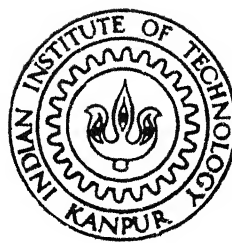


# ELECTRICAL DISCHARGE DIAMOND GRINDING: MECHANISM OF MATERIAL REMOVAL AND MODELING

PHILIP KOSHY



DEPARTMENT OF MECHANICAL ENGINEERING

**INDIAN INSTITUTE OF TECHNOLOGY KANPUR**

JUNE, 1996

TH  
MEE/1996/D  
K  
IEE  
-996  
D  
S  
LE

ELECTRICAL DISCHARGE DIAMOND GRINDING  
MECHANISM OF MATERIAL REMOVAL AND  
MODELING

*A Thesis Submitted  
in Partial Fulfillment of the Requirement  
for the Degree of  
DOCTOR OF PHILOSOPHY*

by  
PHILIP KOSHY

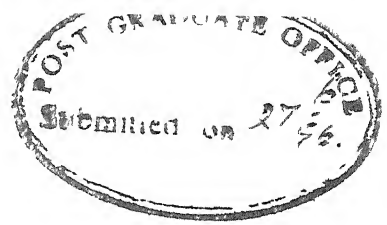
to the  
DEPARTMENT OF MECHANICAL ENGINEERING  
INDIAN INSTITUTE OF TECHNOLOGY – KANPUR

June 1996

RECEIVED

No. A 123597

REC-1386-D-1511-1




## CERTIFICATE

It is certified that the thesis work entitled *Electrical Discharge Diamond Grinding Mechanism of Material Removal and Modeling* by PHILIP KOSHY has been carried out under our supervision, and that it has not been submitted elsewhere for a degree



(Prof V K Jain)



(Prof G K Lal)

Department of Mechanical Engineering  
Indian Institute of Technology  
Kanpur 208 016 India

June 1996



## Acknowledgments

---

Praise be to God Almighty for His persistent grace

I am indebted to my thesis supervisors Prof V K Jain and Prof G K Lal for having given me a free rein in the formulation and implementation of the research work, and for their expert guidance which helped me be on the right track my interaction with them — academic and otherwise, has always been fruitful and pleasant A word of thanks also to Prof A Ghosh, Prof M K Muju, Prof KripaShanker and Dr S K Choudhury for their encouragement during the various phases of my work

The dynamometer donated by Mr Joginder Singh of Kalsi Micro-Measurements and Instrumentation Private Ltd , Kanpur, was of immense help I thank him for his kind gesture Thanks are also due to Mr Jagdish Arora, Krishna Industries, Kanpur for developing a kerosene-resistant polymer coating for the dynamometer

Many thanks to Messrs R M Jha, O P Bajaj, H P Sharma, Namdev and Gupta of the Manufacturing Science Laboratory for their skillful and friendly rendering of all possible help in the setting up and conducting of the experiments

The financial assistance received from the Department of Science and Technology, Government of India, in the form of a Research Associateship is acknowledged Widia (India) Ltd and Sandvik Asia Ltd generously provided work material samples and diamond grinding wheels for experimentation

The time I spent with Ammavan, Prakash, Bala, Ramesh, Verma, Ravindra, Christian, Jimmy, Salim, Siby, Manoj, Taraks Sobha, Sridhar, Jagirdar, Reddy, Rajiv has been very exciting and enlightening as well, they really made life at IIT-Kanpur memorable and great Special mention of Jimmy who meticulously edited my manuscripts My gratitude also to Dr Joseph John and Dr Raghuram, and their families for their warm friendship

I am grateful to Papa, Mumma, Shiju, Achachen and Liz for their unfailing love, patience and support, but for which this work would have hardly been possible

PHILIP KOSHY

To my wife, Elizabeth

---

” in the twenty-first century, sustainable competitive advantage will come much more from new process technologies what used to be secondary (inventing and perfecting new processes), becomes primary ”  
from **HEAD TO HEAD** by *Lester Thurow*

---

## Synopsis

---

Advanced engineering materials, despite their remarkable technological characteristics, have not been exploited yet due to lack of appropriate machining technology. It is hence imperative to evolve novel, cost-effective and rapid machining techniques that are particularly suited to advanced materials. Towards this end, the emphasis of late has been on developing efficacious hybrid machining processes which combine two or more machining techniques, with a view to exploiting their synergy. The thesis is on a new hybrid process called *Electrical Discharge Diamond Grinding* (EDDG) which integrates diamond grinding and electrical discharge machining (EDM) for machining electrically conducting hard materials. In this process, the workpiece is simultaneously subject to heating by electrical spark discharges bridging the metallic wheel bond and the work, and abrasion by diamond grains.

Motivations for the development of EDDG process are manifold. While grinding hard materials, it is essential to frequently dress the wheel surface to maintain a wheel topography conducive to effective grinding, due to acute wheel loading and glazing problems. In EDDG on account of erosion of the wheel bond by the spark discharges, dressing and declogging of the wheel is in-process which saves the unproductive down-time spent on wheel dressing, moreover, electro-discharge dressing is more efficient than mechanical methods, since it does not involve shearing and consequent loss of abrasives, as in the latter. This apart, the spark discharges thermally soften the work material in the grinding zone, akin to hot machining, on a microscopic scale, and thus facilitate grinding and diminish the grinding forces.

EDM-grinding hybrid process is in its early stages of development and the published literature available on the process constitute a thin body of work. Sustained research efforts are required to transform the process into a mature technology. This thesis makes an attempt in this direction. The work reported in the thesis comprises both experimental and theoretical components. The accent in the experimental work is on examining the role of electrical spark discharges incorporated at the wheel-work interface in enhancing the grinding performance. Experiments have been conducted on

high speed steel (HSS) and cemented carbide workpieces to elucidate the material-specific stock removal mechanism. On the theoretical front, in order to model the EDDG process, two approaches to modeling diamond wheel topography are presented in the thesis. The utility of the wheel topography model in simulating surface generation in EDDG is also demonstrated.

Experiments have been conducted on a die-sinking type spark erosion machine. The set-up consists of a grinding spindle assembly and drive, mounted on the ram of the EDM machine to rotate the peripheral, metal-bonded diamond wheel about an axis parallel to the machine table, for material removal in cut-off configuration. The downfeed of the rotating wheel is regulated automatically by the servo control of the EDM system such that the metallic wheel bond and the work surface are separated by a gap, the width of which depends on the local breakdown strength of the dielectric used, for a particular servo reference voltage. The electrical spark discharges that occur in the interelectrode gap thus thermally influence the work surface and the wheel in the grinding zone, while those diamond grains with protrusion height greater than the interelectrode gap-width abrade the work. The role of spark discharges in augmenting the grinding performance is appraised in terms of the material removal rate (MRR) and the grinding forces, and is compared to grinding with no spark assist. The input parameters investigated are the current and wheel speed for HSS, and the current, pulse on-time and duty-factor for cemented carbide.

Diamond grinding experiments on HSS indicate that the wheel rapidly loses its ability to grind effectively due to the formation of wear-flats on the abrasive grains owing to graphitization of diamond. This also leads to an increase in the normal force as grinding progresses. The problem is quite serious at high grinding speeds since the rate of graphitization depends on the temperature at the grain-work interface, which in turn is a function of the wheel speed. The introduction of electrical spark discharges in the grinding zone has been found to alleviate these problems. The continuous renewal of the wheel surface due to bond erosion by the electrical discharges overwhelms abrasive blunting, and results in a higher MRR, the normal force is also rendered stationary which is advantageous from the point of view of machining.

accuracy. Moreover, with an increase in current, the normal force has been observed to decrease considerably, implying thermal softening of the work by the electrical discharges. The tangential grinding force, however, exhibits a maximum with respect to current, since the flow and welding of adhesive junctions between the abrasive grains and the work is facilitated at a particular temperature. Scanning electron micrographs of surfaces ground at various wheel speeds reveal that the effect of the spark discharges decreases with increasing speed, presumably due to discharge instability at high wheel speeds. The experiments on HSS have led to concluding that (i) EDDG is technologically attractive for grinding hard materials, carbide-steel combinations and materials that tend to load the wheel, (ii) the wheel wear, however, has to be optimized for EDDG to be economically viable, and (iii) the thermal softening of the work by the discharges can be taken advantage of to substitute diamond abrasives with relatively inexpensive  $\text{Al}_2\text{O}_3$  abrasives for grinding hard materials.

The behavior of WC-TiC-(TaNb)C-Co cemented carbide is quite different from that of HSS while grinding with electrical spark assist. The experimental results denote that at low current, the grinding performance enhancement while grinding the cemented carbide is due to declogging of the wheel surface. With an increase in current, the MRR in fact decreases as material removal due to plastic deformation dominates over microcracking mechanism, as a consequence of thermal softening of the work. Furthermore, pull-out of abrasives from the bond is prevalent at higher currents, as indicated by micrographs of the ground surface and the force traces, and substantiated by the observation that the MRR increases with decreasing pulse on-time and duty factor, for a particular current. The results imply that electrodischarge dressing of the wheel away from the grinding zone would be more appropriate for grinding cemented carbides. WC-TiC-(TaNb)C-Co has been found to exhibit an increase in wear resistance at low discharge current which is interpreted in terms of the role of fracture toughness in the wear of the composite. Thermal relief of the inherent tensile residual stress in the cementing phase of the composite, through which the rupturing cracks propagate appears to be responsible for the rise in fracture toughness and the concomitant increase

in wear resistance

Information on the topography of diamond grinding wheels is indispensable for modeling the EDDG process. Currently, models for the topography of diamond wheels are not available, and the existing models pertaining to conventional wheels cannot be extended to diamond wheels since these wheels are structurally very different. With this in view, two approaches to model the diamond wheel topography are presented in this thesis. The first is a stochastic simulation methodology which entails a random sampling technique, and the second, a mathematical model based on simple concepts of probability theory. The indices that characterize the topography of a diamond wheel viz., the static grain count, the protrusion height distribution, the distribution of inter-grain spacing, and the projected area due to exposed abrasives are estimated by these models, with reference to wheel grit size and concentration. The study indicates that (i) the protrusion height distribution of a freshly dressed diamond wheel is uniform, and is independent of abrasive concentration, (ii) the inter-grain spacing conforms to a gamma distribution, and (iii) the projected area due to exposed abrasives is independent of abrasive grit size. The results are validated by experimental data available in the literature.

In EDDG, it is expedient to finish-grind components with the current switched off, since the spark discharges deteriorate the roughness of the ground surface. In this light, a simulation of surface generation in diamond grinding, with regard to the kinematics pertaining to EDDG process is presented. The wheel topography data required for the simulation are derived from the stochastic model mentioned earlier. The simulation enables prediction of the roughness of the ground surface for various grit sizes, the results of which are verified by experiments conducted on the EDDG set-up developed. In addition, the simulation yields the statistical properties of the ground surface, and the relationship between the surface roughness parameter  $R_a$  and the average uncut chip cross-sectional area.

The thesis also outlines possible avenues for future research on EDDG.

## Publications

---

- PHILIP KOSHY, V K JAIN and G K LAL, A Model for the Topography of Diamond Grinding Wheels, *Wear* **169** (2), 237–242 (1993)
- PHILIP KOSHY, V K JAIN and G K LAL, Mechanism of Material Removal in Electrical Discharge Diamond Grinding, accepted for publication in the *International Journal of Machine Tools and Manufacture*
- PHILIP KOSHY, V K JAIN and G K LAL, Grinding of Cemented Carbide with Electrical Spark Assist, submitted to *Journal of Materials Processing Technology*
- PHILIP KOSHY, V K JAIN and G K LAL, Stochastic Simulation Approach to Modeling Diamond Wheel Topography, submitted to *International Journal of Machine Tools and Manufacture*
- PHILIP KOSHY, V K JAIN and G K Lal, Simulation of Surface Generation in Diamond Grinding, to be submitted



## Nomenclature

---

$a, b$	parameters of the mathematical model for wheel topography
$a_c$	uncut chip cross-sectional area
$a_m$	mean uncut chip cross-sectional area
$A_p$	projected area due to a protruding grain
$A_p^c$	projected area of contact of the abrasive
$A_{av}^p$	average projected area due to protruding grains
$c$	side of cubic volume of wheel material considered for modeling
$C$	abrasive concentration
$d$	uncut chip thickness
erf	error function
$E[ ]$	expected value
$f$	fraction of pulse power expended at the anode
$f( )$	probability density function
$F_n$	normal force
$F_n^p$	normal force corresponding to pulse power $p$
$F_t$	tangential force
$F( )$	population distribution function
$g$	parameter for calculating the shape parameter $\lambda$
$g_w$	interelectrode gap-width
$G$	geometric mean of inter-grain spacing
$h$	ordinate of the highest point on the work profile
$H$	work-material hardness
$H_b$	height of bond surface from datum
$k$	thermal conductivity
$K$	a constant
$l$	ordinate of the grain center w r t bond level
$L_s$	sampling length
$MRR_g$	rate of material removal due to grinding
$n$	sample size
$[N_1^p, N_2^p]$	95% confidence limits for static grain density
$N_{av}^p$	average number of protruding abrasive grains
$N_{st}$	static grain density
$p$	pulse power

$p_h$	abrasive protrusion height
$p_{h_{max}}$	maximum protrusion height
$q$	power flux
$r$	radius of abrasive grain
$r_a$	radius of spark channel
$R_a$	surface roughness parameter
$S$	abrasive mesh size
$S_k$	skewness
$S_m$	mean abrasive mesh size
$S( )$	empirical distribution function
$t$	thickness of the debris layer adhering to the wheel
$t_{on}$	pulse on-time
$T$	temperature
$T_s$	Smirnov test statistic
$u$	specific grinding energy
$v$	peripheral wheel speed
$V_a$	volume of abrasives in $c^3$ volume of wheel material
$(x/r)$	parameter representing the critical state of bonding of a grain
$y$	ordinate of abrasive grain center

*Greek symbols*

$\alpha$	thermal diffusivity
$\lambda$	shape parameter of gamma distribution
$\mu_r$	mean abrasive grain radius
$\mu_z$	mean profile height
$\rho_d$	density of diamond
$\sigma$	scale parameter of gamma distribution
$\sigma_r$	standard deviation of abrasive grain radius
$\sigma_z$	standard deviation of profile height
$\phi$	integral complementary error function
$\Gamma$	gamma function
$\Lambda_w$	material removal parameter

# List of Figures

1 1	Basic configurations of EDM-grinding hybrid process (a) Combined dressing and grinding zones (b) Isolated dressing and grinding zones (1–wheel, 2–work, 3–power supply, 4–dressing electrode) [17]	8
1 2	The effect of applied voltage on (a) Forces and (b) Wheel wear, while diamond grinding cemented carbide with electrical spark assist [24]	11
1 3	The effect of applied voltage on (a) Straightness and (b) Surface roughness, while diamond grinding cemented carbide with electrical spark assist [24]	12
1 4	(a) A comparison of the MRR obtained in EDM, EDG and AEDG while machining Al-SiC (b) The role of current and pulse on-time on the MRR in AEDG [25]	13
2 1	Photograph depicting the grinding attachment mounted on the ram of the EDM machine	17
2 2	Kinematic configuration of the experimental set-up	17
2 3	Schematic representation of a section of the wheel-work interface in EDDG	18
2 4	Illustration of the model for estimating the reduction in normal force due to the incidence of spark discharges	22
2 5	The effect of pulse power on $F_n^p/F_n$ at different depths-of-cut — simulation results ( $r=80\text{ }\mu\text{m}$ , discharge voltage 40 V, pulse on-time 100 $\mu\text{s}$ , HSS workpiece)	24
2 6	The effect of wheel speed on MRR at different current while grinding HSS	25
2 7	The effect of current on the average radial wheel wear rate while grinding HSS (wheel speed 4 5 m/s)	26

2 8	The size distribution of cubic boron nitride particles of 120 mesh size (a) before EDM-truing (b) after EDM-truing [35]	27
2 9	Micrographs of chips collected at a current of (a) 1A and (b) 5A while grinding HSS (wheel speed 4 5 m/s)	29
2 10	The effect of current on the evolution of normal force while grinding HSS (wheel speed 4 5 m/s)	30
2 11	The effect of current on the normal force at different wheel speeds while grinding HSS	30
2 12	Micrographs of HSS work-surfaces ground at a current of (a) 0 A (b) 1 A (c) 5 A (wheel speed 4 5 m/s)	32
2 13	Micrographs of HSS work-surfaces ground at a wheel speed of (a) 1 5 m/s (b) 6 m/s (current 2 5 A)	33
2 14	The effect of current on the tangential force at different wheel speeds while grinding HSS	34
2 15	MRR vs normal force at 2 5 and 5 A current while grinding HSS	36
2 16	The effect of current on the specific grinding energy at different wheel speeds while grinding HSS	37
2 17	The effect of current on the MRR at different pulse on-time while grinding cemented carbide	40
2 18	The effect of pulse current on the MRR at different duty factor while grinding cemented carbide (10 $\mu$ s pulse on-time)	41
2 19	Time evolution of normal force while grinding cemented carbide at different current (20 $\mu$ s pulse on-time)	42
2 20	The effect of current on the normal force at different pulse on-time while grinding cemented carbide	43
2 21	Force ratio $F_t/F_n$ vs current at different pulse on-time while grinding cemented carbide	43
2 22	The variation of the material removal parameter $\Lambda_w$ with current at different pulse on-time while grinding cemented carbide	44
2 23	The effect of pulse current on the material removal parameter $\Lambda_w$ at different duty factors while grinding cemented carbide (10 $\mu$ s pulse on-time)	45
2 24	Illustration of the effect of clogging of the wheel	47

2 25	Micrograph indicating wheel loading . . .	47
2 26	Micrographs of cemented carbide work surfaces machined at various currents (a) 0 A (b) 0.4 A (c) 2.1 A (10 $\mu$ s pulse on-time)	49
2 27	The role of fracture toughness on wear resistance [55]	51
3 1	Assumed distribution of grain radius . . .	58
3 2	Critical state of bonding of a grain . . .	60
3 3	Schematic representation of the simulated wheel structure	61
3 4	Scheme for identifying protruding abrasive grains .	62
3 5	Projected area due to an exposed abrasive grain	62
3 6	Typical protrusion height distribution of a 90/110 grit wheel for different concentrations	64
3 7	Maximum protrusion height vs grit size	64
3 8	The static grain count as a function of concentration for various grit sizes as obtained by stochastic simulation	66
3 9	Definition of the inter-grain spacing $\Delta y$	67
3 10	Typical plan view of the simulated surface of a 90/110 grit wheel for two different concentrations (the side of the square represents 3 mm)	68
3 11	The role of concentration on the distribution of inter-grain spacing $\Delta y$ (90/110 mesh size)	69
3 12	The shape parameter of the gamma distribution of $\Delta y$ as a function of concentration for various grit sizes	69
3 13	The scale parameter of the gamma distribution of $\Delta y$ as a function of concentration for various grit sizes	70
3 14	The mean projected area due to exposed abrasives vs mesh number for different concentrations	71
3 15	Parameters of the mathematical model	72
3 16	Protrusion height distribution for three different grit sizes ( $c = 1$ mm)	75
3 17	Static grain count as a function of concentration for different grit sizes as computed using the mathematical model	75
3 18	A comparison of the static grain count due to stochastic simulation and mathematical model (90/110 mesh size)	76

3 19	Projected area due to exposed abrasives — a comparison of results due to stochastic simulation and mathematical model (75 concentration)	77
4 1	The effect of current on the surface roughness — HSS workpiece (voltage 40 V, pulse on-time 100 $\mu$ s, duty factor 0.5, wheel speed 4.5 m/s)	79
4 2	The effect of current on the surface roughness — cemented carbide workpiece (voltage 40 V, pulse on-time 10 $\mu$ s, duty factor 0.5, wheel speed 4.5 m/s)	79
4 3	Schematic representation of surface generation in EDDG (adapted from reference [92])	83
4 4	Coordinate system adopted for simulation of surface generation in EDDG	84
4 5	The surface roughness parameter $R_a$ as a function of active grain number for various gap-widths, in cut-off configuration (simulation result)	86
4 6	The 95% confidence limits for the surface roughness parameter $R_a$ as a function of gap-width, in cut-off configuration (obtained by simulation)	87
4 7	The surface roughness parameter $R_a$ in cut-off configuration for various grit sizes — comparison of simulation and experimental results (the error bands denote 95% confidence limits for $R_a$ , as obtained by simulation)	89
4 8	The roughness parameter $R_a$ vs active grain number at various gap-widths during spark-out — simulation results	90
4 9	The roughness parameter $R_a$ for various grit sizes (spark-out) — a comparison of simulation and experimental results	90
4 10	Representative simulated ground work profiles and their profile height distribution at an active grain number of (a) 250 (b) 500 and (c) 1000 (100/120 grit, 40 $\mu$ m gap-width, cut-off)	91
4 11	The skewness of the simulated profile as a function of active grain number (cut-off)	92
4 12	The distribution of chip cross-sectional area for various grit sizes obtained by simulation (40 $\mu$ m gap-width, cut-off)	94

4 13	The roughness parameter $R_a$ as a function of the average chip cross-sectional area (obtained by simulation)	95
4 14	A comparison of the $R_a$ vs $a_m$ characteristic obtained by simulation with that of experiment cited in reference [95]	95

# List of Tables

2 1	Wheel specifications and electrodischarge dressing parameters	20
2 2	Work material (HSS) specifications and the pertinent EDDG pulse parameters	21
2 3	Work material specifications (cemented carbide) and the relevant EDDG pulse parameters	40



# Contents

<b>1</b>	<b>Introduction</b>	<b>1</b>
1 1	Machining of Advanced Materials	1
1 2	Hybrid Machining Technology	4
1 3	Electrical Discharge Diamond Grinding	7
1 4	Scope and Organization of the Thesis	14
<b>2</b>	<b>Mechanism of Material Removal in EDDG</b>	<b>16</b>
2 1	Experimentation	16
2 2	Material Removal Mechanism — HSS	20
2 2 1	Analysis	21
2 2 2	Results and Discussion	24
2 3	Material Removal Mechanism — Cemented Carbide	38
2 3 1	Results	39
2 3 2	Discussion	44
<b>3</b>	<b>Topography Models for Diamond Grinding Wheels</b>	<b>54</b>
3 1	Introduction	54
3 2	Background & Assumptions	56
3 3	Stochastic Simulation	60
3 3 1	Methodology	60
3 3 2	Results and Discussion	63
3 4	Mathematical Model	71
3 4 1	Methodology	71
3 4 2	Results and Discussion	74

4	Simulation of Surface Generation in EDDG	78
4 1	Introduction	78
4 2	Experimentation	82
4 3	Simulation of Surface Generation	83
4 3 1	Methodology	83
4 3 2	Results and Discussion	86
5	Conclusions and Future Work	96
5 1	Conclusions	96
5 2	Scope for Future Work	98

# Chapter 1

## Introduction

---

### 1.1 Machining of Advanced Materials

Rapid progress in the science and technology of materials has resulted in the emergence of a wide range of engineering ceramics and composites. Materials can now be tailor-made to feature a combination of desired properties for advanced applications. Endowed with remarkable technological characteristics such as high strength even at elevated temperatures and excellent wear resistance, these materials offer attractive options for component design, silicon nitride bearings, for instance, can be operated upto 700°C under extremely corrosive conditions without lubrication. However, the very material properties responsible for superior product performance, render the transformation of such materials into useful products difficult.

Lack of appropriate machining technology is evidently the major impediment to exploiting advanced materials. For high precision components, with the present technology, the cost incurred in machining could be as much as 90% of the total component cost, which is quite high in comparison to the cost associated with machining conventional materials. It is hence pertinent to direct research efforts toward developing novel, cost-effective and rapid machining techniques. It is also essential that the machining process induces only tolerable surface damage, in view of the strength of these materials being susceptible to flaws generated during manufacture.

Ceramic parts can be fabricated to near-net shape only in the green state,

for which polycrystalline diamond tools are extensively used. On sintering, machining of the functional surfaces of a part is indispensable to meet tolerances of dimension and form, to achieve specified surface finish, and to remove surface flaws for a better surface integrity. Reference [1] presents an excellent review of the state of art of machining of ceramic materials, and identifies areas for future research. Many machining processes that have been developed for machining metals are currently being extended to advanced materials. Machining of ceramics with a geometrically defined cutting edge necessitates the tool to be harder than the work-material, and be of a configuration that would remove material without overstressing the machined component. Turning and milling of ceramic parts in the hardened state is of limited scope since the tools experience unacceptably high rates of wear, and in the course of machining exert too great a local tensile load on the work resulting in severe surface damage. Machining of hardened ferrous components is however technologically and economically feasible with ceramic tools, on rigid and precise machines [2].

Grinding of hard materials is accomplished with diamond or cubic boron nitride superabrasives. The problems encountered during grinding of advanced materials, on account of their being inherently hard and brittle have paved the way for the development of material-adapted grinding techniques [3]. This refers to the identification and control of grinding conditions to be employed to maximize the rate of material removal, while maintaining the level of surface damage within acceptable limits. Material removal while grinding hard materials is known to be effected by a combination of brittle fracture and plastic deformation mechanisms. Brittle fracture entails two principal crack systems — lateral cracks responsible for material removal, and median cracks which degrade the strength of the parent material. Plastic deformation is similar to chip formation during grinding of metals which involves shearing of the material.

The operative mode of material removal while grinding hard materials depends on the size and density of defects such as voids and cracks in the material, and the extent of the stress field arising out of the interaction of abrasives with the work [4]. When the stress field is larger than the size

of defects, material is removed by way of localized micro brittle fracture, and when the bulk of the stress field is smaller, the mechanism of material removal is primarily plastic deformation. Removal of material can be facilitated, if that is what is of interest, by effectively taking advantage of the phenomenon of brittle fracture by employing appropriate grinding parameters. On the other hand, if sub-surface damage is intolerable, as in the grinding of optical glass, ductile mode is adopted by resorting to operating conditions that correspond to cutting depths less than a certain threshold value specific to the material [5]

Electrical discharge machining (EDM) is perhaps the most popular among electrical machining techniques, for the machining of advanced engineering materials. Apart from the generation of extremely complex geometries by die-sinking and wire-cutting, materials can by this method be processed regardless of hardness or strength, with negligible forces exerted on the work, provided the work material electrical resistivity is not more than  $100 \Omega\text{cm}$ . In EDM, material is removed by utilizing high-density thermal energy. While machining metals, material removal is essentially by melting and vaporization phenomena. This leaves a recast layer of heat-affected material on the work surface which consists of a fine network of microcracks, which has to be removed by polishing if surface integrity is of concern. Material removal has also been known to take place by thermal spalling in case of materials like  $\text{TiB}_2$  which have a high thermal expansion coefficient and low thermal conductivity. The remarkable success of the application of EDM in shaping intractable materials can be appraised by considering the fact that many nonconducting materials, just for the sake of machining, are rendered electrically conductive to the level required for electrodischarge processing by doping them with conductive elements [6]

Besides grinding and EDM, other processes such as honing, lapping, ultrasonic machining (USM), electrochemical machining (ECM) and abrasive water-jet machining, and techniques employing laser, ion or electron beams are also practiced for machining advanced materials. Novel methods of finishing like magnetic abrasive machining are being innovated and continually refined. Lately, the accent has been on developing efficacious hybrid machin-

ing techniques

## 1.2 Hybrid Machining Technology

Hybrid processes combine two or more machining techniques with a view to exploiting their synergy to enhance productivity, particularly for machining difficult-to-machine materials

Perhaps the most well-known among hybrid machining processes is electrochemical grinding (ECG) which involves the combination of ECM and fine grinding for the machining of hard or fragile electrically conducting materials. ECG systems closely resemble conventional grinding machines, grinding wheels with a conducting bond are utilized in ECG, with an electrolyte replacing the coolant. Machining proceeds with a potential applied across the wheel and the work, with the wheel acting as the cathode. Typically, 90% of the material removal is by electrochemical means and the rest by abrasion. The abrasive grains do away with any nonreactive oxide layer formed on the machined surface to ensure unhindered electrolytic action. For materials with a hardness of  $R_c$  60 or more, ECG offers removal rates upto ten times of that of conventional grinding. In case of nonhomogenous materials like cemented carbides, the surface finish obtained is also better. Moreover, no matter how hard, tough or brittle a material is, the finished work surface is free from burrs or grinding-burn marks. Since the dimensional accuracy obtained in ECG is not as good as in conventional grinding, it is a normal practice to finish components with no electrochemical material removal. The application of ECG is primarily in the manufacture of carbide cutting tools, where savings of the order of 80% in wheel costs and 50% in labor costs have been reported [7] to be realized, as compared to conventional grinding.

Electrochemical arc machining (ECAM) which combines ECM and spark erosion, relies on electrical discharge phenomenon in electrolytes for material removal [8]. In this process, a pulsed voltage (full-wave rectified a.c.) is applied between a vibrating cathode tool and the work, which are separated by a gap. The input voltage waveform is tuned to be in phase with the displacement of the tool. During the course of vibration of the tool, in every cycle,

as the interelectrode gap decreases, the current increases and sparking takes place by breakdown of the electrolyte, aided by the generation of gas/steam bubbles in the gap. Material removal is by electrolysis when the gap-width and current are not conducive to sparking. Any metallurgical damage to the work due to spark discharges, can also be alleviated by electrochemical action in this process. Typical material removal rates obtained in ECAM are nearly a hundred and fifty times of that of EDM, and three times that of ECM in hole-drilling applications.

The primary limitation of USM process is the low material removal rate (MRR). The introduction of electrical discharges in the machining zone in USM has to a large extent overcome this constraint. For tungsten carbide material, a 50-85% increase in MRR has been observed [9] on combining EDM and USM, due to activation of the abrasive slurry by the discharges. Scanning electron microscopic studies of the machined surface has indicated that abrasion effectively removes material which is thermally softened by the electrical discharges.

Reference [10] reports a hybrid process which involves the combination of grinding, USM and EDM for processing ceramic components. Imparting an ultrasonic vibration alone to the grinding wheel, in addition to decreasing the grinding forces for various ceramics to about 30% of that in conventional grinding, has been found to render the grinding forces stationary. Grinding of very hard materials like  $TiB_2$  requires the addition of EDM also in the process to obtain constant and low grinding forces, and to maintain the grinding ability of the wheel during the course of machining.

There has been a renewed interest in hot machining with the advent of difficult-to-machine materials. In hot machining, by some external means of localized heating, the work is rendered soft in comparison to the tool, which is expected to result in lower cutting forces, a better surface finish and a longer tool life. Either plasma arcs or laser beams are used as heat sources. Laser beams are however preferred to plasma arcs since they possess a higher power density and strong directionality. Moreover, they are flexible to handle and are amenable to fine control.

Plasma hot machining of ceramic materials is discussed in reference [11]

The response to plasma arc heating of the work while machining has been found to be material-dependent, while silicon nitride exhibited a marked decrease in turning forces as the workpiece was heated to temperatures above 1050°C, the forces were observed to be on an increase with a rise in workpiece temperature in the case of alumina. The mechanism of chip formation for a variety of materials like mullite and silicon carbide, on heating, has been observed to change over from brittle fracture to plastic flow, exemplified by the change in the chip-form from discontinuous to continuous. A remarkable decrease in tool wear — by a factor of eight, has been obtained by plasma hot machining silicon nitride with a diamond tool.

In laser-assisted machining of hard materials, the beam intensity and interaction time are selected such that, during the cutting operation the workpiece is selectively heated to a defined depth which would reduce the cutting forces but cause no thermal damage to the functional surface generated. The resultant low cutting forces permit the machining of fragile or slender components. Milling of a cobalt-based alloy (stellite) with laser-assist using a cubic boron nitride tool has been reported [12] to result in 70% reduction of cutting forces and 90% increase in tool life. The reduction in tool wear is on account of the decrease in stresses experienced by the tool face, brought about by thermal softening of the work. Recently, laser-assisted grinding of hot-pressed silicon nitride has been found [13] to increase the rate of material removal by six times with no mechanical damage imparted to the workpiece.

Research on chemical means of assisting material removal processes are also being pursued. Interactions between chemical compounds added to the cutting fluid, and the work-surface, could influence the coefficient of friction in the cutting zone, the wear of abrasives and the mechanical properties of the work material. The addition of boric acid while drilling polycrystalline alumina with a diamond core drill, for example, has been observed [14] to increase the MRR twofold due to boric acid influencing the grain boundary phase in alumina, promoting intergranular fracture.

The foregoing discussion clearly indicates that hybrid machining technology potentially has a vital role to play in the machining of advanced materials. The work reported in this thesis is on a new hybrid process called



*Electrical Discharge Diamond Grinding* (EDDG) which integrates diamond grinding and EDM for machining electrically conducting hard materials. The following section provides an introduction to this process, and a review of the relevant literature available.

## 1.3 Electrical Discharge Diamond Grinding

The concept of integrating EDM and diamond grinding for machining electrically conducting hard materials was perhaps first highlighted in publications from the erstwhile Soviet Union [15–17]. There are two basic configurations by which the combination of grinding and EDM can be realized [17]. (i) The workpiece itself acts as the dressing electrode whereby the grinding and wheel dressing zones are combined (Figure 1 1a). The work is thus simultaneously under the action of diamond grains and electrical spark discharges which cause abrasion and material softening/removal respectively. The reduction of grinding forces and power, due to spark induced thermal softening of the work, and enhanced wheel performance due to continuous, in-process dressing and declogging of the wheel are the salient features of this set-up. Though the construction is simple, this arrangement precludes independent optimization of grinding and dressing operations, which in some cases might result in wasteful diamond wear. (ii) A separate electrode accomplishes electrodischarge dressing of the wheel outside the grinding zone (Figure 1 1b). The discharges are utilized for the renewal of the wheel topography alone and do not exert any influence on the work. The wheel, however, can be dressed as and when the need arises, at an optimum rate, irrespective of the grinding conditions.

Our interest, in the present work, is on the first configuration (Figure 1 1a) which combines the grinding and dressing zones. It is to be noted that this process is different from the so-called electrical discharge grinding (EDG) process [7] — the terminology of which is a misnomer, as the rotating graphite electrode used therein for spark erosion is never in physical contact with the work, let alone abrade the work material. Considering the apparent similarity between ECG and EDDG, a comparison between the two is in order.

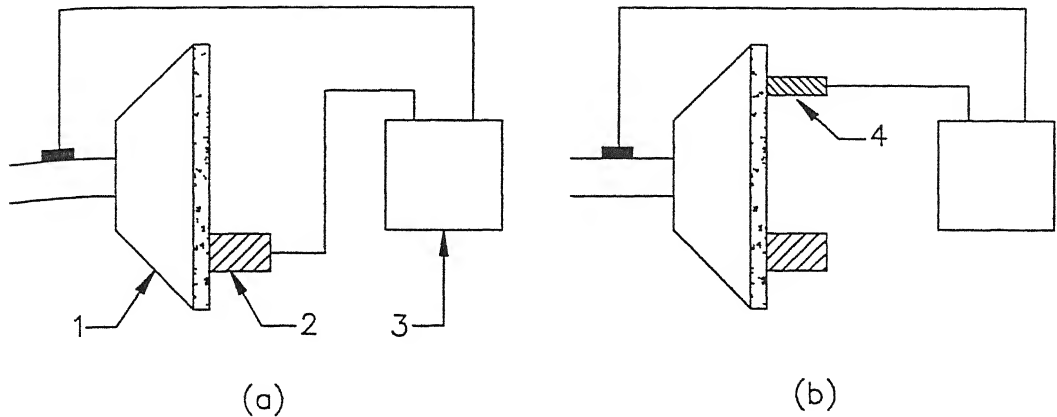


Figure 1.1 Basic configurations of EDM-grinding hybrid process (a) Combined dressing and grinding zones (b) Isolated dressing and grinding zones (1-wheel, 2-work, 3-power supply, 4-dressing electrode) [17]

Material removal in the latter process, in contrast to ECG, is predominantly by abrasion with the spark discharges playing more of a supportive role. An advantage of EDDG over ECG is that it is more environment-friendly with no sludge formation and attendant disposal problems — an aspect becoming increasingly prominent lately.

To appreciate the motivation for the development of EDDG process, it is worthwhile to review certain characteristics of and the problems associated with grinding and EDM of hard materials to understand how they assist each other when combined.

Abrasive machining, by nature, calls for a tool material harder than the workpiece. Grinding of hard materials, therefore, becomes a problem as the work-material hardness approaches that of diamond, which is the hardest known abrasive. In addition, grinding of hard materials is characterized by inordinately high normal force as the indentation of the abrasive grains into the workpiece becomes difficult [4]. High normal force causes significant elastic deformation of the machine tool structure, which reflects detrimentally on the machining accuracy. Under such circumstances, it is essential to explore means of lowering the resistance of the work material to machining. Hybrid machining processes are possibly the key to this end. ECG of  $\text{Al}_2\text{O}_3$ -Mo cermet, for instance, involves lower grinding forces and specific grinding energy

in comparison to conventional diamond grinding, as the electrolytic action weakens the Mo bridges that bind the hard  $\text{Al}_2\text{O}_3$  grains [18] In EDDG, electrical spark discharges are utilized to thermally soften the work-material on a microscopic scale to facilitate grinding and to diminish the grinding forces

While grinding hard materials, wear-flats are formed rapidly on the abrasives, on account of intense attritious wear This is known as glazing of the wheel Another related problem is wheel loading which refers to the accumulation of grinding swarf in the chip pockets on the wheel surface These phenomena collectively give rise to a time-dependent increase of grinding forces and power, and undesirable vibrations Glazing and loading of grinding wheels are serious deterrents to achieving good machining accuracy and surface finish, and eventually culminate in stalling the material removal process Frequent dressing of the wheel is hence imperative to maintain a wheel topography conducive to effective grinding This translates to considerable loss of both wheel material and productive machining time The volumetric diamond wheel wear while grinding polycrystalline diamond, for example, is fifty times the volume of material removed [19] This implies that more time is spent on dressing the wheel, rather than machining In EDDG, dressing of the grinding wheel is continuous and is in-process, as the bond material is subject to spark erosion This obviates the need to interrupt machining for dressing the wheel In the event of wheel clogging, the conducting grinding debris is selectively removed, thus enabling free cutting Moreover, the discharge parameters can be optimized such that the wear rate of the bond corresponds to that of the abrasives, which represents optimal grinding performance

The nature of dressing metal-bonded wheels by electroerosion also deserves mention Presently, mechanical methods are widely practiced wherein dressing is brought about by abrasion of the relatively soft bonding matrix [20] These procedures have the limitations of acute wear of the dressing medium, and the possibility of the loss of abrasive grains by way of grain fracture or pull-out Electrodischarge dressing has been found [21] to alleviate these difficulties Here mechanical shearing of abrasives is absent as dressing

is by bond erosion. A maximum protrusion height close to 60% of the grain dimension is achievable by this method [22] whereas the one obtained through mechanical methods will be lower, depending on the efficiency of dressing. In addition, the negligibly low dressing forces in electrodischarge dressing help retain good form accuracy of the wheel, and facilitate dressing of even thin wheels. Moreover, a wide range of grit sizes and concentrations can be accommodated while electrodischarge dressing by just tuning the discharge parameters, mechanical methods of dressing, on the other hand, would require a large inventory of suitable dressing wheels of different specifications for accomplishing the same task.

Abrasion assisting EDM is another perspective of EDM-grinding combined process. EDM is an inefficient machining process. Thermal modeling of the process has indicated [23] that the fraction of the molten material which is physically not removed but redeposited on the parent material surface could be as high as 80%. The recast layer and the heat affected material immediately beneath contain numerous microcracks which degrade the fatigue strength of the material. In EDDG, the crack-infested layer can be ground off in situ by appropriately selecting the grit size of abrasives used in the wheel. The rate of material removal is also improved considerably.

EDM of composite materials containing electrically nonconducting phases poses a few problems. The nonconducting material particles hamper the process stability and impede the material removal process resulting in very low stock removal rates. More serious is the risk associated with die-sinking this kind of materials [6] as machining progresses, due to inhomogeneity of the work material, if by chance, a localized layer of insulating material surfaces up, the control system of the machine tool would misinterpret the situation as an open-circuit condition. This would result in a feed motion being imparted to the electrode which can result in collision and consequent damage. These problems are taken care of in EDDG. The MRR is enhanced as the abrasive grains remove the nonconducting material particles expending little effort, with the spark discharges having thermally softened the surrounding binding material. Chances of potential collisions are also reduced considerably by the incorporation of abrasion into EDM. The rotating wheel, moreover,

considerably improves the flushing at the interelectrode gap, which is most important with regard to process stability

Publications available on EDM-grinding hybrid machining process are not many. References [15–17] on the process are more of an exploratory nature. An extensive literature survey yielded just two references that report a systematic study of the process, the salient results of which are reviewed in the following.

The role of electrical discharges introduced in the grinding zone while grooving and cutting-off of cemented carbides and a few advanced ceramics has been studied by Aoyama and Inasaki [24]. The responses investigated to evaluate the grinding performance were the grinding forces, wheel wear, surface finish and the geometrical accuracy. Their set-up consisted of a surface grinding machine, with the wheel and the work electrically insulated from the rest of the machine, across which a pulsed d.c. voltage was applied for the spark discharges to occur in the grinding zone. The grit size of the resinoid bonded wheel used was  $100\text{ }\mu\text{m}$ . With an increase in the applied voltage, the normal and tangential components of grinding force were found to decrease, at the expense of an increase in wheel wear (Figures 1.2a and 1.2b). While

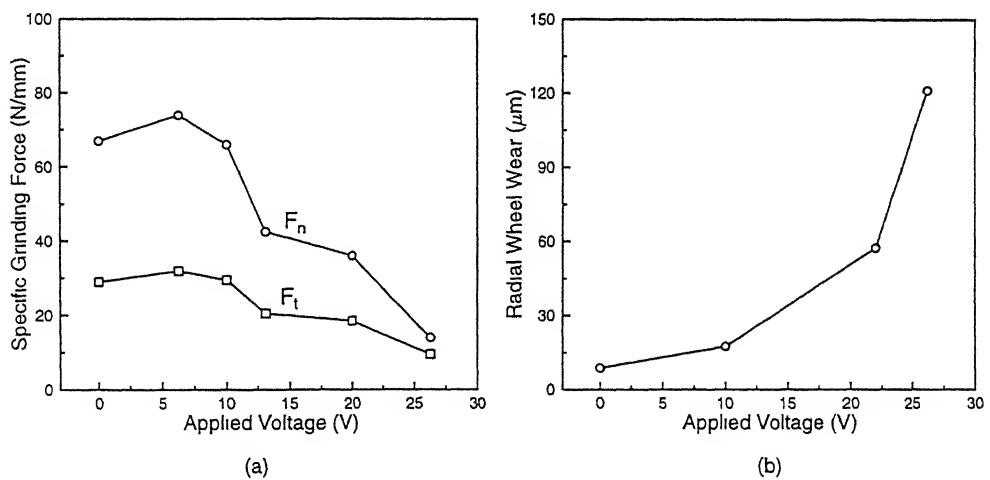


Figure 1.2 The effect of applied voltage on (a) Forces and (b) Wheel wear, while diamond grinding cemented carbide with electrical spark assist [24]

the straightness of the ground groove improved with increasing voltage, due to reduced elastic deformation of the wheel associated with lower grinding forces, the surface finish was found to deteriorate (Figures 1 3a and 1 3b) The electrical discharges have also been found to obviate the problem of chipping of ground edges, which is common while grinding brittle materials

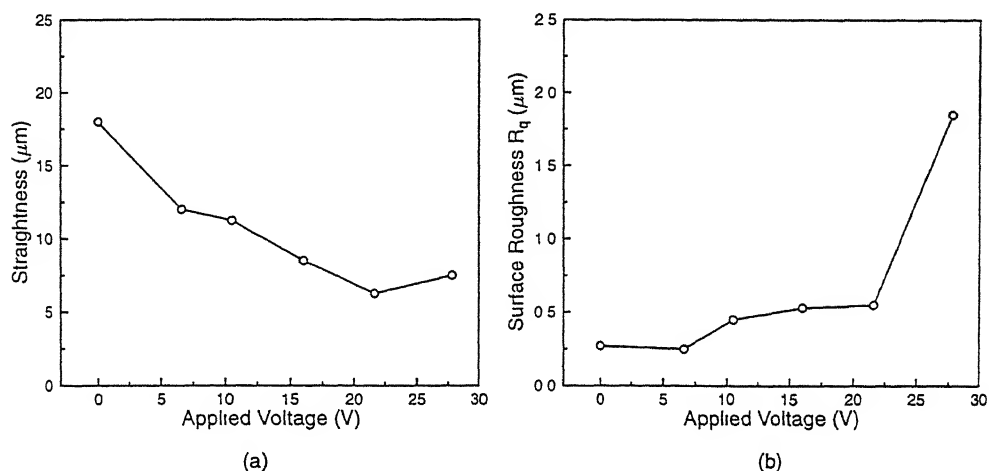


Figure 1 3 The effect of applied voltage on (a) Straightness and (b) Surface roughness, while diamond grinding cemented carbide with electrical spark assist [24]

The decrease in the grinding forces has been attributed to two factors (i) a portion of the material being removed by spark erosion before the abrasive grains cut the material, and (ii) self-sharpening of the grinding wheel brought about by the electrical discharges The grinding forces were found to be reduced remarkably while grinding SiC and Si<sub>3</sub>N<sub>4</sub> ceramics too The primary limitation of the process was found to be the high wear rate of the wheel, which could be circumvented by replacing the resinoid bond of the wheel by tungsten, which is quite resistant to spark erosion

Recently, Rajurkar et al [25] have reported the characteristics of EDM-grinding hybrid process, which they call Abrasive Electrodischarge Grinding (AEDG) The experimental set-up comprises a grinding attachment assembled on a EDM die-sinker Machining experiments have been conducted on Al-SiC and a titanium alloy Their viewpoint of the process has been to study how abrasion could enhance EDM performance, and for this reason, use a fine

grit wheel (220 mesh) The peak current, pulse on-time and wheel speed have been identified to be the main parameters influencing the process responses for a particular wheel and servo reference voltage setting The enhancement of the material removal rate on introducing abrasion into the process has been studied in comparison to conventional EDM, and EDM with a rotating graphite electrode (EDG), as a function of wheel speed and pulse on-time, an increase in wheel speed has been observed to provide a higher material removal rate in AEDG due to enhanced abrasion (Figure 1 4a) Similarly, with an increase in the peak current, more of material is removed on account of intensified electroerosion (Figure 1 4b) The relative contributions of EDM and grinding in removing material, with reference to peak current, has also been qualitatively studied with the aid of scanning electron microscopy

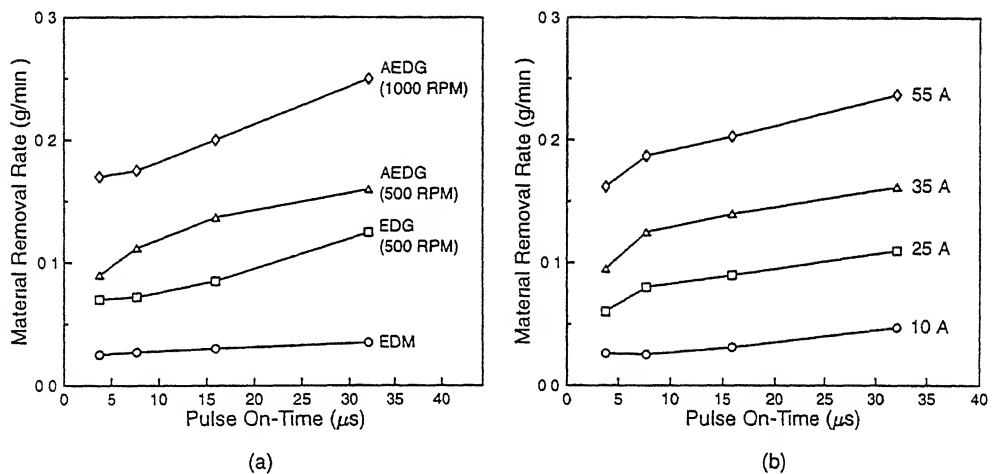


Figure 1 4 (a) A comparison of the MRR obtained in EDM, EDG and AEDG while machining Al-SiC (b) The role of current and pulse on-time on the MRR in AEDG [25]

EDM-grinding hybrid machining process is very much in its early stages of development Sustained research is required to transform the process into a mature technology, for its successful induction into the industry This thesis makes an attempt in this direction The scope of the present work, and the organization of the thesis are described in the following section

## 1.4 Scope and Organization of the Thesis

The thesis comprises both experimental and theoretical components. In studying the EDM-grinding hybrid machining process, the emphasis in the present work is on examining the role of electrical spark discharges incorporated at the wheel-work interface in enhancing the grinding performance. Experiments have been conducted on both high speed steel and cemented carbide workpieces to elucidate the material-specific stock removal mechanism. The effect of wheel speed, current, pulse on-time and duty factor, on the material removal rate and grinding forces have been studied to perceive the underlying physics of the process. Description of the experimental set-up, details of experimentation, and the associated results and discussion constitute Chapter 2 of the thesis.

Metal-bonded diamond grinding wheels are predominantly employed in EDM-grinding hybrid machining process. Modeling of the process with a view to contributing to a better understanding of the same requires a model for the topography of diamond grinding wheels. Despite their extensive use lately, in the grinding of advanced engineering materials, topography models for diamond wheels are presently not available. Chapter 3 presents two approaches to modeling diamond wheel topography in a bid to bridging this knowledge gap. The first approach entails a stochastic simulation methodology, and the second, a mathematical method based on simple concepts of probability theory. Various topographic indices that macroscopically characterize the topography of diamond wheels viz , the static grain count, the protrusion height distribution, the distribution of inter-grain spacing and the projected area due to exposed abrasives are estimated with reference to abrasive grit size and concentration. The models are validated by experimental data available in the literature.

The introduction of electrical spark discharges in the grinding zone, though beneficial in many respects, has however been found to impair the surface finish. It is hence expedient to switch off the current and employ grinding alone while finishing a component. In this light, a simulation of surface generation in EDDG under conditions of no current flow, which utilizes the



topography model described in Chapter 3, is presented in Chapter 4. The roughness of the ground surface is predicted for various grit sizes by simulation, and the results are validated by experiments conducted on the EDDG set-up developed. The distribution of both the ground surface profile height and the uncut chip cross-sectional area is also studied.

The conclusions drawn from the present work are enumerated in Chapter 5. Possible avenues for future research are also outlined.

# Chapter 2

## Mechanism of Material Removal in EDDG

---

This chapter presents the mechanism of material removal while diamond grinding, with electrical spark discharges incorporated at the wheel-work interface. Experiments have been conducted on high speed steel (HSS) and cemented carbide workpieces to explicate the material-specific grinding response. The emphasis is on gaining an insight into how the discharges influence the wheel and the work with reference to the process parameters viz , wheel speed, current, pulse on-time and duty-factor. The role of spark discharges in augmenting the grinding performance is evaluated in terms of the MRR and grinding forces, vis-à-vis grinding with no spark assist.

The following section describes the experimental set-up and the details of experimentation. Subsequent sections dwell on the material removal mechanism, separately for HSS and cemented carbide.

### 2.1 Experimentation

Experiments have been conducted on a ELEKTRA die-sinking type spark erosion machine equipped with a solid-state power supply. The set-up consists of a grinding spindle assembly and a variable-speed drive, mounted on the ram of the machine to rotate the peripheral, metal-bonded diamond wheel about its axis parallel to the machine table (Figure 2.1). While machining,

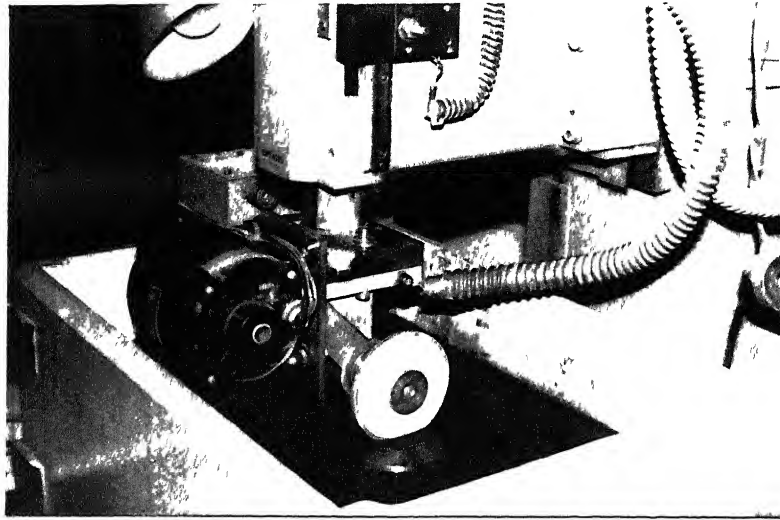


Figure 2 1 Photograph depicting the grinding attachment mounted on the ram of the EDM machine

the rotating wheel is fed downward under servo control of the EDM machine, for material removal in cut-off configuration (Figure 2 2) The downfeed of the rotating wheel is regulated automatically by the servo of the EDM system such that the metallic wheel bond and the work surface are physically

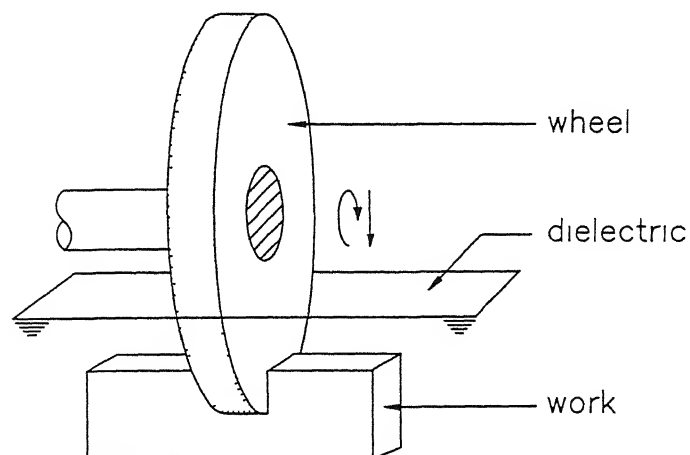


Figure 2 2 Kinematic configuration of the experimental set-up

separated by a gap, the width of which depends on the local breakdown strength of the dielectric for a particular servo reference voltage setting. The workpiece is thus simultaneously subject to heating due to electrical sparks occurring between the wheel bond and the work, and abrasion by diamond grains with protrusion height  $p_h$  more than the interelectrode gap-width  $g_w$  (Figure 2 3)

In conventional grinding operations, a part of the input energy is expended in sliding contact between the wheel bond and the workpiece [26]. In the configuration above, since the non-conducting diamond grains alone are in contact with the work, such frictional energy loss is non-existent.

The diamond wheel on being mounted on the spindle, was initially trued with a silicon carbide wheel (C60L5V) run in mesh with it, truing being accomplished by abrasion of the bond by the debris generated at the interface of the two wheels. The slip between the grinding and truing wheels, necessary for truing action, was obtained by orienting their axes such that their peripheral velocities are not collinear along the line of contact. Truing was carried out until the run-out of the wheel was reduced to less than  $10\text{ }\mu\text{m}$ . The wheel was thereafter electrodischarge dressed under identical discharge conditions (see Table 2 1) before each experiment to obtain a standard wheel topography. The effect of discharge energy on the resultant wheel topography while electrodischarge dressing is discussed in reference [21]. Sufficient grit protrusion is obtained under high discharge energy conditions but at the expense of dislodging some abrasive grains. Arriving at the appropriate

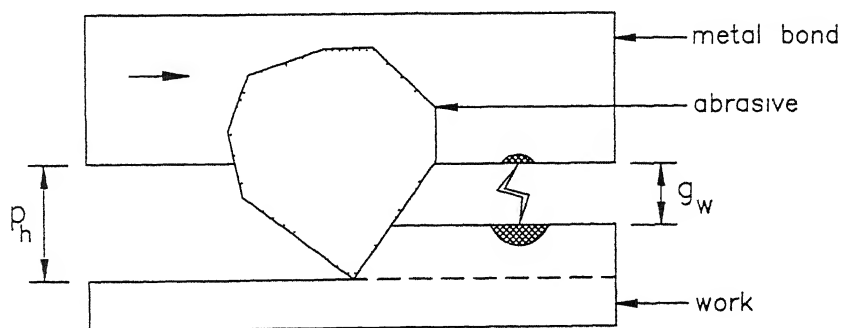


Figure 2 3 Schematic representation of a section of the wheel-work interface in EDDG

level of discharge energy entails a compromise between these two conflicting factors. The dressing conditions employed in the present study were selected to preclude contact between the abrasive grains and the dressing electrode, and to remove radially about 50  $\mu\text{m}$  of the wheel material (approximately 30% of the grain dimension) in reasonable time.

While electrodischarge dressing diamond wheels, the choice of the electrode material is important. At high temperatures, the transformation of diamond to graphite occurs, a reaction catalyzed by the presence of certain metallic elements. It was observed during experimentation that a wheel electrodischarge dressed with a steel electrode rubbed against rather than cut the material, thus giving rise to severe chatter. The color of the wheel surface was also observed to turn black indicating graphitization of protruding abrasive grains. Reference [27] presents a study on the affinity of diamond towards different metals. Remarkable graphitization of diamond has been observed on heating to 900°C in the presence of iron. Of the many materials studied, copper and gold have been reported to be the only materials to induce no thermal erosion in diamond. Dressing of the wheel was hence carried out with a copper electrode employing positive polarity.

To evaluate the grinding performance obtained in EDDG, experiments have also been conducted by switching off the current, to correspond to conventional diamond grinding. (A negligibly small current of approximately 0.04 A however flows through the gap at this setting for the purpose of gap sensing.) The servo sensitivity and the servo reference voltage were kept constant for all experiments.

The MRR was calculated by measuring the weight loss of the sample on machining for a period of five minutes. The normal and tangential forces were measured with an octagonal-ring strain gage dynamometer. The morphology of the ground surface and the wheel, and the grinding debris were examined in a JEOL JSM 840-A scanning electron microscope.

Since the performance characteristics of diamond wheels of even the same specification are prone to vary from one wheel to another, the same wheel was used for each of the two materials studied. The specifications of the diamond wheel used and the dressing parameters employed are listed in Table 2.1. The

current and voltage reported in this thesis pertain to average values, unless mentioned otherwise

---

### Wheel

1A1 diamond wheel, 5.7 mm thick, 100 mm diameter  
G80/100 C75, bronze bond

### Dressing

Voltage	60 V
Current	10 A
Pulse on-time	100 $\mu$ s
Duty factor	0.5
Wheel speed	60 m/min
Duration	2 min

---

Table 2.1 Wheel specifications and electrodischarge dressing parameters

## 2.2 Material Removal Mechanism — HSS

Diamond is an ineffective abrasive for grinding ferrous materials since it wears off rapidly by a graphitization process, with iron acting as a catalyst. This fact, however, is the motivation for having selected HSS as one of the work materials, for evaluating the grinding performance in EDDG, HSS essentially represents very hard materials in so far as it swiftly blunts the diamond abrasives in the grinding wheel.

Diamond grinding of tool steels has been studied by Graham and Nee [28]. They report that during the course of grinding, the normal force component initially increases with time on account of the formation of wear-flats on the diamond grains by a combination of abrasive and chemical phenomena, and later stabilizes at an equilibrium value. Their results indicate that the wear of the wheel, for a given set of grinding conditions, is related to the hardness of the workpiece, and the rate of change of normal force during the course of

grinding

Prins [29] conducted single-grit scratch experiments on steels using diamond indentors to investigate their interaction. The normal force was found to depend mainly on the hardness of the work-material, and to be independent of the cutting speed. The tangential force component, on the contrary, while being insensitive to work hardness, was observed to decrease with an increase in cutting speed.

In the present work, the role of current and wheel speed on the MRR and grinding forces is investigated to elucidate the mechanism of material removal while grinding HSS with electrical spark assist. The work material specifications, and the electrical pulse parameters employed during experimentation are given in Table 2.2. A simple model for assessing the reduction in normal grinding force, due to the incidence of spark discharges on the HSS workpiece is presented next. The subsequent subsection discusses the experimental results.

---

### Work Material

High speed steel (20%W, 4%Cr, 5%V)

Hardness 1200 HV

5.6 mm wide

### EDDG Pulse Parameters

Voltage 40 V

Pulse on-time 100  $\mu$ s

Duty factor 0.5

---

Table 2.2 Work material (HSS) specifications and the pertinent EDDG pulse parameters

## 2.2.1 Analysis

The normal force component in grinding originates from the physical interaction between the abrasive grains and the work. The extent of abrasive-work

interference in grinding depends on the topography of the wheel and process kinematics, and is stochastic in nature. However, for simplicity, it is expedient to consider a single spherical grain of radius  $r$  ploughing through a plane work surface to a depth  $d$  (Figure 2.4). The normal force  $F_n$  in this case is given by

$$F_n = H A_c^p \quad (2.1)$$

where  $H$  is the hardness of the work material and  $A_c^p = \frac{\pi}{2}(2rd - d^2)$  is the projected area of contact in a plane perpendicular to the line of action of  $F_n$ . A spark discharge incident on the work material just ahead of the grain would bring about a hardness gradient across the depth of cut due to a rise in temperature. The hardness  $H(y)$  at a depth  $y$  would depend on the temperature  $T(y)$ . The normal force  $F_n^p$  corresponding to this situation can be calculated as

$$F_n^p = \int_0^d H(y) A_c^p(y) dy \quad (2.2)$$

High speed steels retain about 80% of their room-temperature hardness upto a temperature of 600°C. At higher temperatures the hardness decreases rapidly at first and gradually thereafter as the temperature approaches the melting point [30]. The hardness becomes zero at the melting temperature.

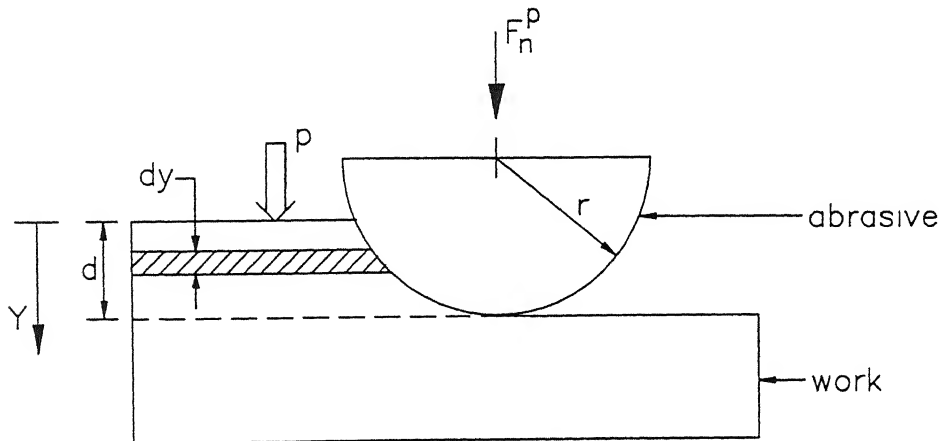


Figure 2.4 Illustration of the model for estimating the reduction in normal force due to the incidence of spark discharges



(1250°C) In the present work, for computation,  $H(y)$  is evaluated as a function of the temperature  $T(y)$  by fitting piecewise polynomials that conform to this trend

To compute the temperature field in the material due to a single spark, the anode erosion model discussed in reference [31] is adopted in the present work. The temperature  $T(y)$  along the axis of the spark is of interest and is given by the expression

$$T(y) = \frac{2q\sqrt{\alpha t_{on}}}{k} \left[ \phi \left( \frac{y}{2\sqrt{\alpha t_{on}}} \right) - \phi \left( \frac{\sqrt{y^2 + r_a^2}}{2\sqrt{\alpha t_{on}}} \right) \right] \quad (2.3)$$

In the above equation, the power flux  $q$  incident on the anode is evaluated as

$$q = \frac{fp}{\pi r_a^2(t_{on})} \quad (2.4)$$

where  $p$  is the pulse power,  $f$  is fraction of the pulse power expended at the anode, and  $r_a$  is the radius of the circular spark channel assumed to follow the relationship  $r_a(t_{on}) = 0.8 t_{on}^{3/4} \mu\text{m}$ ,  $t_{on}$  being the pulse on-time,  $k$  denotes the thermal conductivity of the work material, and  $\alpha$  the thermal diffusivity,  $\phi$  represents the integral complementary error function

The variation of the thermophysical properties of the work material over the temperature range from ambient to melting is accounted for by employing average values. The material constants used for computation are  $k = 25 \text{ W/mK}$  and  $\alpha = 6.83 \times 10^{-6} \text{ m}^2/\text{s}$ . The heat of fusion is neglected as it incurs a maximum error of just about 2%. The fraction of the pulse power incident on the work is assumed to be 8% [31].

The model is simulated to study the effect of pulse power and the depth of cut on  $F_n^p/F_n$ . The results are depicted in Figure 2.5.  $F_n^p/F_n$  decreases with increasing pulse power at a rate depending on  $d$ . Despite the simplifying assumptions adopted in the model, the simulation results will be seen to qualitatively agree with those of experiments, discussed later (Figure 2.11).

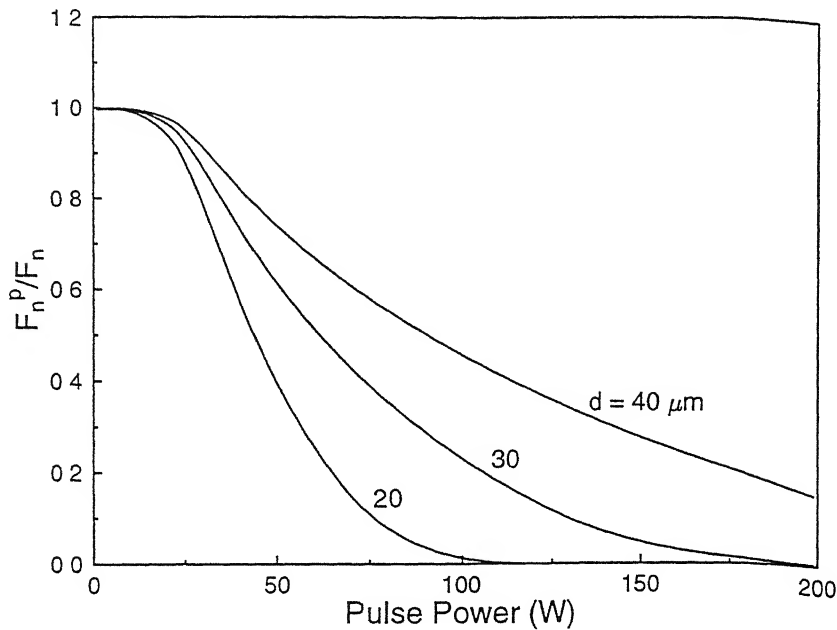


Figure 2.5 The effect of pulse power on  $F_n^p/F_n$  at different depths-of-cut — simulation results ( $r=80 \mu m$ , discharge voltage 40 V, pulse on-time 100  $\mu s$ , HSS workpiece)

## 2.2.2 Results and Discussion

### Material Removal Rate

In EDDG only those abrasive grains with protrusion height more than the interelectrode gap-width physically interact with the work. Such an abrasive, in order to remove material has to satisfy the following conditions (i) the uncut chip-thickness has to be greater than the critical depth of penetration, which is linearly dependent on the grain-tip radius, and (ii) the rake angle of the grain needs to be less negative than the critical rake angle at which chip formation ceases. Thus in practice, only a fraction of the number of abrasive grains interacting with the work will indeed be removing material. The current and wheel speed are seen to influence these two aspects and thus have an effect on the MRR in EDDG.

Figure 2.6 exhibits the role of wheel speed on MRR at different current while grinding HSS. At a current of 0 and 1 A the MRR initially increases

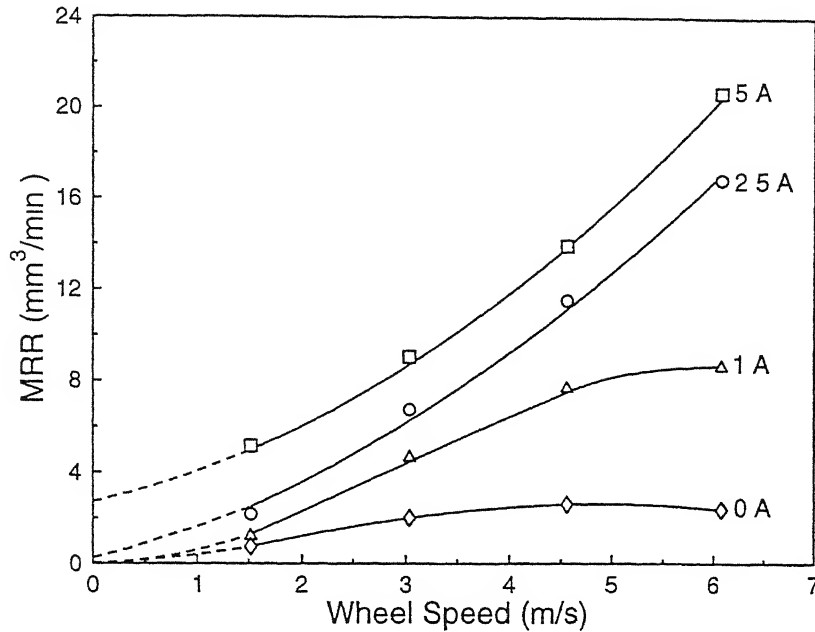


Figure 2.6 The effect of wheel speed on MRR at different current while grinding HSS

with wheel speed but tends to decrease at the higher end of the wheel speed. The trend exhibited by the MRR-wheel speed characteristics at 2.5 and 5 A, however, is different in that the MRR increases monotonically with wheel speed. The flow of current through the grinding zone by way of spark discharges is seen to beneficially increase the MRR at all wheel speeds tested.

The decline in the material removal capability of the wheel at 0 and 1 A current at the higher end of wheel speed is evidently due to blunting of the abrasives. While grinding steel, diamond abrasive grains have been known to wear rapidly owing to graphitization of diamond, with iron acting as a catalyst [32–34]. The rate of the reaction depends on the temperature at the grain-work interface which is dependent on the wheel speed. The implications of wear-flat formation on an abrasive grain with regard to its ability to remove material are twofold: the grain-tip radius and hence the critical depth of penetration is increased, while the uncut chip-thickness is itself decreased. Hence, with the formation of wear-flats, a number of grains which hitherto have been actively involved in material removal, tend to just plough and displace but not remove material. This reduces the MRR.

To understand the mechanism of improved grinding with the flow of current in the grinding zone, it is essential to examine the magnitude and mode of wheel wear in EDDG. The average radial wheel wear rate as a function of current is shown in Figure 2.7. The wheel wear rate is seen to increase with increasing current. This implies that the continuous renewal of the wheel surface due to in-process dressing counteracts grain blunting and this enhances the grinding performance.

Grain fracture is another plausible mechanism of wheel wear in EDDG. Particle size analysis of swarf collected while EDM-truing cubic boron nitride wheels presents evidence in support of this phenomenon [35]. The spark discharges have been observed to alter the size distribution of abrasives from normal to log-normal, with the grain size shifting toward smaller values (Figure 2.8). Particles with log-normal distribution of size are known to evolve due to impulsive forces [36] which suggests thermally originated fracture of the abrasives. Rapid thermal excursion of sintered diamond compacts has also been found to induce cracks in diamond grains by a chemically

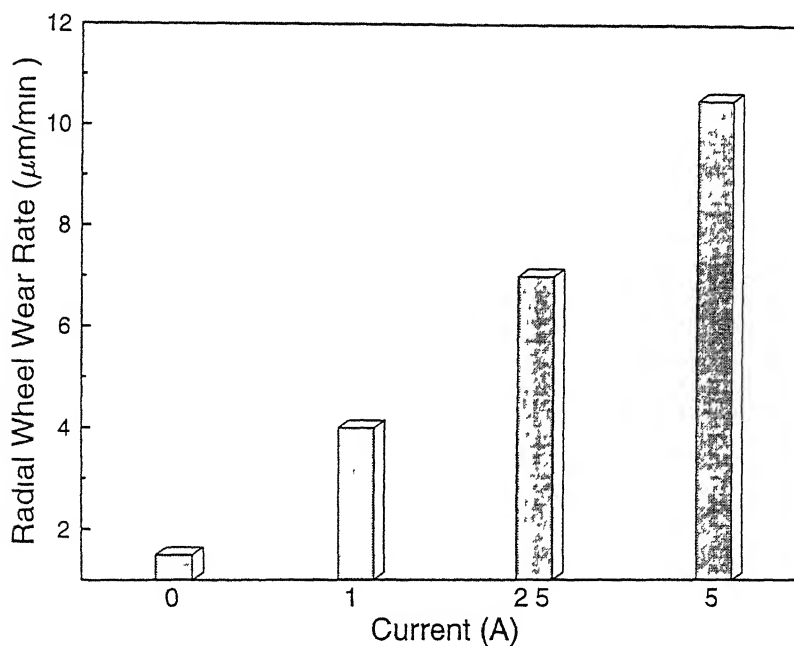


Figure 2.7 The effect of current on the average radial wheel wear rate while grinding HSS (wheel speed 4.5 m/s)

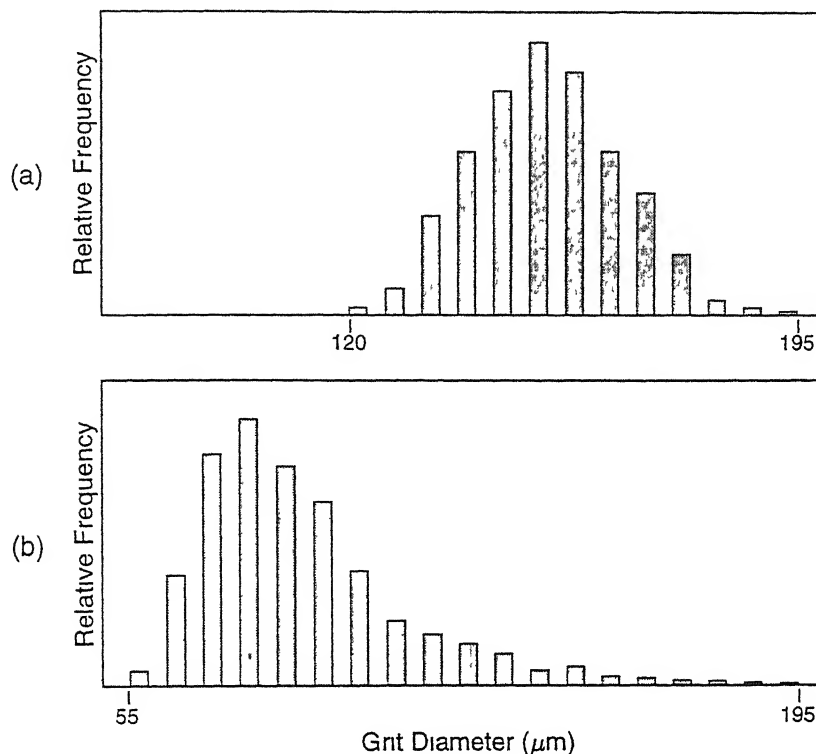


Figure 2.8 The size distribution of cubic boron nitride particles of 120 mesh size (a) before EDM-truing (b) after EDM-truing [35]

activated mechanism [37]. The micro-fracture of abrasive grains augments grinding performance as sharp and angular abrasives are more effective than their blunt counterparts in removing material [38]. Grain fracture can be expected to be the dominant wheel wear mechanism at low current.

The critical rake angle is primarily dependent on the coefficient of friction between the contacting surfaces. An increase in the temperature of the workpiece has been observed to shift the critical rake angle towards more negative values in slow-speed abrasion experiments on steel [39]. This is an important factor considered to improve the MRR in EDDG with the work under the thermal influence of the electrical sparks. Especially so, since in grinding the abrasive grains pose highly negative rake angles to the work.

The degree of interaction between the wheel and the work, and hence the MRR in the configuration of EDDG adopted in the present work, depends

on the dynamics of the gap-width. With increasing wheel speed, the reduced contamination at the gap results in decreasing gap-width which would increase the undeformed chip-thickness (see Figure 2.3). Provided the wheel is sharp, this has the effect of non-linearly increasing the MRR with respect to wheel speed as seen for 2.5 and 5 A current in Figure 2.6. Since the 2.5 and 5 A characteristics are almost parallel to each other, it seems that a maximum current of 2.5 A is sufficient to maintain the cutting ability of the wheel in the range of wheel speeds investigated.

Examination of the grinding detritus is one of the diverse approaches helpful in understanding the mechanism of abrasive-work interaction. Scanning electron micrographs of chips obtained in EDDG at a current of 1 A and 5 A are shown in Figure 2.9. The chips obtained at a current of 1 A can be seen to have a lamellar structure pointing to chip-formation mechanism. The presence of spherical particles is conspicuous in chips collected at a current of 5 A. These spherical particles are due to material removed by EDM and should not be confused with those reportedly obtained in ordinary grinding, that are formed by oxidation of the chips on leaving the grinding zone. Such a mechanism is absent in EDDG as the grinding zone is completely immersed in a hydrocarbon dielectric. This indicates that, in EDDG, depending on the current, a part of the material is removed by EDM. The non-spherical particles found at 5 A current do not have a chip-like shape and appear to be segments of highly distorted material, characteristic of debris formed by abrasive grains with rake angle more negative than  $-45$  degrees [40].

The extrapolation of the curves in Figure 2.6 to zero wheel speed is for separating the component of the MRR due to EDM alone, and is explained later.

### Normal Force

The normal force component in grinding, although not of concern with regard to the power consumed, is important with regard to machining accuracy considerations.

Figure 2.10 depicts the trend of the evolution of the normal grinding force  $F_n$  for various current, normalized with respect to the initial values. It can

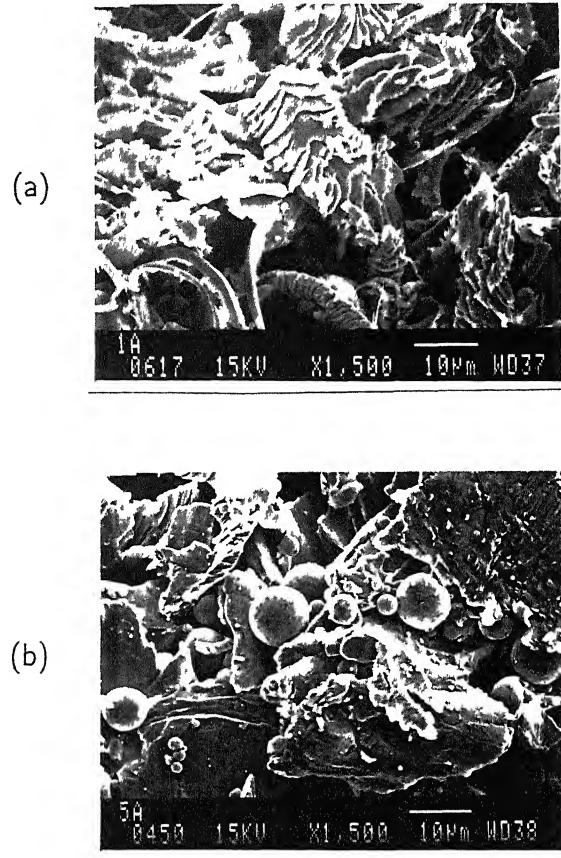


Figure 2.9 Micrographs of chips collected at a current of (a) 1A and (b) 5A while grinding HSS (wheel speed 4.5 m/s)

be seen that the normal force increases with time before attaining steady state at currents of 0 and 1 A. At higher currents (2.5 and 5 A) the increase in force is only marginal since the spark discharges preclude the formation of wear-flats on the abrasives.

Figure 2.11 illustrates the variation of the stabilized normal force with current at various wheel speeds. The normal force decreases with increasing current for all wheel speeds. It is also seen that for a particular current, the normal force is higher for a larger wheel speed.

Scanning electron micrographs of ground surfaces obtained at different

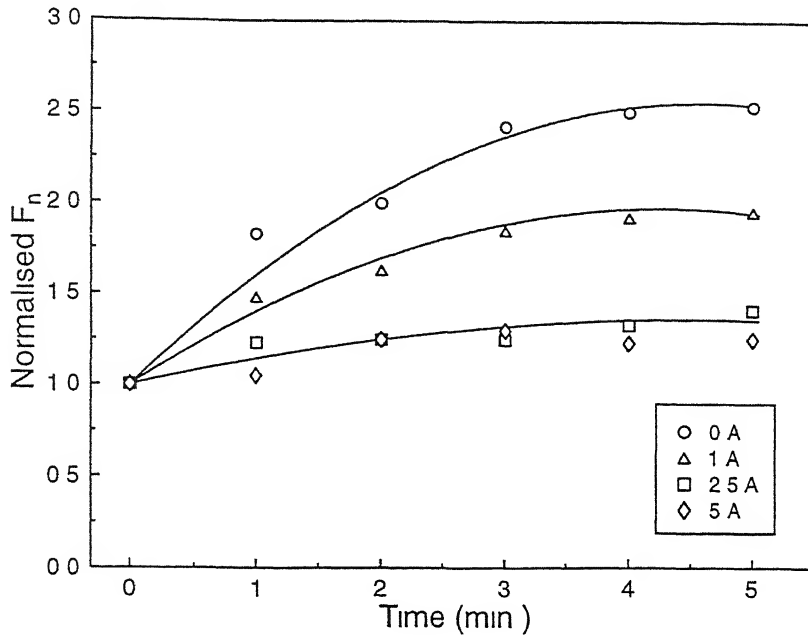


Figure 2.10 The effect of current on the evolution of normal force while grinding HSS (wheel speed 4.5 m/s)

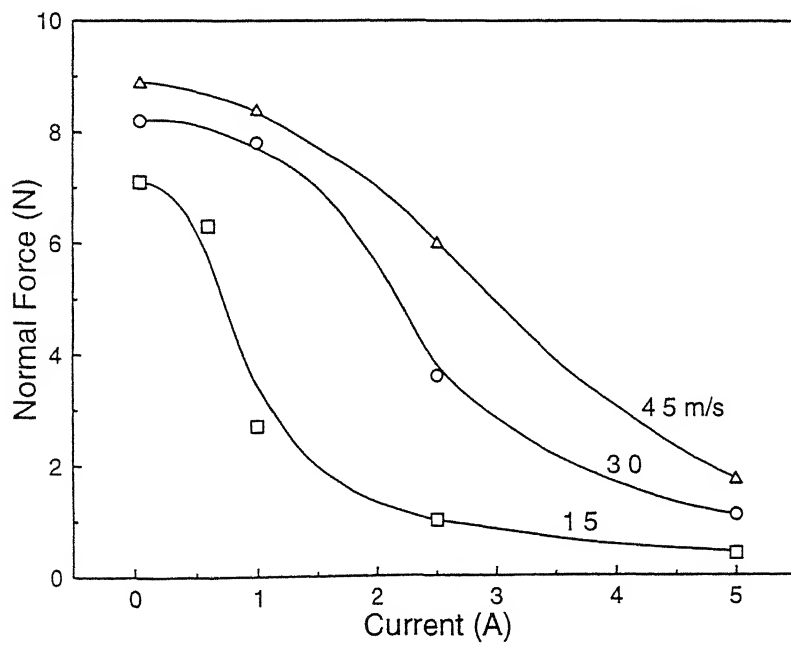


Figure 2.11 The effect of current on the normal force at different wheel speeds while grinding HSS



current and wheel speed clarify their effect on the normal force. Micrographs in Figure 2.12 reveal the role of current. At zero current condition, grooves formed by the abrasive grains are visible (Figure 2.12a). The black spots found are presumably graphite particles detached from the diamond grains and deposited on the machined surface. Incipient melting of the surface is evident at a current of 1 A (Figure 2.12b). The extent of melting is seen to increase with current as indicated by the micrograph corresponding to 5 A current (Figure 2.12c). Higher current causes more thermal softening which results in decreasing normal force (Figure 2.11).

The increase in normal force with wheel speed at a current of 0 A is due to the increase in the rate of formation of wear-flats on the abrasives with an increase in the wheel speed. This is on account of the rate of graphitization of diamond abrasives being dependent on the temperature at the grain-work interface, which in turn is a function of wheel speed. With a current flowing through the gap, the blunting of grains is however not prevalent, but other factors come into picture as discussed below.

Figure 2.13 shows micrographs of surfaces machined at a current of 2.5 A for two wheel speeds. The micrographs denote that there is a transition in the mechanism of material removal from predominantly EDM to grinding, as the wheel speed increases. Possible reasons for the increase in normal force with wheel speed at a particular current are as follows: (i) With an increase in wheel speed, as the number of abrasive-workpiece interactions per unit time increases, the number of spark discharges available per active grain decreases. This would lead to a higher normal force. (ii) The presence of solid, conducting impurities suspended in the dielectric fluid influences the discharge phenomenon in EDM [41]. A certain amount of contamination at the interelectrode gap is essential for the discharges to materialize. At high wheel speeds, the effectiveness of discharges decreases due to discharge instability owing to swift removal of debris from the gap. With an increase in wheel speed, the energy transferred to the workpiece and hence the extent of thermal softening decreases which would contribute to an increase in the normal force. (iii) A change in the gap-width would also influence the normal force. At a particular current, an increase in wheel speed reduces the gap-

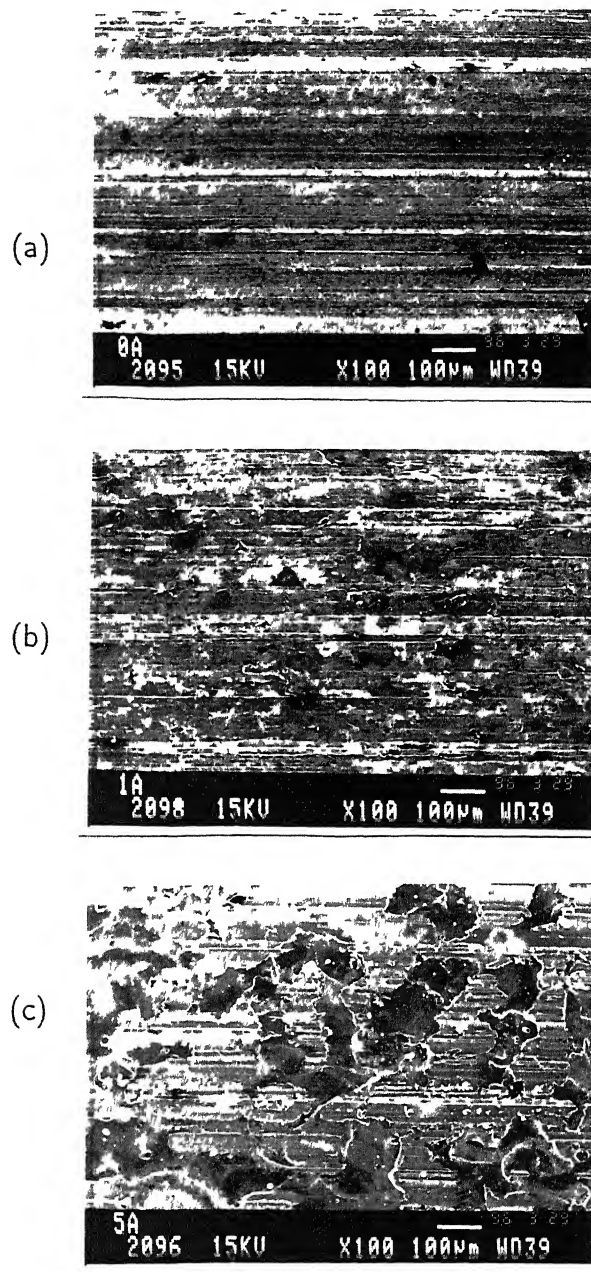


Figure 2 12 Micrographs of HSS work-surfaces ground at a current of (a) 0 A (b) 1 A (c) 5 A (wheel speed 4 5 m/s)

width This results in more interference between the wheel and the work, and hence a higher normal force (The effect of wheel clogging, if any, on the other hand, will be to counteract this by receding the wheel away from the

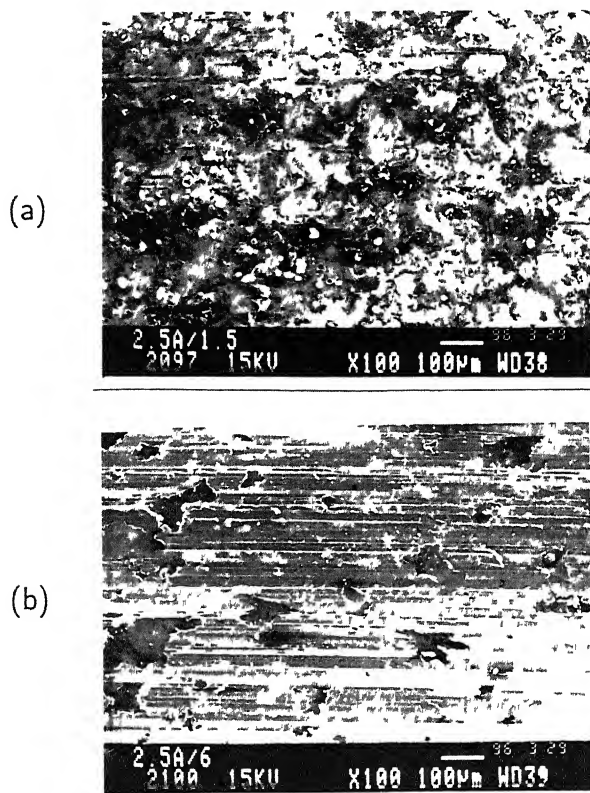


Figure 2.13 Micrographs of HSS work-surfaces ground at a wheel speed of (a) 1.5 m/s (b) 6 m/s (current 2.5 A)

work to maintain the gap-width )

### Tangential Force

The effect of current on the tangential force at different wheel speeds while grinding HSS is presented in Figure 2.14. At zero current, the tangential force decreases with wheel speed, the trend of which reverses with a current flowing through the gap. The characteristics also exhibit distinct maxima with respect to current for each wheel speed. The maximum shifts toward higher values of current with increasing wheel speed.

The resistance to the lateral motion of an abrasive grain comprises (1) the

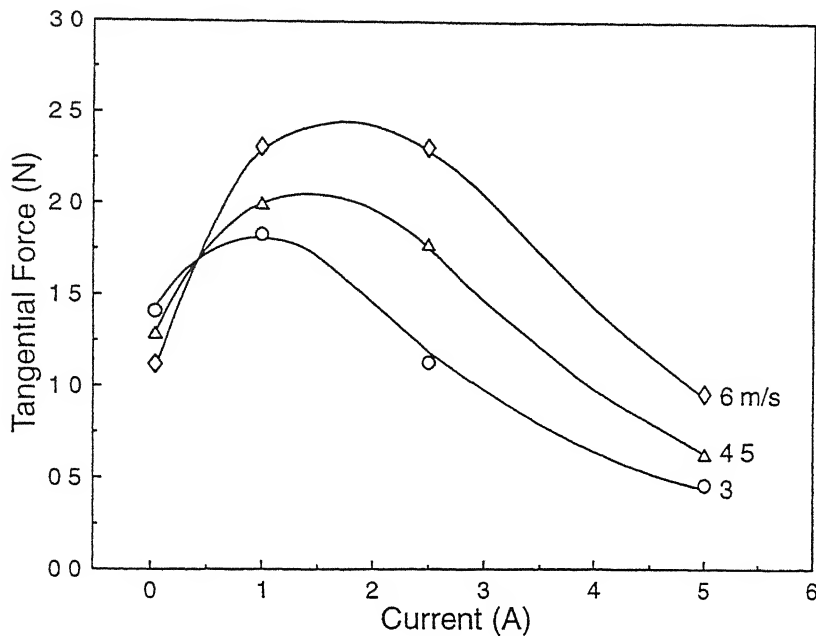


Figure 2.14 The effect of current on the tangential force at different wheel speeds while grinding HSS

force required to shear the junctions formed between the work and the grain, and (ii) the force needed to displace the material ahead of the grain. These force components are influenced by the bulk physical properties of the work material.

The formation of adhesion junctions between the work and the grain at points of contact is deemed to arise out of a cold-welding process [42]. The force required to shear the junction thus formed, as the grain moves, is dependent on the shear strength and the area of the junction. The temperature of the contact interface plays a significant role in facilitating the flow and welding of the adhesion junctions between the abrasives and the work. This explains the dependence of the tangential force on current in EDDG.

The role of temperature on the shear strength of adhesion junctions formed between surfaces in contact is reported in reference [43]. Strong adhesion force is found to initiate at a temperature about half the melting temperature of the softer metal. Above this temperature, the adhesion force increases markedly to reach a maximum and decreases thereafter. The in-

crease in adhesion force with temperature is attributed to junction growth, the rate of which is largely temperature dependent. At the temperature corresponding to the maximum adhesion force, the real area of contact approaches the apparent area. Once the maximum area of contact is attained, a further increase in temperature results in decreasing shearing forces due to work material softening. This interprets the maxima that occur in the tangential force-current characteristics. The maxima shift toward higher current with increasing wheel speed as a higher current is required to offset the decrease in the pulse energy expended on the work, with an increase in wheel speed.

The decrease in the tangential force with increasing wheel speed, at a constant depth of cut, in conventional diamond grinding (0 A current) of steel has been reported in reference [29] too, this has been ascribed to a fundamental change in the material deformation mechanism, as indicated by the morphology of the chip-forms. Softening of the work in the primary shear deformation zone due to plastic deformation-induced heating is a possible reason for the decrease in the tangential force with increasing wheel speed. With the flow of current through the interelectrode gap, the tangential force increases with wheel speed for a particular current due to the combined effect of increasing wheel-work interference, and reduced thermal softening associated with increasing wheel speed.

### Specific Grinding Energy

Specific grinding energy is the energy expended in grinding a unit volume of a material. Consideration of the magnitude of specific grinding energy and its dependence on the operating conditions provides vital clues to figuring out the mechanism of abrasive-work interaction. Typical values of specific grinding energy for steels are much higher than the melting energy per unit volume. This is due to large negative rake angles of the abrasive grains which is a severe constraint to material removal [44].

In this sub-section, the dependence of specific grinding energy in EDDG on the wheel speed and current is studied. To evaluate the specific grinding energy in EDDG, the component of MRR due to grinding alone has to be

separated from the total MRR

Referring to Figure 2.6, extrapolation of the 0 A characteristic to zero wheel speed corresponds to zero MRR. This is understandable as no material removal is possible with the wheel remaining stationary under pure grinding conditions. The same is observed for 1 A too. The absence of spherical particles among chips collected at 1 A current (Figure 2.9a) also suggests that no appreciable amount of material is removed by EDM at that current. Extrapolating 2.5 and 5 A curves, however, appear to yield positive intercepts on the MRR axis. The magnitude of these intercepts ought to be the MRR due to EDM at the respective currents, averaged over the wheel speeds investigated. To corroborate the methodology given above, the MRR is plotted against the corresponding normal force for these currents in Figure 2.15. The relationship is found to be linear. As EDM is devoid of any machining force, extrapolation of these lines to zero normal force can be expected to give the MRR due to EDM. The results of these two exercises are found to agree within 15%. The average of these values gives an indication of the MRR due to EDM. The MRR due to grinding ( $MRR_g$ ) is now obtained

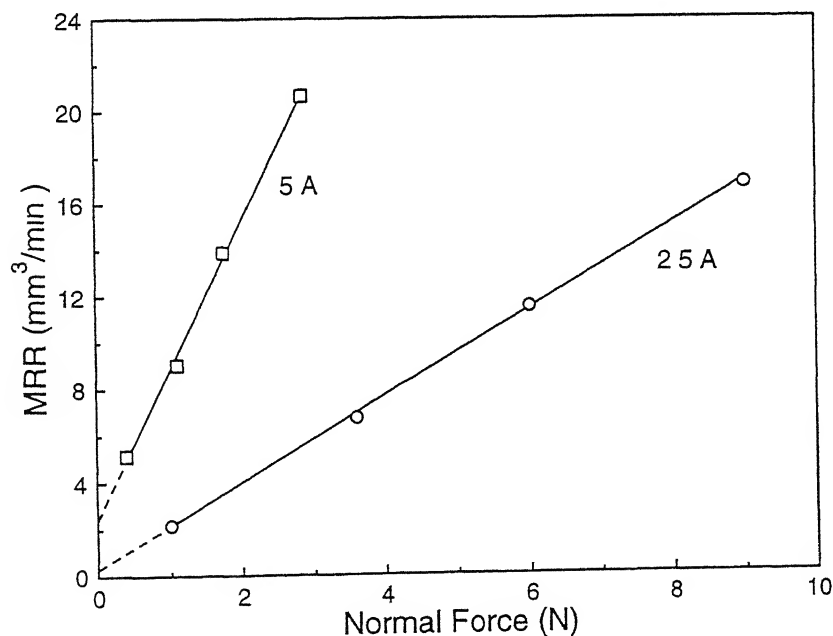


Figure 2.15 MRR vs normal force at 2.5 and 5 A current while grinding HSS

by subtracting the component of MRR due to EDM from the total MRR

The specific grinding energy  $u$  is evaluated as

$$u = \frac{F_t v}{\text{MRR}_g} \quad (2.5)$$

where  $F_t$  is the tangential force and  $v$  is the wheel speed. Figure 2.16 depicts the variation of specific grinding energy with current for various wheel speeds. For all wheel speeds investigated, the specific grinding energy decreases exponentially with current. This confirms the efficacy of the mode of material removal in EDDG, and thermal softening of the work as discussed in the foregoing. It is interesting to note that the specific grinding energy at the higher end of current tends toward the melting energy per unit volume ( $10.5 \text{ J/mm}^3$ ) of steels [44]. For a given current, an increase in wheel speed corresponds to a higher specific grinding energy. This corroborates the premise that the extent of thermal softening decreases with increasing wheel speed.

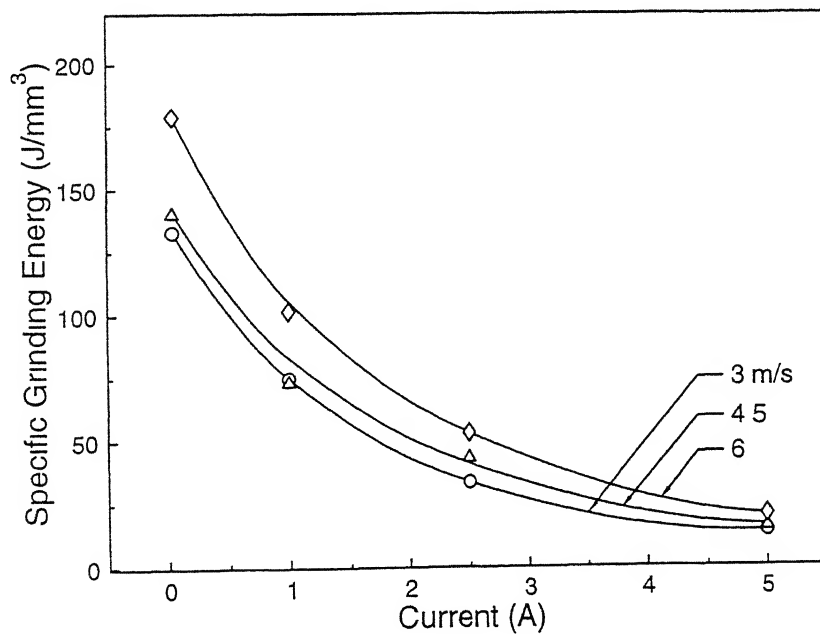


Figure 2.16 The effect of current on the specific grinding energy at different wheel speeds while grinding HSS

## 2.3 Material Removal Mechanism — Cemented Carbide

Cemented carbides constitute an important class of materials, the applications of which, especially in the metal cutting industry cannot be overemphasized. Inevitable shrinkage of these materials on sintering, among other factors, often necessitates subsequent machining to impart the specified dimensions and form to the end-product. Owing to high material hardness, machining is generally performed with diamond grinding wheels. EDM is also widely practiced.

To prepare the ground for the study of EDDG of cemented carbides, the available published literature emphasizing the mechanism of material removal, on grinding and EDM of the same, is reviewed in the following.

In view of their technological significance, attempts to elicit the mechanism of wear of cemented carbides have been many. Our interest, however, with reference to the present work, will be confined to wear due to hard abrasives. While diamond and silicon carbide abrasives cut cemented carbides effectively, alumina which has a hardness only of the order of that of WC has been found [45] to be able to only partially penetrate or abrade them.

Reference [46] reports the simulation of abrasive wear of WC-Co by sliding a loaded, conical diamond indenter. The indenter was observed to generate permanent grooves on the specimen surface on application of a load exceeding a certain threshold. The mechanism of groove formation was primarily plastic deformation, accompanied by microfracture of the binder and carbide phases, especially at high loads. With these mechanisms operative, the wear volume was found to have a good correlation with the product of hardness and fracture toughness of the specimen. Under repeated scratching conditions, the mechanism of wear was found to be gradual extrusion of the binder which weakens the groove surface thereby making it susceptible to removal during the subsequent passes of the indenter.

Examination of diamond ground WC-Co surfaces in a scanning electron microscope [47] has revealed the presence of grooves along the grinding di-



rection. X-ray microanalysis indicated the grooves to be devoid of cobalt, in contrast to the ridges which were rich in them, understandably due to binder extrusion mechanism. The chips collected during grinding cemented carbide were found to be similar to flow-type chips obtained while grinding metals. The appearance of distinct shear front lamellae on the WC grains, confirmed plastic flow which precedes and accompanies crack propagation through the carbide phase.

The detritus collected during wire EDM of WC-Co, on observation in a scanning electron microscope has been found [48] to be composed of spherical cobalt particles — some of which were hollow, and WC particles, irregular in shape as in the composite. This indicates that the temperature to which the WC-Co surface is exposed to during EDM, is high enough to melt/evaporate the metallic binder which is the lower-melting constituent. Due to the higher electrical conductivity of Co as compared to WC, the spark discharges can be expected to be by and large localized on the Co matrix. The WC network is therefore debilitated due to selective loss of binder by spark erosion. Individual WC grains are eventually dislodged, presumably by shock waves arising out of the abrupt collapse of the plasma bubble during the off-time of the pulse.

The work reported in this thesis is concerned with the effect of introduction of electrical discharges at the wheel-work interface, while grinding WC-TiC-(TaNb)C-Co cemented carbide. The role of current, pulse on-time and duty factor on the MRR and grinding forces is studied to comprehend the mechanism of material removal. Specifications of the cemented carbide used in the work and the experimental parameters employed are presented in Table 2.3. The next two subsections dwell on the experimental results and discussion.

### 2.3.1 Results

Figure 2.17 depicts the effect of current flowing through the wheel-work interface on MRR at different pulse on-time. The data-point corresponding to 0 A current pertains to grinding with no electrical discharge effect. Ex-

**Work Material**

Cemented carbide (86%WC, 2.5%TiC, 6%(TaNb)C, 5.5%Co)

Grain size 2-3  $\mu\text{m}$

Width 5.6 mm

**EDDG Pulse Parameters**

Voltage 40 V

Duty factor 0.5

Wheel speed 4.5 m/s

Table 2.3 Work material specifications (cemented carbide) and the relevant EDDG pulse parameters

periments repeated at this condition indicated that the scatter of the results was less than 5% of the mean value. The characteristics exhibit maxima at a current of about 0.5 A. The maximum MRR with respect to current

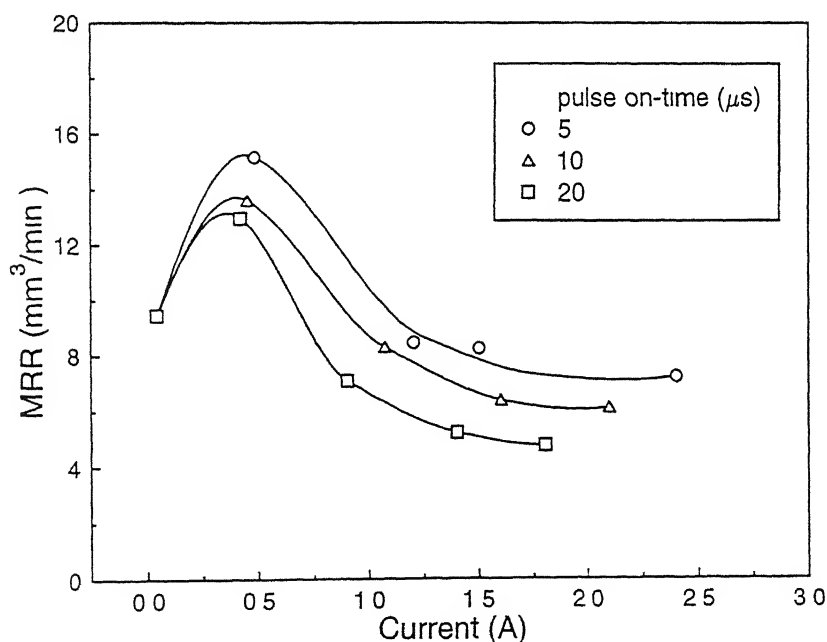


Figure 2.17 The effect of current on the MRR at different pulse on-time while grinding cemented carbide

is distinct for each pulse on-time, with shorter pulse on-time yielding higher MRR. For a given pulse on-time, the MRR on reaching a maximum, decreases thereafter with a further increase in current. It is seen that in the range of current investigated MRR increases with a decrease in pulse on-time, for a particular current. The material removal rates are much higher than that obtained while electrical discharge machining cemented carbides, a representative value of which is around  $0.4 \text{ mm}^3 \text{min}^{-1} \text{A}^{-1}$  [49]. The effect of duty factor of the discharges on the MRR, as a function of pulse current is shown in Figure 2.18 which indicates that the MRR increases with a decrease in duty factor, in the range of pulse current investigated. (Note that the graphs corresponding to duty factor as one of the variables [Figures 2.18 and 2.23] have been plotted with reference to pulse current rather than the average current as in the other figures, since the average current tends to decrease with a decrease in duty factor, for the same pulse current setting.)

The time evolution of grinding forces during EDDG of cemented carbide is dependent on current. Typical variation of the normal grinding force with

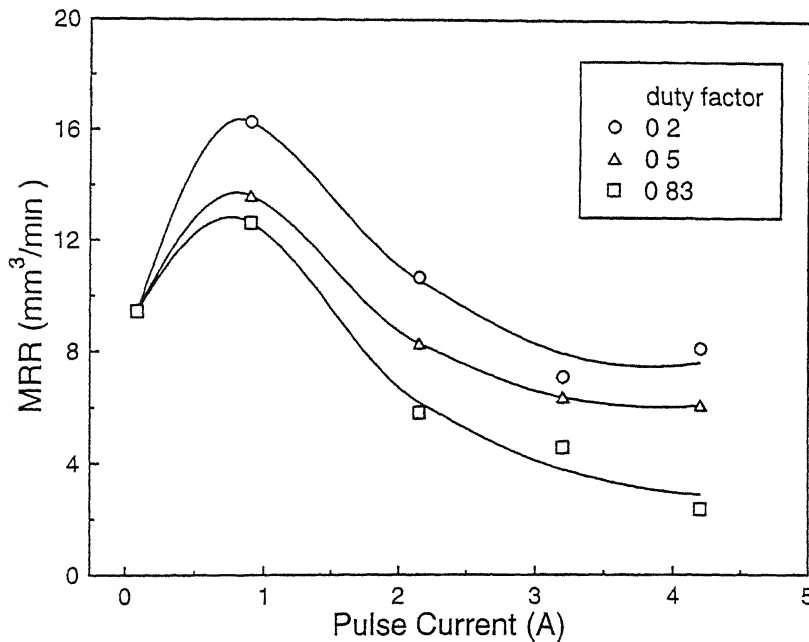


Figure 2.18 The effect of pulse current on the MRR at different duty factor while grinding cemented carbide ( $10 \mu\text{s}$  pulse on-time)

time, for different current, normalized with respect to their initial values is shown in Figure 2.19. At low current (0.4 A), the normal force undergoes a uniform increase with time before stabilizing at an equilibrium value as in conventional grinding operations, at an intermediate current (0.9 A) the force remains more or less stationary, and at a higher current (1.4 A) the normal force initially decreases with time and eventually attains steady state. The tangential force follows a similar trend as the normal force.

The trend of the variation of the stabilized normal force, as far as the initial increase with respect to current at different pulse on-time (Figure 2.20) is concerned, is seen to be similar to that of MRR (Figure 2.17). At the higher end of current, the normal force appears to become independent of pulse on-time. The force ratio ( $F_t/F_n$ ) is independent of current and pulse on-time (Figure 2.21), and is numerically consistent with the value quoted elsewhere [26] for diamond-carbide combination.

The role of electrical spark discharges in enhancing the grinding performance while machining cemented carbide is appraised in terms of a material

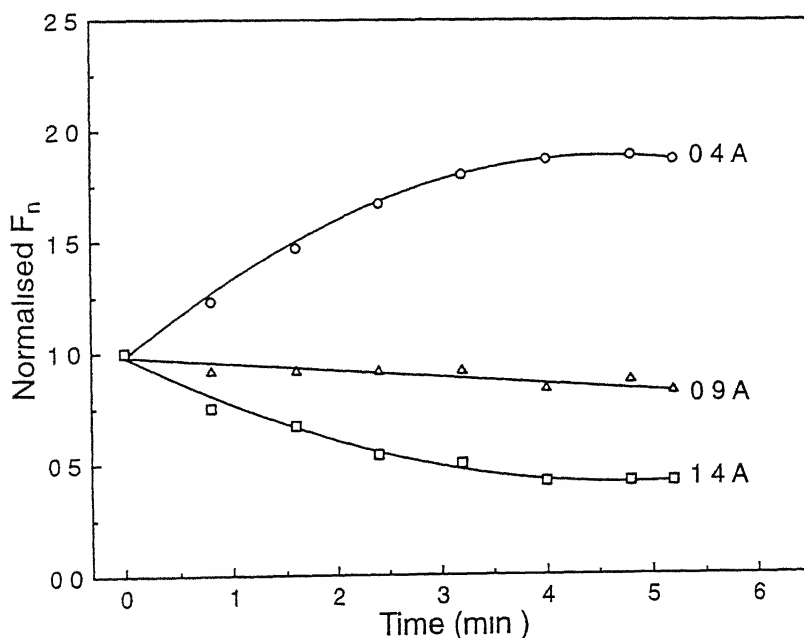


Figure 2.19 Time evolution of normal force while grinding cemented carbide at different current ( $20 \mu\text{s}$  pulse on-time)

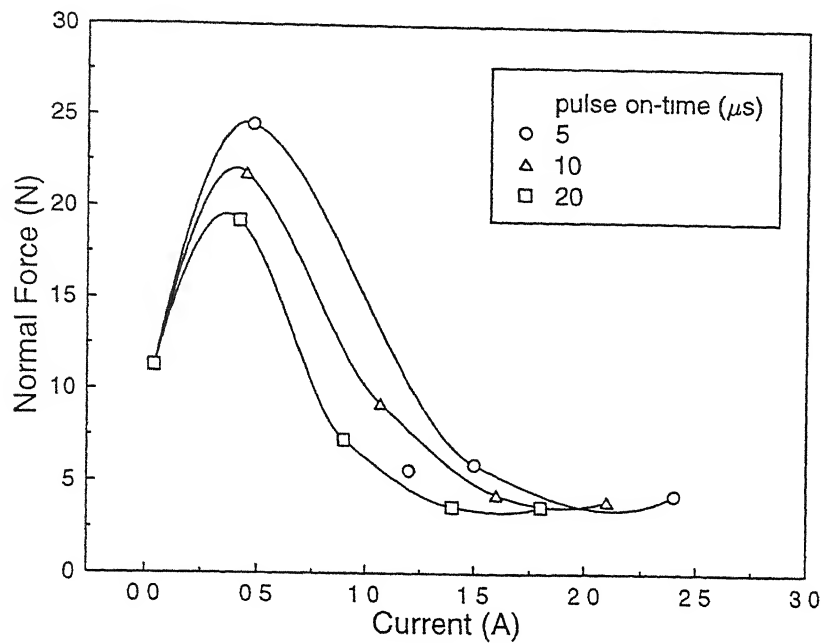


Figure 2 20 The effect of current on the normal force at different pulse on-time while grinding cemented carbide

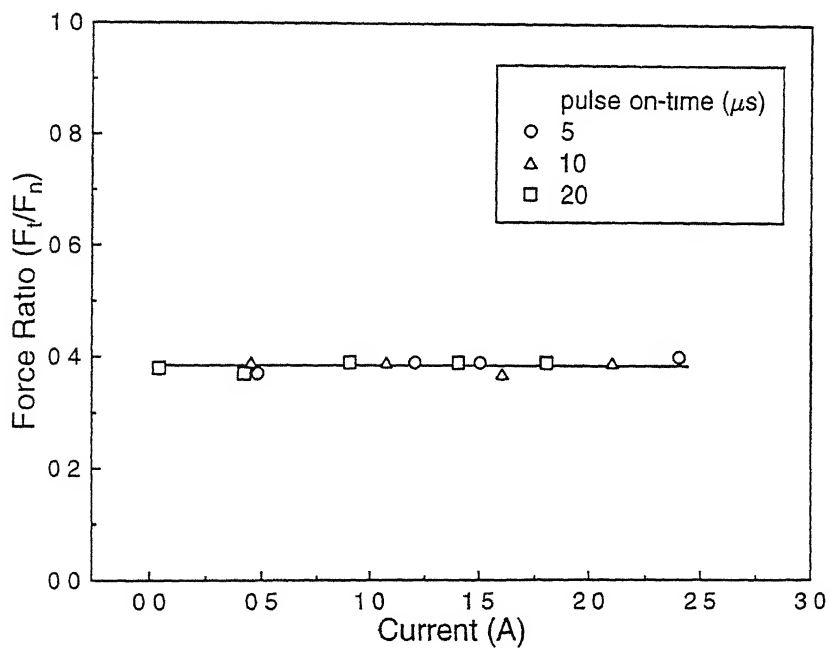


Figure 2 21 Force ratio  $F_t/F_n$  vs current at different pulse on-time while grinding cemented carbide

removal parameter ( $\Lambda_w$ ) defined as the volume of material removed in unit time per unit normal force.  $\Lambda_w$  is a measure of the resistance of the work material to wear. The variation of  $\Lambda_w$  with current at different pulse on-time is illustrated in Figure 2.22.  $\Lambda_w$  initially decreases with an increase in current, is minimum at a current of about 0.5 A and thereafter increases with current, for all pulse on-time investigated. Pulse on-time does not appear to have any influence on  $\Lambda_w$ . Figure 2.23 depicts the effect of duty factor on  $\Lambda_w$  at various pulse current. While duty factors of 0.5 and 0.83 exhibit similar characteristics, a duty factor of 0.2 seems to have no effect on  $\Lambda_w$  in the range of pulse current investigated.

### 2.3.2 Discussion

Grinding is a complex, dynamic process. To comprehend the nature of the characteristics discussed in the foregoing section, it is essential to develop a systems approach to the abrasive wear of cemented carbides from the point of view of both the wheel and the work, and thereafter analyze the outcome

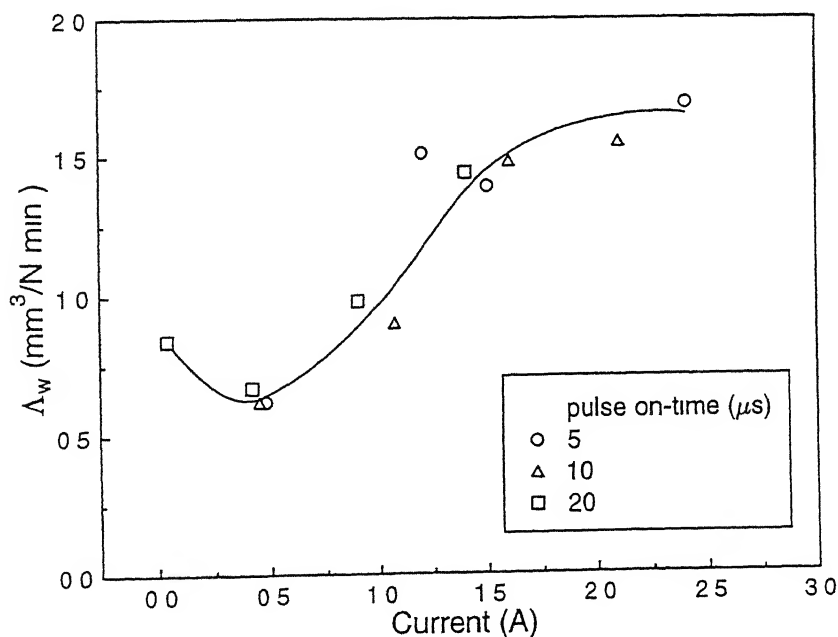


Figure 2.22 The variation of the material removal parameter  $\Lambda_w$  with current at different pulse on-time while grinding cemented carbide

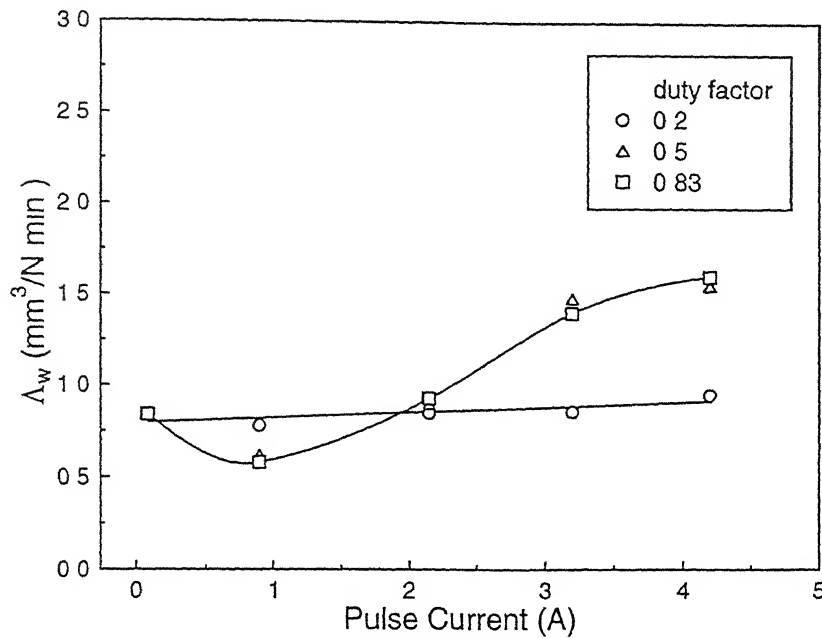


Figure 2.23 The effect of pulse current on the material removal parameter  $\Delta_w$  at different duty factors while grinding cemented carbide ( $10 \mu\text{s}$  pulse on-time)

of the inclusion of electrical discharges in the grinding zone, on the system response

Cemented carbides, on account of their possessing the unique combination of high hardness and significant toughness, represent a grey zone between metals and ceramics with reference to their response to abrasion. In case of ductile metals, wear during abrasion is predominantly due to plastic deformation, with the generation of grooves and eventual detachment of wear debris in the form of chips. For brittle solids, in contrast, provided the depth of indentation of the sliding abrasive is more than the critical value, the tensile stress associated with sliding initiates the propagation of median and lateral cracks, emanating from the plastic zone induced beneath the indenter. Material is removed by way of fracture when the lateral cracks reach the free surface or link amongst themselves to form loose fragments. The rate of material removal associated with fracture mechanism is of an order of magnitude higher than that of plastic deformation, since the volume removed by crack propagation is large compared to the groove dimensions [50].

The fracture of cemented carbide during indentation is discussed in reference [51]. It has been observed that in cemented carbides, the cracks remain within the plastic zone of indentation unlike in brittle solids, where they penetrate the surrounding elastic region. Since abrasion of cemented carbide entails both plastic deformation and brittle microcracking mechanisms, the relative extent of these mechanisms will govern the rate of material removal.

The progressive loss of the cutting ability of a diamond wheel while grinding hard materials is generally due to one, or a combination of the following phenomena: (i) attritious wear of grits resulting in the formation of wear-flats, (ii) wheel loading and (iii) pull-out of abrasives. However, during diamond grinding of cemented carbide, fine microfracture of the abrasive grains, to a large extent reduces wear-flat formation [52], and wheel loading is the major problem [53]. Wheel loading refers to the adhesion of grinding debris on the active grains and the wheel bond. This leads to increased friction and is a dominant factor in determining the frequency of dressing in grinding operations. A study on the loading of grinding wheels [54] indicates that the rate of loading is high at the outset, and tends to saturate as grinding proceeds. Pull-out of grains is not quite common in fine grinding, but is so during EDDG of cemented carbides, and will be discussed later.

The behavior exhibited by the MRR and normal force characteristics with regard to current and pulse on-time (Figures 2 17 and 2 20) can now be rationalized in the framework of the concepts reviewed above.

Since the current at which the maximum MRR occurs (Figure 2 17) corresponds to the minimum  $\Lambda_w$  (Figure 2 22), it is conclusive that the increase in MRR on introducing electrical discharges in the grinding zone is not because of removal of material being made any easier. The possibility of an increase in normal force (Figure 2 20) due to grit-blunting is ruled out, as it would have showed up as a decrease in the force ratio, which is not the case (Figure 2 21). Moreover, during preliminary experimentation, it was observed that the rise in normal force was reversible — the force reverted back, on switching off the current — which endorses the view that the abrasive grains do not undergo any significant blunting. It is apparent that the increase in MRR and normal force is due to declogging of the wheel by electrical discharges. The effect is



schematically illustrated in Figure 2 24 Under pure grinding condition (0 A

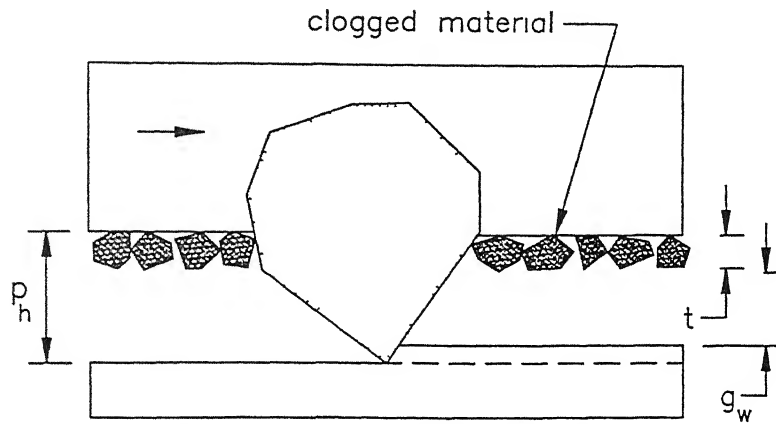


Figure 2 24 Illustration of the effect of clogging of the wheel

current), there is adherence of work material chips on the abrasive grains and the bond (Figure 2 25) For a thickness  $t$  of electrically conducting adherent layer (refer Figure 2 24), the undeformed chip-thickness for an active grain of protrusion height  $p_h$  will be  $p_h - (g_w + t)$  With the introduction of electrical



Figure 2 25 Micrograph indicating wheel loading

discharges in the interface, declogging of the wheel occurs whereby  $t \rightarrow 0$  and the undeformed chip-thickness increases to  $(p_h - g_w)$ . In this process of the wheel moving towards the work, many grains which hitherto have not been interacting with the work become active. The increase in the effective mechanical interference between the wheel and the work results in a higher MRR and concomitant higher normal force. It is also likely that the uncut chip-thickness due to some abrasives would graduate to the microcracking regime from that of plastic deformation, thus enhancing material removal.

For a particular pulse on-time, the decrease in MRR and normal force with current, after attaining a maximum (Figures 2 17 and 2 20) is due to a multiplicity of factors. (i) With increasing current, thermal softening of the work occurs as implied by the increase in  $\Lambda_w$  (Figure 2 22). With the decrease in the hardness of the work, plastic deformation would dominate over microcracking, and will be the rate-controlling mechanism. This decreases the MRR. (ii) The time evolution of normal force (Figure 2 19) shows that at higher current, the normal force initially decreases with time before attaining steady state. This is an indication of pull-out of abrasives from the bond. At higher current, the abrasive grains held mechanically in the bond are dislodged rather easily on application of a tangential grinding load, due to thermal softening of the bond material. This decreases the contribution of grinding towards material removal which results in the diminution of the MRR. (iii) The increase in gap-width with an increase in current [41] also contributes to some extent in decreasing the abrasive-work interaction.

The notions stated above are clearly brought out in the micrographs of surfaces machined at different current. The micrographs of the surface generated under pure grinding condition (Figure 2 26a) clearly indicates that material removal takes place by a combination of microcracking and plastic deformation. At a current of 0 4 A (Figure 2 26b), microcracking is predominant. With the current increased to 2 1 A (Figure 2 26c), the role of grinding in removing material appears to be on a decrease, the grooves generated by the sliding abrasives evident at currents of 0 and 0 4 A are fairly reduced in number as the current is increased to 2 1 A.

$\Lambda_w$  being more or less independent of pulse on-time (Figure 2 22) discloses

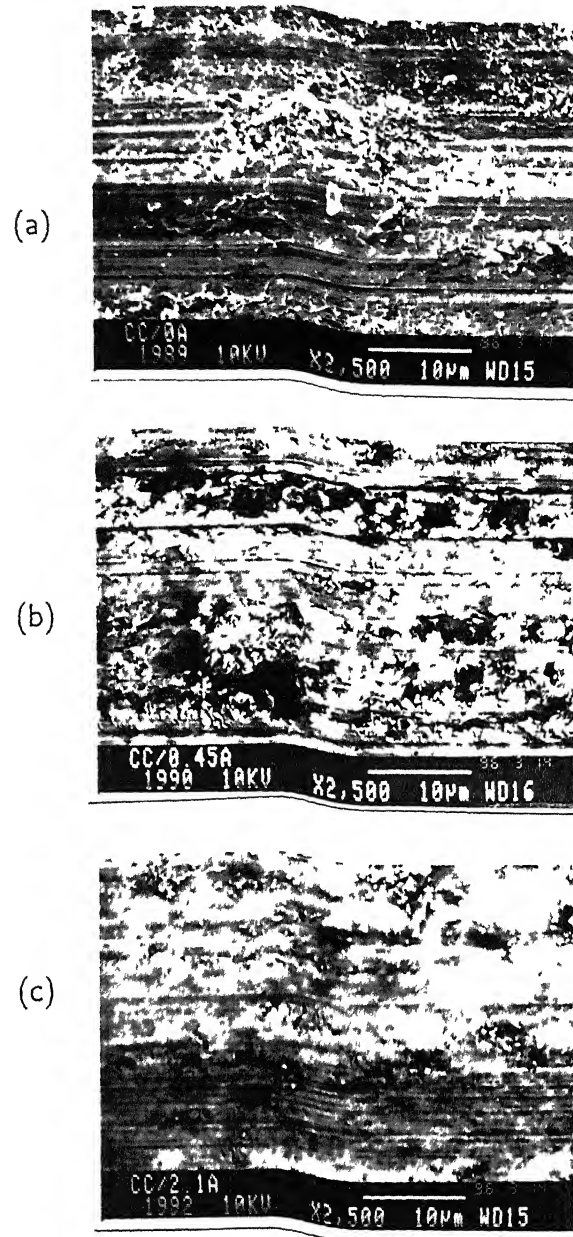


Figure 2.26 Micrographs of cemented carbide work surfaces machined at various currents (a) 0 A (b) 0.4 A (c) 2.1 A (10  $\mu$ s pulse on-time)

the fact that the dependence of MRR and normal force on pulse on-time (Figures 2.17 and 2.20) is due to the change in pulse on-time influencing the wheel rather than the work. In EDM the relative volume of material eroded

from the electrodes depends on the respective contributions of electrons and positive ions, resulting from the ionization of the dielectric at the gap, to the total current flow [8]. Since the positive ions are about  $10^4$  times as massive as the electrons, the latter reach the anode surface and liberate their kinetic energy therein in the form of heat, well before the ions reach the cathode. Thus the electron current predominates in the initial stages of discharge. The technological significance of this phenomenon is that undesirable wear of the tool can be minimized, if not done away with, by employing short pulse on-time and tool-negative polarity. This is the reason behind the reduction in the wear of the cathodic wheel on shifting towards shorter pulse on-time, observed during EDDG of cemented carbides [24]. On extending the concept to the present study, it is evident that for a particular current, the extent of grain pull-out would reduce with decreasing pulse on-time. This results in increasing wheel-work interference which leads to higher MRR and normal force. This is also supported by the fact that a decrease in duty factor increases the MRR for a particular pulse current (Figure 2.18).

The initial decrease in  $\Lambda_w$  (i.e., an increase in wear resistance) with increasing current (Figure 2.22) is quite counter-intuitive. The incidence of electrical discharges on the work, will in the first instance, be expected to at least maintain status quo, if not increase  $\Lambda_w$  due to thermal softening of the work. This phenomenon has been observed in reference [24] too. To elucidate this peculiar behavior, the influence of fracture toughness on the wear of materials has to be inquired — an excellent exposition of which can be found in reference [55]. This study on the abrasive wear resistance of many metals and ceramics has indicated that the wear resistance exhibits a maximum with respect to fracture toughness, the location of the maximum being dictated by the properties of the wear system (Figure 2.27). To the left of the maximum, wear resistance increases with fracture toughness despite decreasing hardness, in this regime, loss of material has been observed to be primarily related to microcracking. To the right of the maximum, the material wears by a combination of microcutting and ploughing and is dependent on hardness alone.

To explain the dependence of wear resistance of the cemented carbide

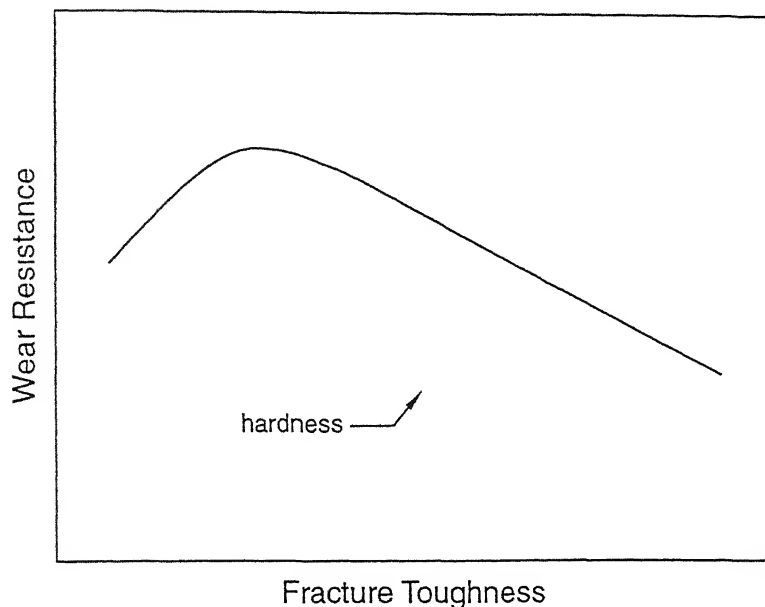


Figure 2 27 The role of fracture toughness on wear resistance [55]

on current in EDDG, it is therefore only necessary to examine the effect of temperature on the hardness and fracture toughness of the composite

The hardness of WC-TiC-(Ta Nb)C-Co cemented carbide decreases with increasing temperature [56] Plotted in semi-logarithmic co-ordinates, the hot hardness characteristic is represented by two linear segments with a point of inflection at approximately 670 K

Elevated-temperature fracture toughness studies of cemented carbides [57] indicate that the fracture toughness of WC-Co (6% Co), largely independent of temperature upto about 875 K, presents a marked increase around 975 K WC-TiC-(Ta Nb)C-Co is identical to WC-Co in so far as fracture related behavior is concerned, for reasons discussed later

Plausible reasons attributed to the increase in fracture toughness with temperature include (i) increased local plasticity at the crack-tip owing to the transformation of cobalt from hexagonal to cubic structure, (ii) enhanced plasticity of WC observed around this temperature, (iii) crack healing by sintering [57], and (iv) thermally activated residual stress relief [56]

The allotropic modification of cobalt takes place around 675 K [58], well

CENTRAL LIBRARY  
I I T., KANPUR

No. A 123597

below the temperature at which an increase in fracture toughness is witnessed which leaves the first premise above suspect. Moreover, an increase in fracture toughness due to crack blunting, on account of enhanced plasticity at elevated temperatures may not be significant, as the onset of plasticity is observed at a temperature of about 1125 K. Semi-empirical analysis, and metallographic examination of the path followed by the rupturing crack in WC-TiC-(TaNb)C-Co cemented carbide indicate [56] that the crack propagates within the cementing phase and along the grain boundaries, circumventing the carbide grains. In that instance, increased plasticity of WC at high temperatures can also be hardly expected to contribute to an increase in fracture toughness. In EDDG, since the abrasive-work interaction events take place rapidly and material is being continually removed, any alteration in the work material behavior due to temperature rise ought to occur in a very small interval of time. This excludes crack healing by sintering as a probable mechanism responsible for the increase in fracture toughness, since it entails a time scale of the order of minutes [59].

Of the mechanisms listed above, the thermal residual stress relief hypothesis proposed by Spath [56] appears to gain credence in the context of the present work. The same is validated in the light of it having analytically predicted [56] the rise in fracture toughness with temperature to become less prominent with an increase in cobalt content, as experimentally observed in reference [60].

Due to the mismatch of the thermal expansion coefficient of Co and WC (coefficient of Co is roughly three times that of WC), on cooling to room temperature after sintering the cementing phase is under tension and the carbide grains under compression. Around 870 K, even under short time holding, these residual stresses have been experimentally found [56] to be non-existent. This is due to thermally aided springback of elastically displaced atoms, which relieves most of the residual microstress.

The strength of a composite in which the rupturing crack traverses through the cementing phase will depend on the resistance offered by the cementing phase to crack propagation. Temperature affects this resistance owing to its influence on the residual stress field. With an increase in temperature, the

cracks which hitherto had been passing relatively easily through the tensile-loaded cementing phase, will encounter more resistance to their propagation on account of the relief of the microstress. The increase in the resistance to crack propagation manifests itself as an increase in fracture toughness and consequent increase in wear resistance.

WC-TiC-(Ta Nb)C-Co cemented carbide has a three phase structure consisting of (Ti,Ta Nb,W)C solid-solution crystals, structurally free WC and a cobalt base cementing phase. In this composite, the path of the rupturing crack is confined to the cementing phase and the grain boundary, as a result of effective wetting of the carbide crystals by cobalt during sintering, which results in a discontinuous carbide skeleton as in WC-Co system. Hence WC-TiC-(Ta Nb)C-Co and WC-Co have similar fracture related behavior.

The increase in wear resistance due to the rise in fracture toughness at a particular temperature will be evinced by only those composites satisfying the following conditions: (i) thermal expansion coefficient of the binder higher than that of the carbide, and (ii) crack propagation in the material predominantly through the cementing phase. With an increase in carbide grain size, the effect will be rendered insignificant, since in such a composite the cracks tend to be trans-granular. If the thermal expansion coefficient of the binder is lower than that of the carbide, the cementing phase will be under residual compression and hence thermal relief of the microstress would in fact, promote material removal. The benefit of combining grinding and dressing zones in EDDG will be significant for machining such materials.

# Chapter 3

## Topography Models for Diamond Grinding Wheels

---

### 3.1 Introduction

Material removal in diamond grinding entails the relative motion of the wheel with respect to the work surface, with which it is in physical contact. The topography of the operating face of the wheel which contains partly embedded diamond abrasives, in conjunction with the kinematic parameters of the grinding process, therefore influences the mode and rate of material removal, the forces developed and the roughness of the generated work surface.

Modeling of grinding processes with a view to contributing to a better understanding of the same, which would lead to increased efficiency and high product quality, requires a true description of the wheel surface. Diamond wheel topography is characterized macroscopically in terms of (i) the protrusion height distribution, (ii) the static planar grain density (iii) the distribution of inter-grain spacing, and (iv) the percentage projected area due to exposed abrasives. These quantities are random variables and for a particular wheel are dependent on the dressing conditions and technique used for wheel preparation. Moreover, the state of the wheel surface is time-dependent, and varies during the course of grinding mainly due to the wear of abrasives.

Characterization of the topography of conventional grinding wheels has



induced considerable interest among researchers in the past. Consequently, many experimental techniques like profilometry, microscopy and dynamometry in addition to scratch, imprint and thermocouple methods — the details and limitations of which are available in references [44, 61], have been developed. Of the aforementioned methods, profilometry is perhaps the most popular for purposes of process modeling and topography evaluation. Reference [62] describes a three-dimensional measuring system which extends the scanning region of a profilometer from a straight line to a plane, to study the effect of dressing parameters on the topography of metal-bonded diamond wheels. Two-dimensional profiles of wheel surfaces obtained by the stylus method have been modeled on a microscopic scale using various statistical approaches like Markov chain theory [63], autocorrelation function [64] and data dependent systems [65]. Recently, the application of fractal analysis to diamond wheel profiles [66] has brought out the correlation between the fractal dimension of profiles of diamond wheels and their grinding performance.

Reference [67] presents a survey of the models available for the topography of conventional wheels, all of which can be reduced to a single basic model. Despite the current widespread utilization of diamond wheels for the grinding of advanced engineering materials, attempts to model their topography have been scant. Diamond wheels are structurally quite different from conventional wheels in two respects: (i) the volumetric percentage of abrasives in conventional wheels (40 to 60%) is much higher than those of diamond wheels, which is generally less than 20%, and (ii) conventional wheels consist of voids separated by bridges of abrasives held in a binder, whereas diamond wheels are of negligible porosity. Hence, models available for conventional wheels can hardly be extended to diamond wheels. For instance, the structure of conventional wheels has been modeled with reference to known crystallographic designs [68], to do likewise for diamond wheels would invariably lead to erroneous results since the simple cubic structure, which has the lowest packing factor of 0.52, is itself about twice as densely packed as commonly used diamond wheels.

Buttner [69] has been cited in reference [67] to have derived a topography model for diamond grinding wheels on the basis of physical observations,

considering the diamond grains to be ellipsoidal in shape. This model relates the static count of grains on the wheel surface  $N_{st}$  to the average mesh size of the abrasives  $S_m$  and concentration  $C$  as

$$N_{st} = \frac{6C}{\pi \rho_D K S_m^2} \quad (3.1)$$

where  $\rho_D$  is the density of diamond, the constant  $K$  in the above equation is evaluated empirically, which limits the practical utility of the model. To the best of the author's knowledge, the above model is the only one available for the topography of diamond grinding wheels.

The motivation for modeling the diamond wheel topography in the present work is to facilitate the simulation of EDDG process, which is presented in the next chapter of the thesis. The model is, however, general in nature and can be applied to simulate any diamond grinding process.

Since the size of abrasives and their location on the wheel surface are random, it is relevant to resort to probabilistic means of modeling the wheel topography. In this thesis, two approaches to modeling diamond wheel topography are presented: the first approach involves a stochastic simulation methodology, and the second, a mathematical technique which is based on simple concepts of probability theory. The objective is to characterize the topography of diamond wheels in terms of the topographical indices viz., the protrusion height distribution, the static grain count, the distribution of inter-grain spacing and the projected area due to exposed abrasives, with reference to abrasive grit size and concentration.

The following section provides the background and explains the assumptions based on which the diamond wheel topography has been modeled.

## 3.2 Background & Assumptions

1. Diamond abrasives are of varied shape. Polycrystalline diamond grits possess no definite geometry whereas monocrystalline grits generally tend to be cubic or cubo-octahedral in shape as a result of differences in their respective synthesis techniques. However, from the point of view of modeling, it is expedient to consider the abrasive grains to

be spherical. This assumption brings about a substantial saving of modeling effort, since a single parameter — the grain radius, is sufficient to characterize the abrasives. Moreover, the orientation of grains in the bond is inconsequential, which would otherwise render the problem unwieldy.

- 2 The two basic parameters that specify a diamond wheel are the size and concentration of the abrasives used in the wheel. Abrasive grains are classified according to size by passing them through a stack of standardized sieves, the mesh size of the sieves getting finer downstream. Two numbers  $S_a/S_b$  are used to denote the abrasive size.  $S_a$  refers to the sieve that would let the abrasive grains pass through, and  $S_b$  to the sieve that would detain most of them. The grit radius  $r$  is related to the sieve number  $S$  as

$$r(\text{mm}) = 7.62S^{-1} \quad (3.2)$$

The proportion of abrasives in the wheel is designated by a concentration number  $C$ , which on division by four gives the volumetric percentage of abrasives.

In the formation of particles, a large number of chance factors are at work. This leads to the emergence of a normal distribution of particle size, which has been observed to hold for narrow distributions [70]. Hence, the distribution of abrasive radius is assumed to be normal (Figure 3.1), and symmetric about the mean grain radius  $\mu_r$  given by

$$\mu_r = \frac{r_a + r_b}{2} \quad (3.3)$$

The standard deviation of the grain radius  $\sigma_r$  is evaluated as

$$\sigma_r = \frac{r_a - r_b}{6} \quad (3.4)$$

since the range of normally distributed random variables, in general, is six times the standard deviation.

- 3 Diamond grinding wheels consist of abrasive grains discretely dispersed in a continuous bonding medium. The wheel material is assumed

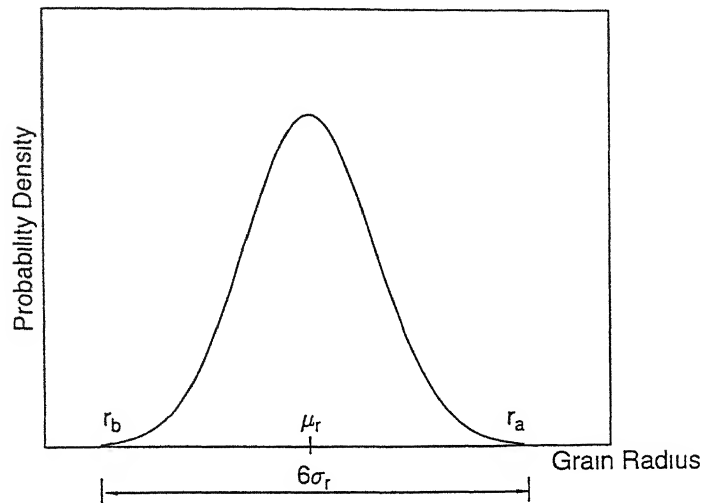


Figure 3.1 Assumed distribution of grain radius

to consist of two phases, with the abrasive grains embedded in the resin/metallic bond. It is presumed that there is no porosity.

The first step in the manufacture of diamond wheels is the mixing of appropriate amount of abrasive grains and bond-material powder in an automatic mixing machine [71]. The mixture is thereafter hot pressed and subsequently sintered. The mixing process ensures a homogeneous structure of the wheel material. The wheel material is hence presupposed to be stochastically homogeneous with reference to the location of abrasive grains; i.e., there is equal probability of encountering an abrasive grain at any point in the volume considered. For low packing densities such as in diamond wheels, this assumption has been generally found to be true [70].

4. A diamond wheel on being mounted on the machine tool spindle is subjected to a dressing operation after truing, to condition the wheel topography. During the course of dressing, the wheel surface might sustain grit fracture and/or pull-out. Fracture of abrasive grains has the effect of altering the protrusion height distribution while pull-out decreases the planar grain density. The present work assumes that the dressing operation induces no grit loss either by way of grain fracture

or dislodgement. Wheel dressing techniques that employ electrical discharge [21] or electrochemical [72] phenomena, under appropriate operating conditions relate to such a situation. Mechanical methods such as the braked truing wheel used at high speeds and rotary wire brush technique have also been reported [73] to dress the wheel with little or no damage to the grits. The model is not relevant to cubic boron nitride wheels, as flattening of grain-tips and grain fracture are inevitable while dressing them [44].

- 5 Diamond grains are held mechanically in the bond. As dressing of the wheel progresses, the bond material around the grains is continually removed due to abrasion by the dressing medium, resulting in an increase in the protrusion height of individual abrasives. With the receding of the bond level, eventually, the grains that are not rooted deep enough in the matrix to withstand the dressing load get levered off the bond. The dislodgement of an abrasive from the bond is a complex event. The failure strength of the adhesive joint between the abrasive grain and the bond material, apart from depending on the stress concentrations at flaws distributed in the interface, is strongly influenced by the local variation of stresses governed by the geometry, the elastic and plastic properties of the constituents, and the loading conditions of the bonded system [74]. Considering the three-dimensional nature and complexity of the problem, it is evident that it would lend itself tractable only to numerical analysis techniques like the finite element method. It was hence expedient to look for experimental information in the literature. The mechanism of release of a diamond grain from resin bond is discussed in reference [75]. It has been reported therein, on the basis of scratch tests, that dislodgement of a grain of radius  $r$  (see Figure 3.2) occurs when the non-dimensional parameter  $(x/r)$  representing the critical state of bonding of the grain assumes a value of 0.2. This is in conformity with the published data available [22, 76] for metal-bonded wheels, and hence has been adopted for topography modeling in the present work.

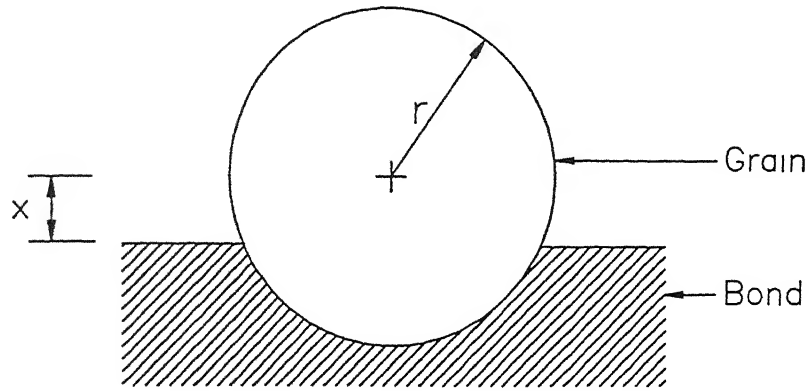


Figure 3.2 Critical state of bonding of a grain

### 3.3 Stochastic Simulation

This section deals with the stochastic simulation of the three-dimensional structure of diamond wheels, whence the desired topographic information is extracted. Stochastic simulation is a versatile numerical technique to simulate systems that are inherently probabilistic, by random sampling. The advent of high-speed computers has facilitated the application of this technique to a variety of problems in science and engineering. Such class of problems is sometimes referred to as Monte-Carlo simulation in the literature. However, stochastic simulation is a more appropriate terminology as the result output by the simulation is probabilistic, computational techniques that involve random numbers to solve deterministic problems are termed Monte-Carlo [77].

The subsections to follow present the simulation methodology, and the results and discussion.

#### 3.3.1 Methodology

A cube of side  $c$  of the wheel material is considered for simulation. For a wheel of concentration  $C$ , the total volume of abrasive grains  $V_a$  in the volume  $c^3$  is given by

$$V_a = \frac{Cc^3}{400} \quad (3.5)$$

The first step in the simulation is to generate  $N_a$  normally distributed random numbers with mean  $\mu_r$  and standard deviation  $\sigma_r$  which correspond to the

grain radius  $r$  such that

$$\frac{4}{3}\pi \sum_{i=1}^{N_a} r_i^3 \approx V_a \quad (3.6)$$

where  $\mu_r$  and  $\sigma_r$  are derived from the mesh size  $S_a/S_b$  (equations 3.3 and 3.4)

Now  $N_a$  sets of three random numbers  $(x_i, y_i, z_i)$ , uniformly distributed between  $(-0.2r_i)$  and  $(+0.2r_i)$  are generated to represent the X,Y,Z co-ordinates of the centers of each of the  $N_a$  grains, vide assumptions 3 and 5. Generation of the co-ordinates of the  $i$ th grain is subject to the condition,

$$\sqrt{(x_i - x_j)^2 + (y_i - y_j)^2 + (z_i - z_j)^2} \geq r_i + r_j, \quad j = 1 \text{ to } i-1 \quad (3.7)$$

since no two grains can occupy the same Euclidean space

Having assigned the spatial location of the abrasive grains as above, the wheel structure can be physically visualized as schematically illustrated in Figure 3.3. The grains protruding below, and belonging to the bond surface at an arbitrary height  $H_b$  within the simulated volume (Figure 3.4) could have the Z co-ordinate of their centers  $z_i$  either above or below the bond surface. These grains can be identified by segregating those satisfying the following conditions

$$\begin{aligned} (H_b - z_i) &\leq 0.2r_i, \quad \forall z_i < H_b \\ (z_i - H_b) &< r_i, \quad \forall z_i > H_b \end{aligned} \quad (3.8)$$

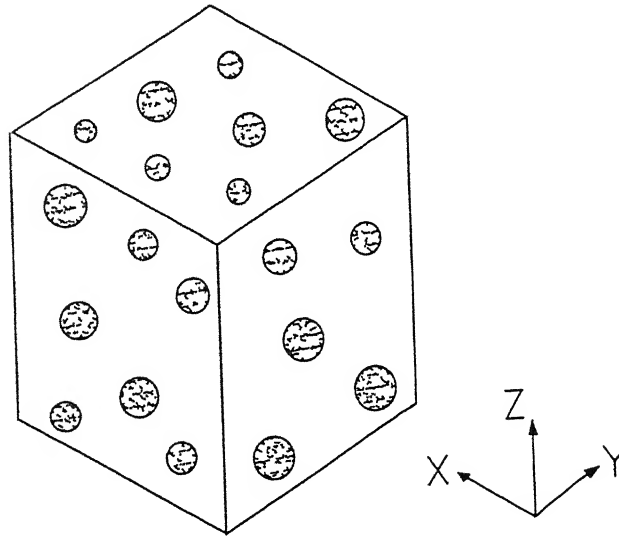


Figure 3.3 Schematic representation of the simulated wheel structure

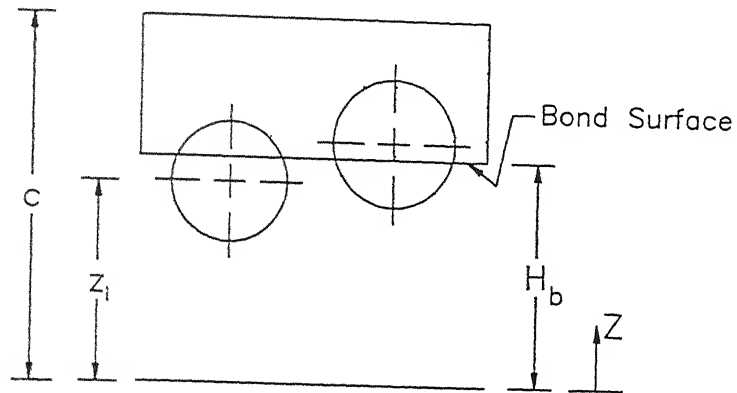


Figure 3.4 Scheme for identifying protruding abrasive grains

The protrusion height  $p_{h_i}$  of an exposed grain of radius  $r_i$  is given by

$$p_{h_i} = H_b - z_i + r_i \quad (3.9)$$

and the projected exposed area  $A_p = \pi(AB)^2$  of a protruding grain (see Figure 3.5) can be calculated as

$$A_p = \begin{cases} \pi(2r_i p_{h_i} - p_{h_i}^2) & \text{if } z_i < H_b \\ \pi r_i^2 & \text{if } z_i \geq H_b \end{cases} \quad (3.10)$$

For random values of  $H_b$  between 0 and  $c$  (Figure 3.4), different samples of the wheel surface of  $c^2$  units of projected bond area can thus be realized for evaluating the topographic indices

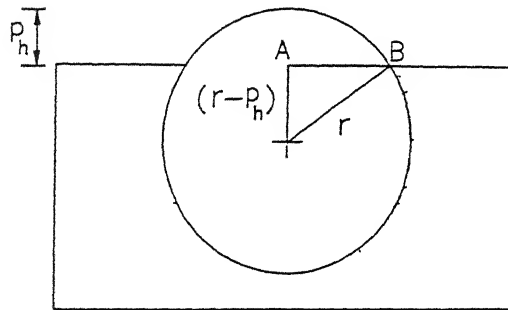


Figure 3.5 Projected area due to an exposed abrasive grain



### 3.3.2 Results and Discussion

#### Protrusion height distribution

The protrusion height is an important parameter on which the grinding performance is dependent to a large extent. It exercises control over the roughness of the ground surface and the wear of the grinding wheel. Inadequate protrusion of abrasive grains leaves little space for accommodating grinding debris and hence promotes wheel loading, which in turn leads to an increase in the grinding forces. Information on the distribution of protrusion height facilitates selection of a wheel for a particular application, and for a selected wheel formulation of the optimum operating conditions.

Typical simulated protrusion height distribution of a 90/110<sup>1</sup> grit, freshly dressed wheel is shown in Figure 3.6 for three different concentrations, which indicates that the distribution is more or less uniform. Experimental results available in the literature on the protrusion height distribution of diamond wheels are of a conflicting nature: a normal distribution of protrusion height is reported in reference [76] on the basis of measurements done on a scanning electron microscopic stereo pair, whereas it is observed in reference [62] by means of profilometry that the distribution changes from exponential to uniform as the dressing conditions become coarser. The difference is possibly due to the extent of grit loss due to fracture and/or dislodgement of abrasives during dressing. The simulation results presented here relate to ideal conditions wherein no grit loss is involved. The maximum protrusion height is seen to decrease with increasing mesh number (Figure 3.7), and the values obtained through simulation are quite in agreement with published data available in references [62,75,76].

The plots in Figure 3.6 indicate the possibility of the protrusion height distribution being independent of abrasive concentration. A two-sided  $k$ -sample Smirnov test [78] was carried out to confirm the same.

The data consisted of 5 random samples corresponding to 5 different concentrations (25 to 125 in steps of 25) of 500 protrusion heights each. The

---

<sup>1</sup>The non-standard 90/110 grit size interval has been chosen to correspond to 100 mesh size used in reference [62].

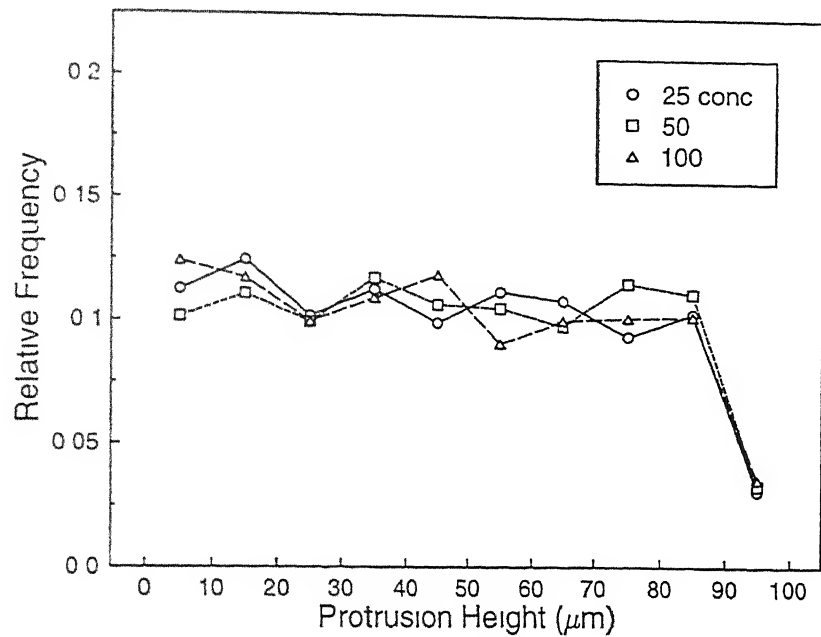


Figure 3.6 Typical protrusion height distribution of a 90/110 grit wheel for different concentrations

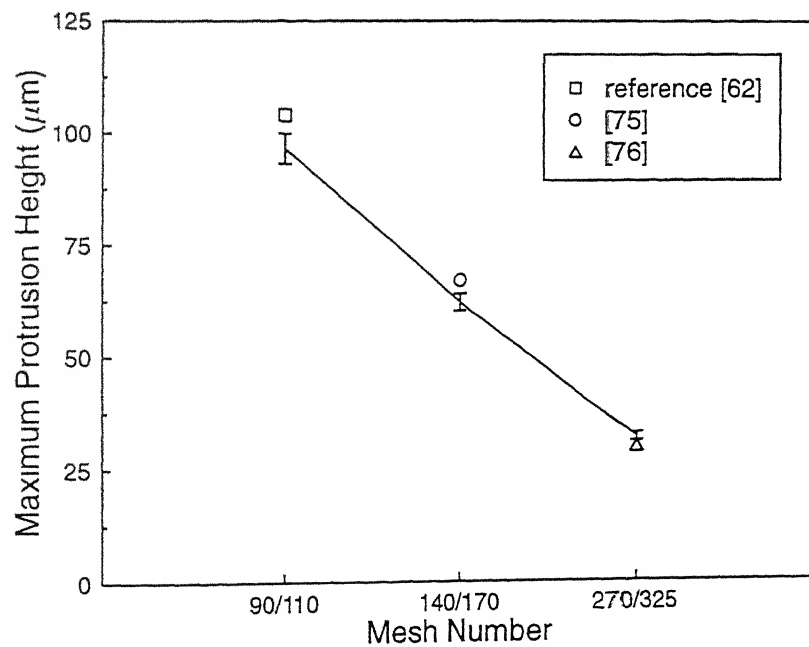


Figure 3.7 Maximum protrusion height vs grit size

population distribution functions of these samples, in order, were denoted by  $F_1(p_h), F_2(p_h), \dots, F_5(p_h)$ . The null hypothesis

$$H_0: F_1(p_h) = F_2(p_h) = \dots = F_5(p_h) \quad \forall p_h \quad (3.11)$$

was tested against the alternative hypothesis

$$H_1: F_i(p_h) \neq F_j(p_h) \quad \text{for some } i \text{ and } j \quad (3.12)$$

The sample with the largest protrusion height ( $98.31 \mu\text{m}$ ) in this case happened to be that of concentration 125 and that with the lowest ( $94.69 \mu\text{m}$ ), of concentration 75. The empirical distribution functions of these samples were denoted as  $S^{(5)}(p_h)$  and  $S^{(1)}(p_h)$ , respectively.

The Smirnov test statistic  $T_s$  defined as

$$T_s = \sup[S^{(1)}(p_h) - S^{(5)}(p_h)] \quad (3.13)$$

was evaluated to be 0.046. The tabulated value given by  $(1.73/\sqrt{n})$ , where  $n$  is the sample size, takes a numerical value of 0.077. Since  $T_s$  is less than the quantile, the null hypothesis — the protrusion height distribution is independent of concentration — was accepted at 5% significance level. The practical implication of the above result is that the roughness of diamond ground surfaces will be independent of abrasive concentration, as has in fact been reported in reference [79] on the basis of experiments.

### Static grain count

The static grain count is the number of protruding grains on the wheel surface per unit area, as opposed to the kinematic grain count which is the planar density of the grains actually interacting with the work to remove material. The kinematic grain count can be evaluated as a fraction of the static count through simulation, by duly incorporating the process kinematics. Conventionally, scratch experiments have been conducted with a single abrasive grain of known geometry, to study the material removal mechanism in grinding processes. To relate the outcome of such experiments, say the force system, to the actual grinding process wherein a large number of grains are dynamically involved, knowledge of the grain density is indispensable.

Figure 3.8 depicts the variation of the static grain count as a function of abrasive concentration for four different grit sizes, for which published experimental data is available for validation. The static grain count increases with an increase in abrasive concentration, and for a particular concentration, is higher for a larger mesh number. Despite the simplifying assumptions adopted, the simulation results can be seen to conform remarkably to reported experimental values, except for 140/170 grit, in case of which the predicted value is somewhat higher than the reported one. It may be noted here that the counting of grains on the wheel surface is prone to error especially for fine grit wheels due to the associated high planar grain density.

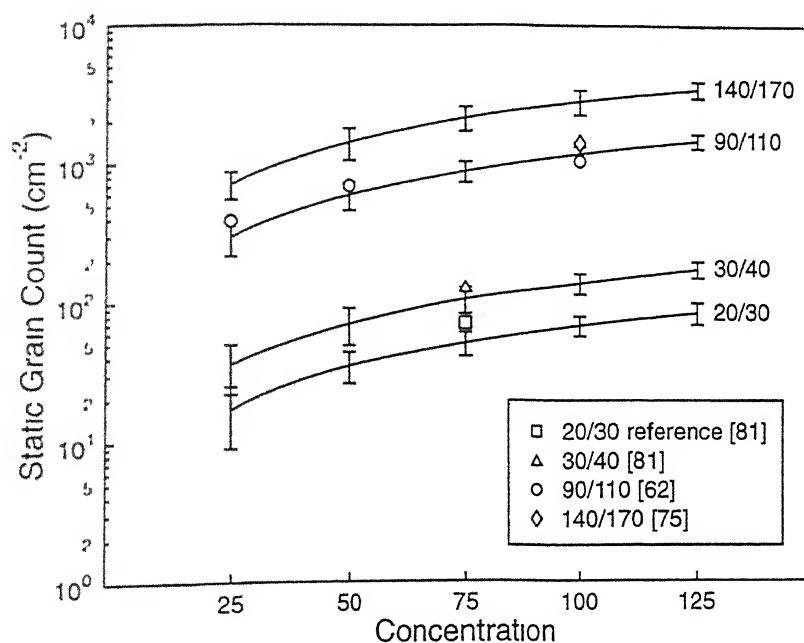


Figure 3.8 The static grain count as a function of concentration for various grit sizes as obtained by stochastic simulation

### Inter-grain spacing

The inter-grain spacing  $\Delta y$  is the distance between two successive grains on the wheel surface, along the grinding direction, lying within a section of width equal to the nominal grain diameter  $\mu_d$  (Figure 3.9). In conjunction with the protrusion height and the kinematic parameters of the grinding process,  $\Delta y$

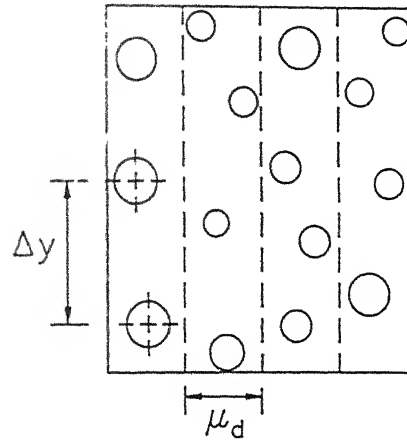


Figure 3.9 Definition of the inter-grain spacing  $\Delta y$

determines the chip cross-sectional area, and hence influences the grinding forces and the roughness of the work surface. It also affects the ease of chip removal and the rate of heating and cooling of the work.

The plan view of the simulated surface of a 90/110 grit wheel for 50 and 100 concentration is shown in Figure 3.10. Due to random position of grains on the wheel surface,  $\Delta y$  is appropriately portrayed in terms of its distribution. The analysis of the distribution of the same revealed that the magnitude of  $\Delta y$  could be described by a gamma model, whose probability density function is given by

$$f_{\Delta y}(\Delta y, \sigma, \lambda) = \frac{1}{\sigma \Gamma(\lambda)} \left( \frac{\Delta y}{\sigma} \right)^{\lambda-1} \exp \left( -\frac{\Delta y}{\sigma} \right), \quad \Delta y, \sigma, \lambda > 0 \quad (3.14)$$

where  $\sigma$  is the scale parameter,  $\lambda$  is the shape parameter and  $\Gamma$  denotes the gamma function.

The parameters  $\sigma$  and  $\lambda$  which completely specify the gamma distribution were estimated by employing the following algorithm given in reference [80]. The arithmetic mean  $\overline{\Delta y}$  and the geometric mean  $G$  of the sample data were determined as

$$\overline{\Delta y} = \frac{1}{n} \sum_{i=1}^n (\Delta y)_i, \quad G = \left( \prod_{i=1}^n (\Delta y)_i \right)^{1/n} \quad (3.15)$$

where  $n$  is the number of data-points in the sample. The shape parameter  $\lambda$

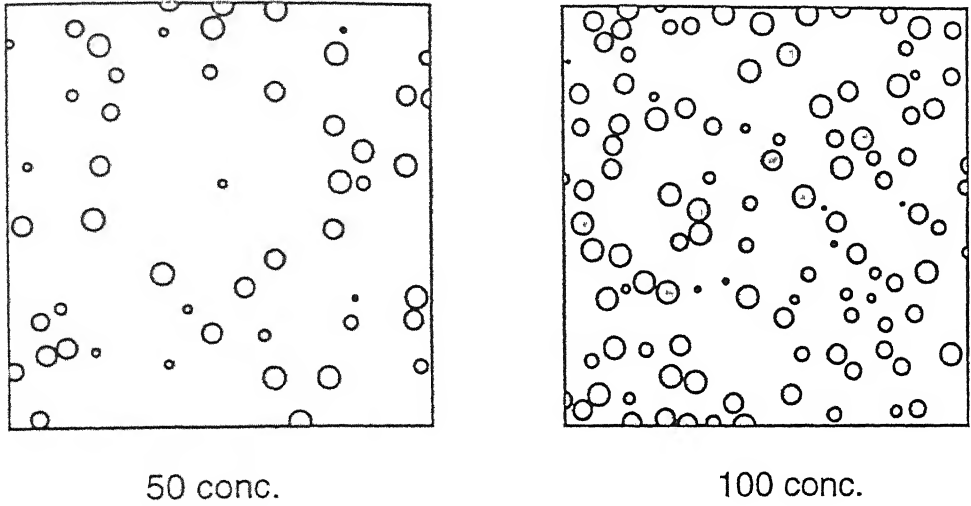


Figure 3.10 Typical plan view of the simulated surface of a 90/110 grit wheel for two different concentrations (the side of the square represents 3 mm)

is given by

$$\lambda = \begin{cases} (0.5001 + 0.1619g - 0.0544g^2)g^{-1} & 0 < g \leq 0.577 \\ (17.8 + 11.97g + g^2)^{-1}(8.899 + 9.06g + 0.9775g^2)g^{-1} & 0.577 < g \leq 17 \end{cases} \quad (3.16)$$

where  $g = \ln(\overline{\Delta y}/G)$ . The scale parameter  $\sigma$  is evaluated as

$$\sigma = \overline{\Delta y}/\lambda \quad (3.17)$$

The goodness-of-fit of the estimated probability density function was ascertained by the standard  $\chi^2$  test at 5% significance level.

The effect of abrasive concentration on the distribution of  $\Delta y$  is depicted in Figure 3.11. The characteristics corresponding to different concentrations can be seen to cross over at an inter-grain spacing approximately equal to five times the mean grain dimension. This was observed for other grit sizes too. Figure 3.11 also indicates that the most probable inter-grain spacing, for a particular grit size, is independent of abrasive concentration. The shape and scale parameters as a function of grit size and concentration are shown in Figures 3.12 and 3.13. The shape parameter varies linearly with abrasive

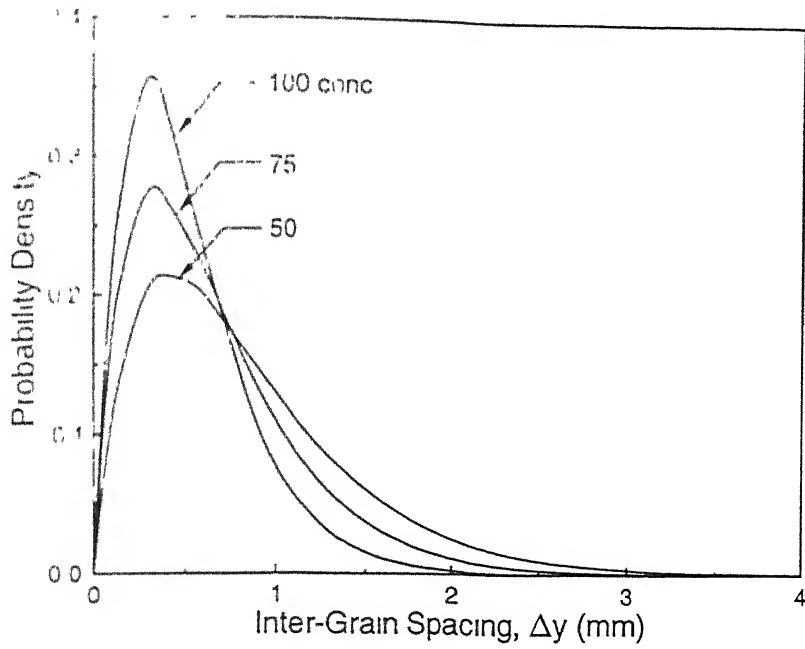


Figure 3.11 The role of concentration on the distribution of inter-grain spacing  $\Delta y$  (90/110 mesh size)

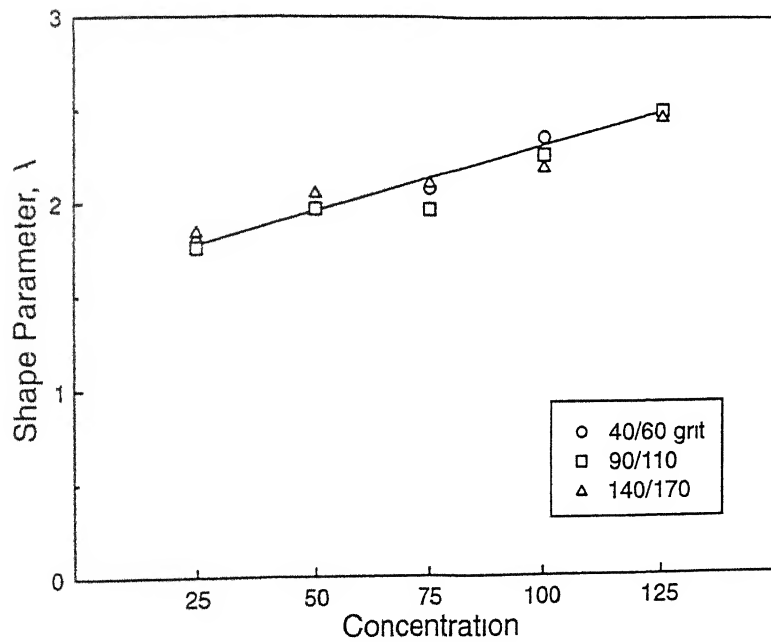


Figure 3.12 The shape parameter of the gamma distribution of  $\Delta y$  as a function of concentration for various grit sizes

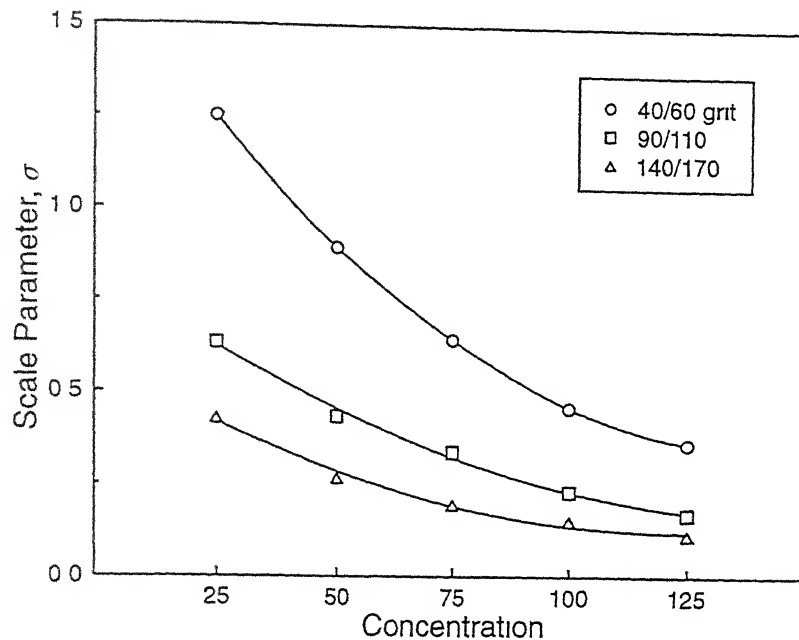


Figure 3.13 The scale parameter of the gamma distribution of  $\Delta y$  as a function of concentration for various grit sizes

concentration, and is independent of grit size. The scale parameter decreases with an increase in concentration, and for a given concentration is smaller for a larger mesh number. It would be of interest, in future, to characterize the performance of diamond wheels in terms of these parameters.

### Projected area due to exposed abrasives

The projected area due to exposed abrasives is an index which characterizes the diamond wheel topography. It is an important parameter that would influence the process response in EDDG, as the component of material removal due to spark erosion will be dependent on the projected conducting bond area on the wheel surface.

The simulated mean projected area due to abrasive grains as a percentage of the wheel area is presented in Figure 3.14. The mean projected area increases with abrasive concentration, but is evidently independent of the abrasive grit size. In reference [81], an area of 14% is reported for an abrasive concentration of 75, which compares quite well with the simulated result.



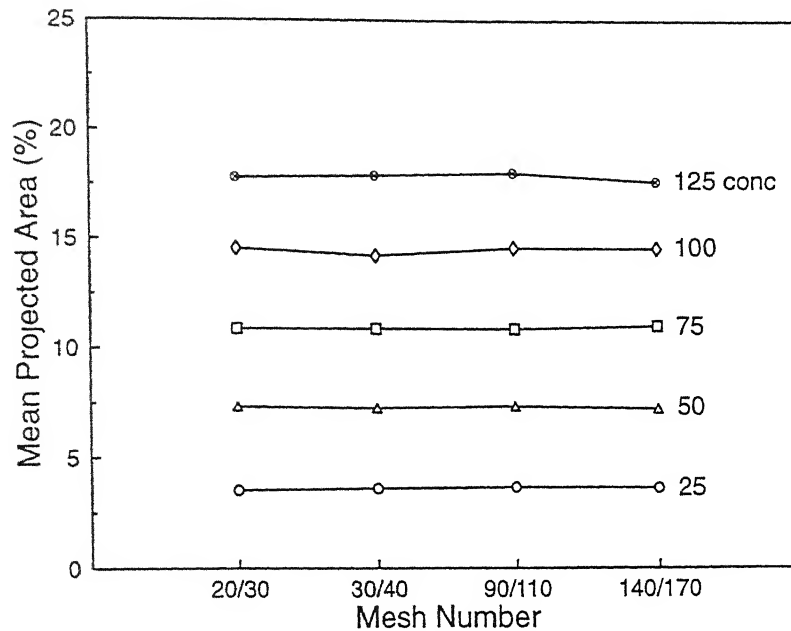


Figure 3.14 The mean projected area due to exposed abrasives vs mesh number for different concentrations

of 11%. That the projected area due to abrasives in diamond wheels is independent of abrasive grit size has also been confirmed by means of quantitative microscopy in reference [81] which further conclusively validates the simulation methodology, its implementation and the assumptions adhered to in the present work

### 3.4 Mathematical Model

In this section, a mathematical model for the topography of diamond wheels is presented. The assumptions adhered to herein are essentially the same as those enumerated in Section 3.2

#### 3.4.1 Methodology

The probability density function  $f_R(r)$  of normally distributed grain radius  $r$  is

$$f_R(r) = \begin{cases} \frac{1}{\sigma_r \sqrt{2\pi}} \exp \left[ -\frac{1}{2} \left( \frac{r - \mu_r}{\sigma_r} \right)^2 \right], & r_b \leq r \leq r_a \\ 0, & \text{otherwise} \end{cases} \quad (3.18)$$

Here  $\mu_r$  is the average grain radius and  $\sigma_r$  is the standard deviation of grain radius as defined in equations 3.3 and 3.4

A cube of volume  $c^3$  units of the wheel material is modeled (Figure 3.15). GR represents the grain radius and  $y$  the ordinate of the center of the grain. The distribution of  $y$  in accordance with assumptions 3 and 5 (Section 3.2) is

$$y \sim U(-0.2\mu_r, c + 0.2\mu_r) \quad (3.19)$$

Now the probability of the tip of the grain (represented by the point R) to be between two arbitrary heights  $a$  and  $b$  is given by

$$P(a \leq r + y \leq b) = \frac{1}{c + 0.4\mu_r} \int_{-0.2\mu_r}^{c+0.2\mu_r} P(c + a - y \leq r \leq c + b - y) dy \quad (3.20)$$

The probability density function  $f_R(r)$  of  $r$  being represented by equation 3.18,

$$P(a \leq r + y \leq b) = \frac{1}{c + 0.4\mu_r} \int_{-0.2\mu_r}^{c+0.2\mu_r} \int_{c+a-y}^{c+b-y} f_R(r) dr dy \quad (3.21)$$

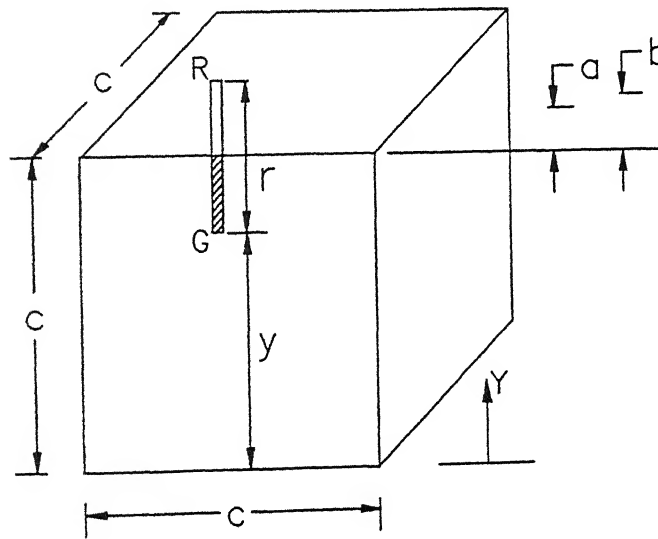


Figure 3.15 Parameters of the mathematical model

For ease of computation, the right hand side of equation 3.21 can be reduced to

$$\frac{1}{2(c + 0.4\mu_r)} \int_{-0.2\mu_r}^{c+0.2\mu_r} \left[ \operatorname{erf}\left(\frac{c+b-y-\mu_r}{\sigma_r\sqrt{2}}\right) - \operatorname{erf}\left(\frac{c+a-y-\mu_r}{\sigma_r\sqrt{2}}\right) \right] dy \quad (3.22)$$

where erf represents the error function

Calculation of the integral has been accomplished by Romberg numerical integration technique [82]. The distribution of protrusion height is obtained by evaluating the integral over small intervals.

The concentration number  $C$  of a wheel divided by four gives the volumetric percentage of abrasive grits in it. Hence, the volume of abrasives  $V_a$  in a volume of  $c^3$  units of wheel material is

$$V_a = \frac{Cc^3}{400} \quad (3.23)$$

The expected number of abrasives  $E[N_a]$  which constitutes the total volume of abrasives  $V_a$  can be shown [36] to be

$$E[N_a] = \int_{r_b}^{r_a} \left[ \frac{V_a}{\frac{4}{3}\pi r^3} \right] f_R(r) dr \quad (3.24)$$

The second moment of  $N_a$ ,  $E[N_a^2]$  is evaluated as

$$E[N_a^2] = \int_{r_b}^{r_a} \left[ \frac{V_a}{\frac{4}{3}\pi r^3} \right]^2 f_R(r) dr \quad (3.25)$$

The standard deviation of the number of abrasive grains  $\sigma_{N_a}$  in  $c^3$  volume of the wheel material is given by

$$\sigma_{N_a} = \sqrt{E[N_a^2] - E^2[N_a]} \quad (3.26)$$

The average number of protruding abrasive grains  $N_{av}^p$  can now be calculated as

$$N_{av}^p = E[N_a]P(a \leq r + y \leq b) \quad (3.27)$$

where  $a = 0$ , and  $b$  is greater than the maximum protrusion height for the concerned grit size. The 95% confidence limits  $[N_1^p, N_2^p]$  for the number of protruding abrasives is given by

$$[N_1^p, N_2^p] = N_{av}^p \pm 2\sigma_{N_a} P(a \leq r + y \leq b) \quad (3.28)$$

For a typical grain shown in Figure 3.5, the area occupied by the abrasive on the surface of the bond is

$$\pi(AB)^2 = \pi(2\mu_r p_h - p_h^2) \quad (3.29)$$

If  $p_{hmax}$  is the maximum protrusion height and  $N_{av}^p$  the average number of projecting grains in  $c^2$  units of projected wheel area, the average area  $A_{av}^p$  occupied by the abrasives can be approximated as

$$A_{av}^p = \sum_{i=1}^{N_{av}^p} \pi(2\mu_r p_{h_i} - p_{h_i}^2) \quad (3.30)$$

where

$$p_{h_{i+1}} = p_{h_i} + \frac{p_{hmax}}{N_{av}^p}, \text{ and } p_{h_0} = 0$$

### 3.4.2 Results and Discussion

Figure 3.16 presents the protrusion height distribution for three grit sizes, computed employing the mathematical model. The distributions are seen to be uniform. The results are in agreement with those of the stochastic simulation in so far as the distribution and the maximum protrusion height are concerned (Figure 3.6 and 3.7). It is apparent from the model (equation 3.20) that the protrusion height distribution is independent of the abrasive concentration and is a function of the mesh size of the abrasives alone.

The static grain count as a function of concentration for various grit sizes is depicted in Figure 3.17. Comparison of these results with those presented in Figure 3.8 indicates that the results due to the mathematical model and stochastic simulation are in agreement as far as the mean values are concerned, the 95% confidence bands due to the mathematical model are however wider than what is obtained by stochastic simulation. To make

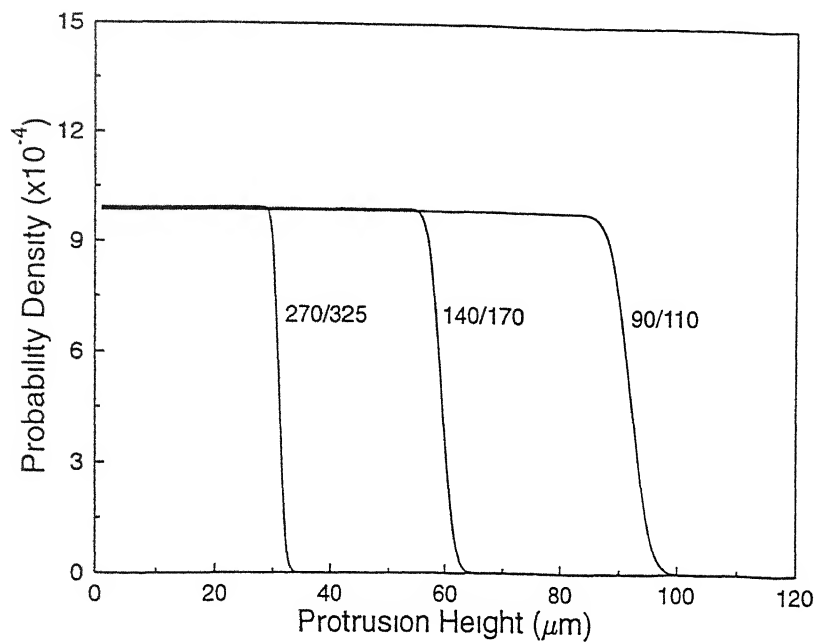


Figure 3 16 Protrusion height distribution for three different grit sizes ( $c = 1 \text{ mm}$ )

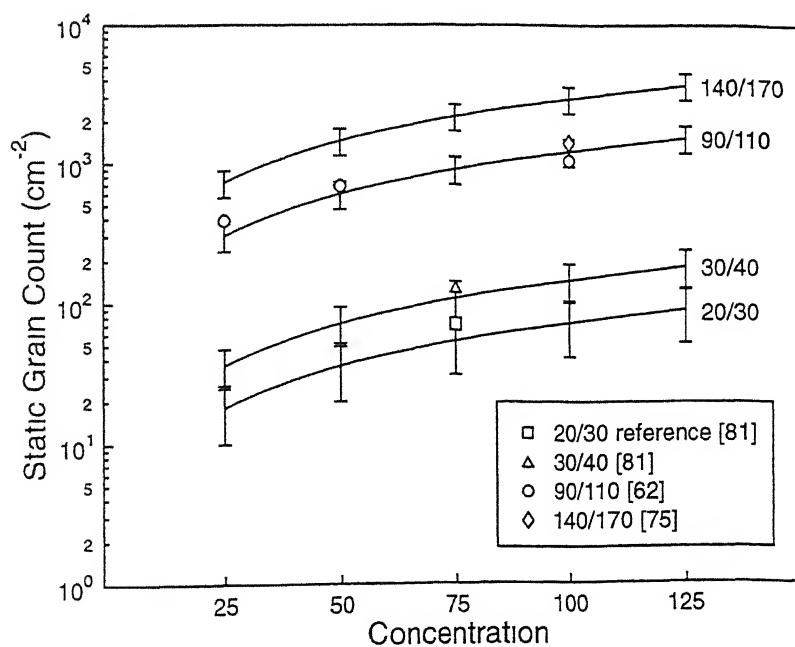


Figure 3 17 Static grain count as a function of concentration for different grit sizes as computed using the mathematical model

things more clear. Figure 3 18 presents a comparison of the mean static grain count due to the mathematical model and stochastic simulation, along with the experimental results for 90/110 grit size as a function of concentration. The difference between the static grain count predicted by the mathematical model and stochastic simulation is only marginal, and that too only at the higher end of concentration. The predicted static grain count can be observed to be in good agreement with the experimental result.

The mean projected area due to exposed abrasives on the wheel surface, as predicted by the mathematical model and stochastic simulation, for a concentration of 75, for various grit sizes is compared in Figure 3 19. The value due to the mathematical model is about 2% higher than that predicted by stochastic simulation. This was found to be true for all concentrations. The mean projected area due to the abrasives is independent of abrasive grit size, as confirmed experimentally in reference [81]. The measured value of projected area for a concentration of 75, as reported in the above reference is 1.4% which is quite in agreement with the predicted result.

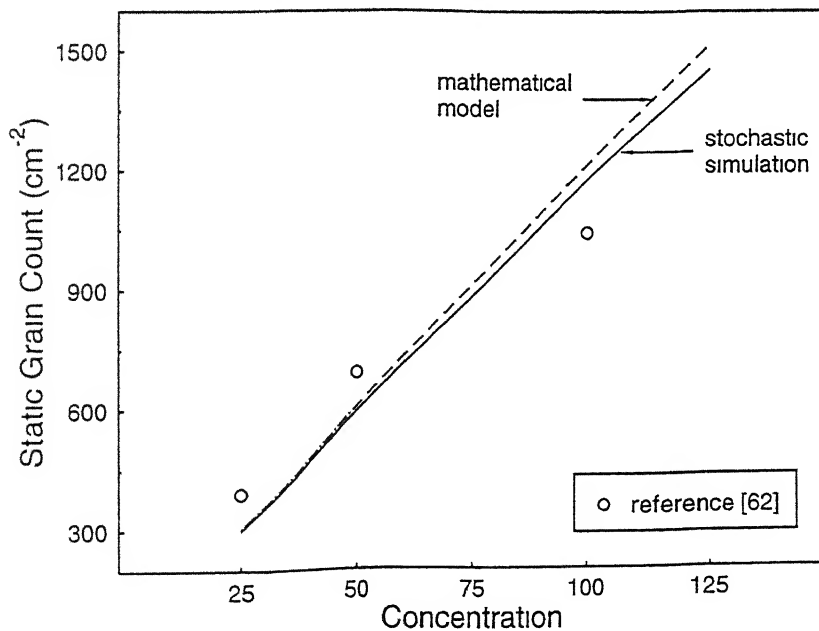


Figure 3 18 A comparison of the static grain count due to stochastic simulation and mathematical model (90/110 mesh size)

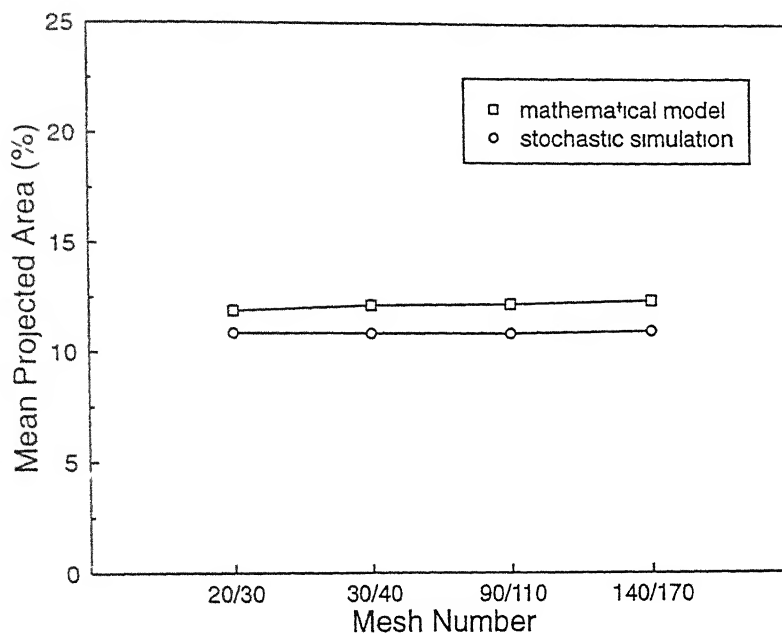


Figure 3.19 Projected area due to exposed abrasives — a comparison of results due to stochastic simulation and mathematical model (75 concentration)

A comparison of the utility of the models presented in this chapter is in order. The mathematical model is approximate whereas the stochastic simulation is a more realistic representation. However, stochastic simulation is computationally intensive in comparison to the mathematical model. If the topographical indices alone are of interest, use of the mathematical model is recommended. On the other hand, if the topographic data is to be used for grinding simulation, the stochastic simulation approach would be more appropriate, since the data required for process simulation are directly obtained from the simulated three-dimensional wheel structure. Use of wheel topography data obtained by stochastic simulation for simulating surface generation in diamond grinding is demonstrated in the next chapter.

# Chapter 4

## Simulation of Surface Generation in EDDG

---

### 4.1 Introduction

The primary advantages derived by way of introduction of electrical spark discharges in the grinding zone in EDDG are the in-process dressing and delogging of the wheel which results in enhanced grinding performance, and the reduction in grinding forces due to thermal softening of the work, as discussed in Chapter 2 of this thesis. Experimental results presented in Figures 1.1 and 1.2 indicate that the spark discharges, however, impair the finish of the ground surface. This has been observed by Aoyama and Inasaki [24] too while grinding cemented carbide with electrical spark assist (refer Figure 1.3b). The detrimental effect of spark discharges on the finish of the ground surface is quite clearly evident in micrographs shown in Figure 2.12. This problem which appears to be the limitation of the EDDG process can nevertheless be circumvented by switching off the current, and employing grinding alone while finishing a component. In this light, a simulation of surface generation in diamond grinding in cut-off configuration, incorporating the kinematics pertaining to EDDG process is presented in this chapter. The simulation enables prediction of the roughness of the ground surface with reference to abrasive grit size, in addition to obtaining the statistical characteristics of both the ground surface and the uncut chip cross-sectional



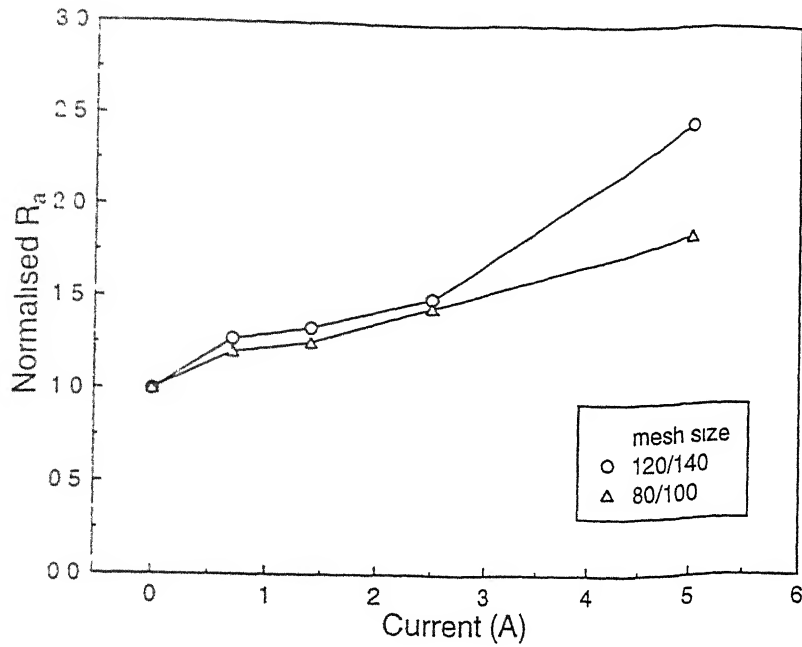


Figure 4.1 The effect of current on the surface roughness — HSS workpiece (voltage 40 V, pulse on-time 100  $\mu$ s, duty factor 0.5, wheel speed 4.5 m/s)

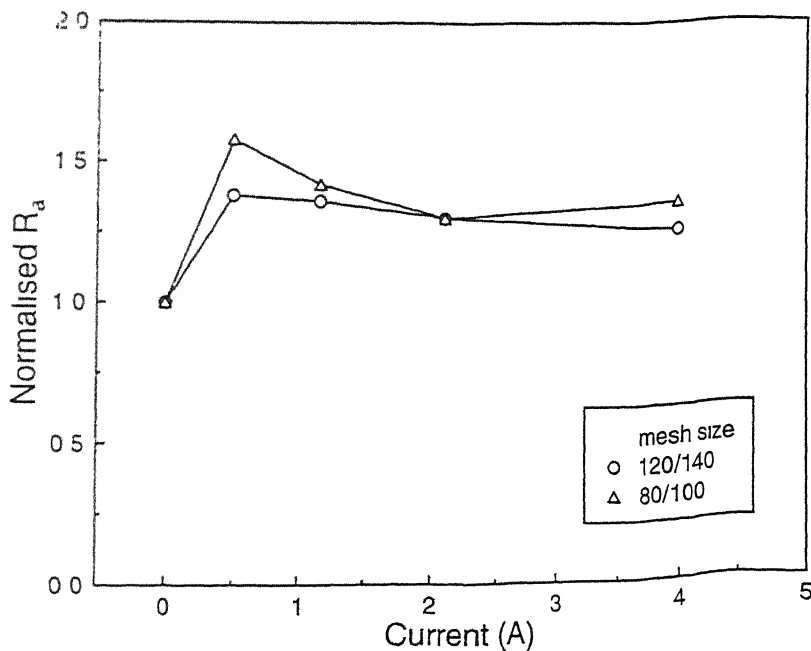


Figure 4.2 The effect of current on the surface roughness — cemented carbide workpiece (voltage 40 V, pulse on-time 10  $\mu$ s, duty factor 0.5, wheel speed 4.5 m/s)

area

The surface generated in grinding is the cumulative outcome of numerous abrasive-workpiece interaction events. By simulating these individual events, it is hence possible to predict the characteristics of the ground surface. Implementation of the same, requires information on the topography of the grinding wheel and the kinematics of the grinding process.

There have been many attempts in the past to model the surface generated in grinding. Baul and Shilton [83] were perhaps the first to employ random digital simulation technique to study the nature of surface interactions that occur in grinding, in such terms as the probability of contact and the relative proportions of cutting and ploughing contacts. A similar technique was used by Yoshikawa and Sata [84] to investigate the distribution of grain spacing on the grinding wheel and the undeformed chip cross-sectional area. Random numbers were generated to assign three dimensional spatial locations to the grain-tips of planar, triangular shaped grits. The assumption of the grains existing independent of each other on the wheel surface is the major drawback of this model.

Bhateja [85] evolved a hypothesis that the ground surface texture is complementary to the envelope of a large number of active transverse wheel profiles that traverse the grinding zone. Based on this approach, the relationship between the roughness of the wheel and the workpiece could be established. A generalized, semi-empirical model for estimating the roughness in grinding, based on wheel surface characteristics was presented by Suto and Sato [86]. The constants that occur in the model have been evaluated by conducting grinding experiments.

Hamed et al [87] developed a theory for the generation of ground surfaces, and verified it through computer simulation and experiment. The ordinates of the generated profile were found to be normally distributed, with an exponential autocorrelation function. The form of the autocorrelation function was observed to contain information on the process of surface formation. Law and Wu [88] explored the complex surface interactions in grinding and the resultant workpiece topography. The computed active grain density and axial pitch have been reported to compare well with experimental results.

Steffens [89] performed grinding simulation utilizing digitized wheel topography data. The peak-to-valley heights obtained through simulation for different grinding conditions were seen to be linearly related to the actual values, though one to two orders of magnitude smaller. A simple probabilistic model to evaluate the surface roughness in fine grinding was proposed by Basuray et al. [90] based on the concepts of radial distribution parameter and the effective profile depth. The results of their approximate analysis have been found to conform to those of experiments reasonably well. An explanation of certain structural properties of a ground surface in terms of the basic parameters and dimensions of the grinding wheel has been put forth by Sayles and Thomas [91]. The model explains the reduction in the roughness of ground surfaces during spark-out, and predicts the surface roughness parameter.

Approaches to modeling surface generation in grinding discussed above are for conventional wheels. The structure of diamond wheels is quite different in comparison to conventional ones. Diamond wheels possess a rather continuous bonding medium as opposed to the porous structure of conventional wheels, and have a volumetric abrasive concentration normally about half as less. Therefore, the models available for conventional wheels are not applicable as such to diamond grinding. Moreover, these models entail either experiments to determine constants that occur in the model, or wheel topography characterization by profilometry technique. The latter method is tedious and is prone to errors of measurement and digitization. The finite radius of the stylus tip filters off fine details, and introduces spurious lateral thickening of grain peaks. This apart, interpretation of the recorded profile is based on arbitrary criteria [44].

With these in view, in the present work, a simulation is presented to predict the characteristics of diamond ground surfaces obtained in EDDG under conditions of no flow of current, utilizing the topography model of the wheel obtained by a random sampling technique, described in Chapter 3 of this thesis. The simulation results are validated by experiments conducted on the EDDG set-up.

## 4.2 Experimentation

The simulation of surface generation in diamond grinding has been done with reference to the kinematics of the EDDG set-up described in Section 2.1. Removal of material, in this set-up, is realized in cut-off configuration, with the downfeed of the rotating diamond wheel regulated automatically by the servo control of the EDM machine (Figure 2.2). The servo system ensures that the metallic bond of the wheel and the work surface are separated by a gap of width  $g_w$  which depends on the local dielectric breakdown strength for a particular servo reference voltage. In this configuration, only those grains with protrusion height  $p_h$  greater than  $g_w$  are likely to remove material (Figure 2.3). During the course of material removal, as and when the gap-width increases, the servo imparts an incremental downfeed to the rotating wheel to maintain the gap-width.

Experiments have been conducted with the current switched off to correspond to pure grinding conditions. Three different wheels of grit sizes 80/100, 100/120 and 120/140, each of concentration 75 were used during the experimentation. The wheel preparation technique was essentially the same as reported in Section 2.1. After truing, the wheels were electrodischarge dressed before each experiment, employing the conditions listed in Table 2.1. Experiments have been carried out on high speed steel and cemented carbide workpieces in both cut-off and sparkout conditions, at a wheel peripheral speed of 4.5 m/s, with the voltage fixed at 40 V. In the cut-off mode, the grinding duration was limited to 30 seconds to isolate the effect of wear of abrasives, in the sparkout condition, grinding was continued for 5 minutes, with the wheel downfeed turned off.

The surface roughness parameter  $R_a$  was measured using a Surtronic 10 instrument (manufactured by Rank Taylor Hobson), with a diamond stylus of 5  $\mu\text{m}$  tip-radius. A traverse length of 5 mm and a cut-off length of 0.8 mm were adhered to during the roughness measurements. The reported roughness values are the average of 5 readings.

## 4.3 Simulation of Surface Generation

### 4.3.1 Methodology

The scheme adopted to simulate the surface generation in EDDG is depicted in Figure 4.3. Neglecting the curvature of the wheel, the wheel rim is developed into a strip which slides past the stationary work surface along the Y-direction. The surface of the wheel bond is positioned at a height equal to the gap-width  $g_w$  from the highest point on the work surface. The gap-width is shown exaggerated in the figure for the sake of clarity. The work surface which is initially plane is thus continually modified by each passing active abrasive which leaves its impression on the workpiece.

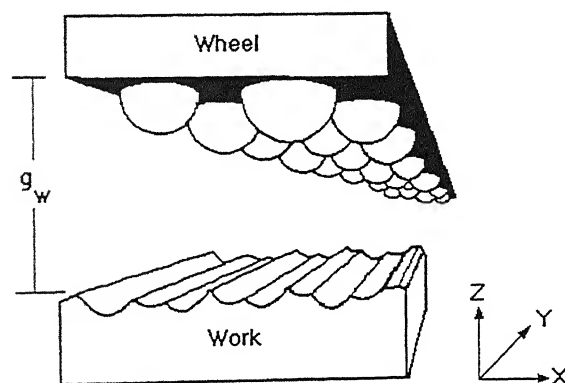


Figure 4.3 Schematic representation of surface generation in EDDG (adapted from reference [92])

The relevant topographic details required for the simulation are derived from the wheel structure, simulated in accordance with the methodology explained in Section 3.3.1. A cubic volume of the wheel material of side 3 mm was simulated at an abrasive concentration of 75 for each of the three grit sizes considered. Sample topographic realizations obtained at random heights  $H_b$  (refer Figure 3.4) between 0 and 3 mm, placed one after the other, lengthwise, in the Y-direction constitutes the wheel strip shown in Figure 4.3. For cut-off configuration, it suffices to consider just a plane section across the grinding lay, as the profile is identical along the direction of grinding. The

problem is thus rendered two-dimensional, in the X-Z plane. The pertinent data which characterize the wheel topography are the X, Z co-ordinates of the center of the abrasives ( $x_i, z_i$ ) with reference to the co-ordinate system presented in Figure 4.3, and their radii  $r_i$ .

The modification of the profile of the work surface as each active grain slides past the work surface is modeled by transforming the co-ordinates of the profile of individual active abrasive grains to the workpiece, based on geometrical considerations alone. It is assumed that the cross-sectional shape of the groove formed by the sliding abrasives on the work surface conforms to the circular profile of the abrasives i.e., material removal is by ideal ductile microcutting with no pile-up of material towards the sides of the groove.

The principle of modification of the work profile adopted in the present work has been applied in the past to simulate grinding [84, 87, 88] and to study abrasive wear [92]. The same is explained with reference to Figure 4.4. Initially a plane work surface AB of length 3 mm along the X-direction at a height  $h$  from the datum is considered. The co-ordinates of the profile AB are stored for discrete values of X in the simulation domain at a spatial resolution of  $1\text{ }\mu\text{m}$ . The centers of the abrasive grains ( $x_i, z_i$ ) are defined with respect to the co-ordinate system fixed to the workpiece. For each grain, while the abscissa  $x_i$  is provided directly by the topography model, the ordinate  $z_i$  is

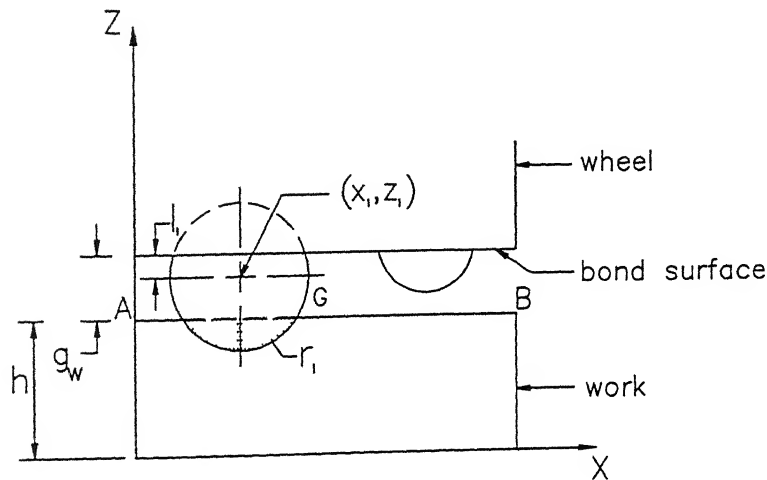


Figure 4.4 Coordinate system adopted for simulation of surface generation in EDDG

computed as

$$z_i = h + g_w + l_i \quad (4.1)$$

where  $l_i$  the ordinate of the grain center with respect to the bond level, obtained from the topography model. With reference to Figure 4.4, it can be seen that an active grain such as G of radius  $r_i$  would modify the work profile only within the interval  $(x_i \pm r_i)$ . The co-ordinates of the profile left by the abrasive on the work in this interval can be computed by solving the equation of the circle for discrete values of  $x$  and modifying the appropriate co-ordinates of the work profile.

The downfeed imparted to the wheel to compensate for any increase in gap-width during the course of material removal is realized in the simulation by updating the value of  $h$  in equation 4.1 to the maximum height of the work profile everytime before an abrasive modifies the work profile. The undeformed chip cross-sectional area  $a_c$  (shown dotted in Figure 4.4) is computed by numerical integration using trapezoidal rule. A sample profile of the ground surface is obtained after the passage of a number of grains has thus been simulated.

For studying the characteristics of the ground surface, a projected profile length of 2.4 mm was considered at a resolution of 1  $\mu\text{m}$ , which was split into three sampling lengths of 0.8 mm each. For each sampling length the mean line was computed such that the area of the solid above the line is equal to the area of the void below. The roughness parameter  $R_a$  has been calculated as

$$R_a = \frac{1}{L_s} \int_0^{L_s} |z(x)| dx \quad (4.2)$$

for each sampling length where  $z(x)$  is the height of the profile from the mean line and  $L_s$  is the sampling length, to compute the average roughness of the profile. The skewness  $S_k$  of profile height has been evaluated as

$$S_k = \frac{1}{n} \sum_{i=1}^n \left[ \frac{z_i - \mu_z}{\sigma_z} \right]^3 \quad (4.3)$$

where  $n$  is the number of sampling points,  $z_i$  is the profile height,  $\mu_z$  and  $\sigma_z$  are the mean and standard deviation respectively, of the profile height.

### 4.3.2 Results and Discussion

Figure 4.5 depicts the variation in the roughness parameter  $R_a$  of the simulated profile as each active grain traverses the work surface in cut-off configuration, at different gap-widths, for a 100/120 grit wheel. The roughness of the profile initially increases steeply, which subsequently decreases and becomes essentially stationary. This behavior has been observed experimentally by Hamed et al. [87], who simulated surface generation in grinding by tracking a Vickers indenter across micropolished surfaces at random locations within the simulated width, during the formation of the surface, it has been observed that once an equilibrium value of  $R_a$  is attained, further removal of material is seen to hardly alter the distribution of the roughness parameter. Figure 4.5 also indicates that a higher value of roughness is associated with a smaller gap-width. The 95% confidence limits for the roughness parameter  $R_a$ , as a function of the gap-width is presented in Figure 4.6. It can be noted that the range of variation of  $R_a$  is higher for a smaller gap-width.

The cyclic variation of  $R_a$  on reaching equilibrium (Figure 4.5), observed

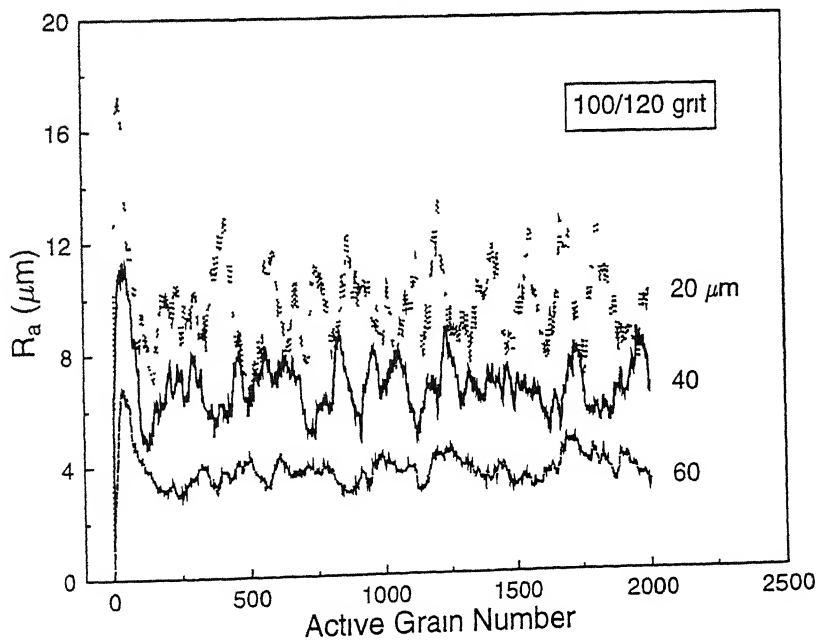


Figure 4.5 The surface roughness parameter  $R_a$  as a function of active grain number for various gap-widths, in cut-off configuration (simulation result)



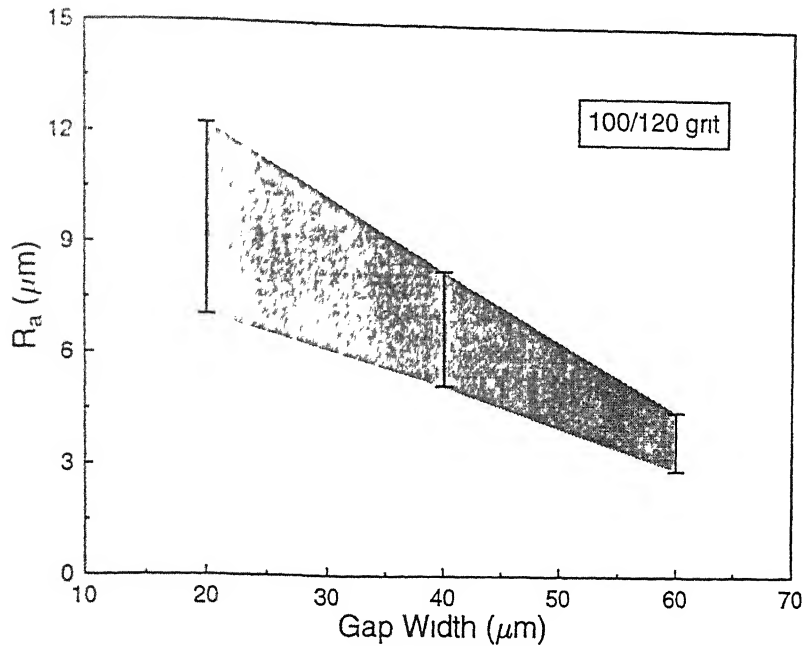


Figure 4.6 The 95% confidence limits for the surface roughness parameter  $R_a$  as a function of gap-width, in cut-off configuration (obtained by simulation)

at all gap-widths simulated is due to the intermittent feed motion imparted to the wheel, for material removal at constant gap-width. The increase in roughness at the beginning of a cycle corresponds to the discrete down-feed imparted to the wheel to compensate for the increase in gap-width which occurs during the course of removal of material. The subsequent decrease of  $R_a$  in the cycle is due to smoothing of the profile due to material removal taking place with the ram remaining stationary. For this reason, the range of roughness is also higher for a smaller gap-width, an infeed given to the wheel at a smaller gap-width results in an increase in the depths-of-cut of individual abrasives leading to a higher roughness value.

With reference to grinding performance, the two basic parameters that specify a diamond wheel are the abrasive grit size and concentration. The roughness of diamond ground surfaces while strongly dependent on the abrasive grit size [93], is independent of abrasive concentration [79]. This is on account of the protrusion height distribution being independent of abrasive concentration, as theoretically established in Chapter 3 of this thesis. For

the gap-width vs roughness relationship obtained through simulation for a particular grit size, as presented in Figure 4.6, to be of practical use in predicting the bounds for roughness obtained in EDDG with respect to that grit size. Information on the magnitude of gap-width is required.

The interelectrode gap-width in electrical discharge machining, for a set voltage, depends on the local breakdown strength of the dielectric which is considerably influenced by the size and concentration of debris present in the gap. Reference [41] is possibly the only source in the literature reporting typical experimentally measured values of frontal gap-width in EDM for the range of machining parameters pertinent to die-sinking, the gap-width has been reported therein to be between 20 and 100  $\mu\text{m}$  corresponding to a wide range of discharge parameters.

In the present work, the gap-width has been evaluated by tuning the mean value of the roughness obtained by simulation to the experimental result as follows. Experiments done with a 100/120 grit wheel on high speed steel and cemented carbide workpieces at a wheel speed of 4.5 m/s and an average voltage of 40 V indicated that the  $R_a$  value of the ensuing ground surface is around 7  $\mu\text{m}$ . Referring to Figure 4.6, this corresponds to a gap-width of about 40  $\mu\text{m}$  which is well within the range reported in reference [41]. A gap-width of 40  $\mu\text{m}$  was hence used in the simulation program for predicting the roughness limits of 80/100 and 120/140 grit wheels, the results of which are presented in Figure 4.7. The simulation results can be seen to agree well with the experimentally measured values. It may be noted here that the roughness obtained in EDDG is in the coarse-machining range and is much higher than what is obtained in conventional diamond grinding, for identical grit size. This is due to the fact that the maximum protrusion height of electrodischarge dressed wheels is about 60% of the nominal grit size, whereas it is less than 10% of the grit size for mechanically dressed wheels [22], due to grit fracture.

The variation of the surface roughness parameter  $R_a$  with active grain number under spark-out condition, i.e. with no infeed given to the wheel, for a 100/120 grit wheel at various gap-widths is shown in Figure 4.8. The roughness initially increases as in the case of cut-off configuration (Figure 4.5), but

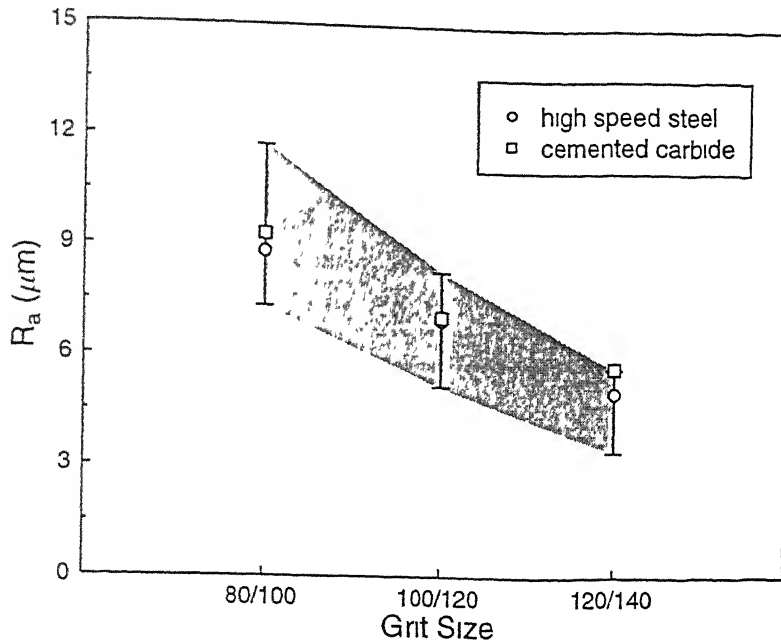


Figure 4.7 The surface roughness parameter  $R_a$  in cut-off configuration for various grit sizes — comparison of simulation and experimental results (the error bands denote 95% confidence limits for  $R_a$ , as obtained by simulation)

thereafter decreases exponentially to a steady-state value. It is also seen that the characteristics corresponding to different gap-widths although do follow different paths, finally converge to the same limiting value. Comparison of the simulated limiting roughness value with experimentally measured values for different grit sizes and work material (Figure 4.9) however indicates that the simulated roughness values are lower than what is obtained experimentally. Though the spark-out roughness is lower than what is obtained in cut-off (compare with Figure 4.7), the difference is not as high as what is predicted by simulation. This is clearly due to the assumption adhered to in the simulation that material removal is by ideal microcutting wherein the abrasive is considered to remove the entire geometric section of the work which interferes its path. In reality, however, the proportion of the volume of the groove removed depends on the hardness of the work material, the ratio of the penetration depth to the tip-radius of the abrasive, and the attack angle involved [45]. The fraction of material removed could be anywhere between zero and one — which respectively correspond to pure ploughing

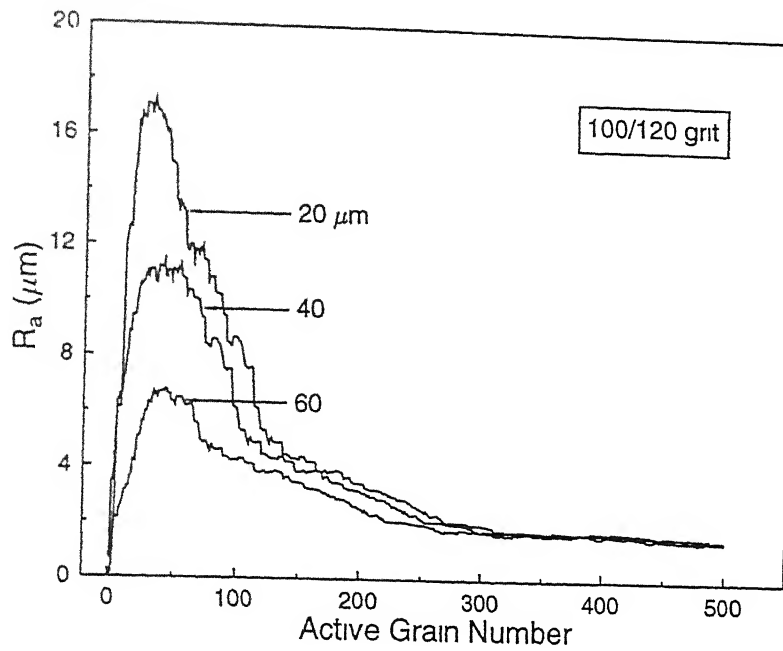


Figure 4.8 The roughness parameter  $R_a$  vs active grain number at various gap-widths during spark-out — simulation results

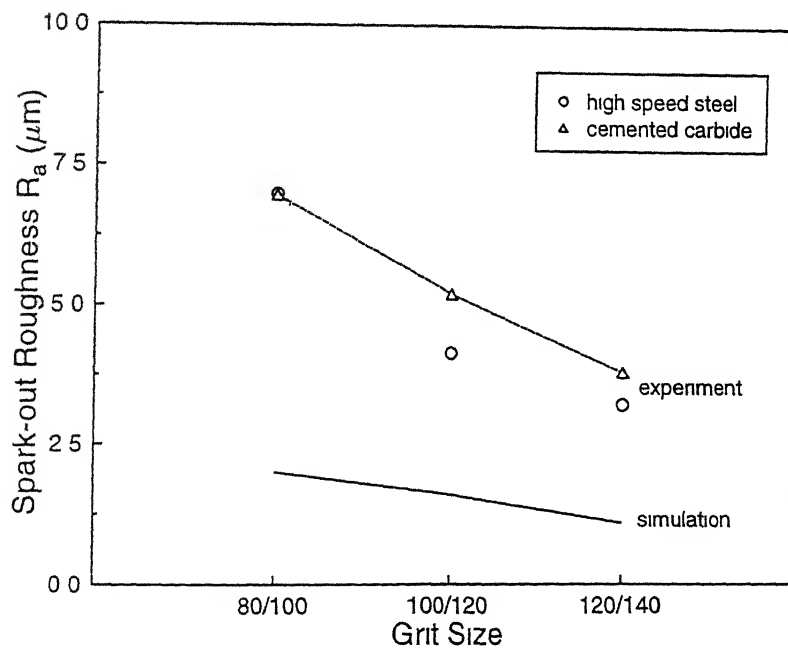


Figure 4.9 The roughness parameter  $R_a$  for various grit sizes (spark-out) — a comparison of simulation and experimental results

wherein all the material is just displaced but not removed, and ideal cutting wherein all the material is removed. Under spark-out conditions, as the profile is progressively smoothed, the ratio of the penetration depth to the tip radius of abrasives continuously decreases. This increases the tendency of the material to get displaced rather than removed, which prevents further improvement in the finish of the surface.

Figure 4.10 depicts sample simulated ground work profiles that correspond to a 100/120 grit wheel at a gap-width of  $40\text{ }\mu\text{m}$  in cut-off configuration for different active grain number, along with the distribution of their profile heights.

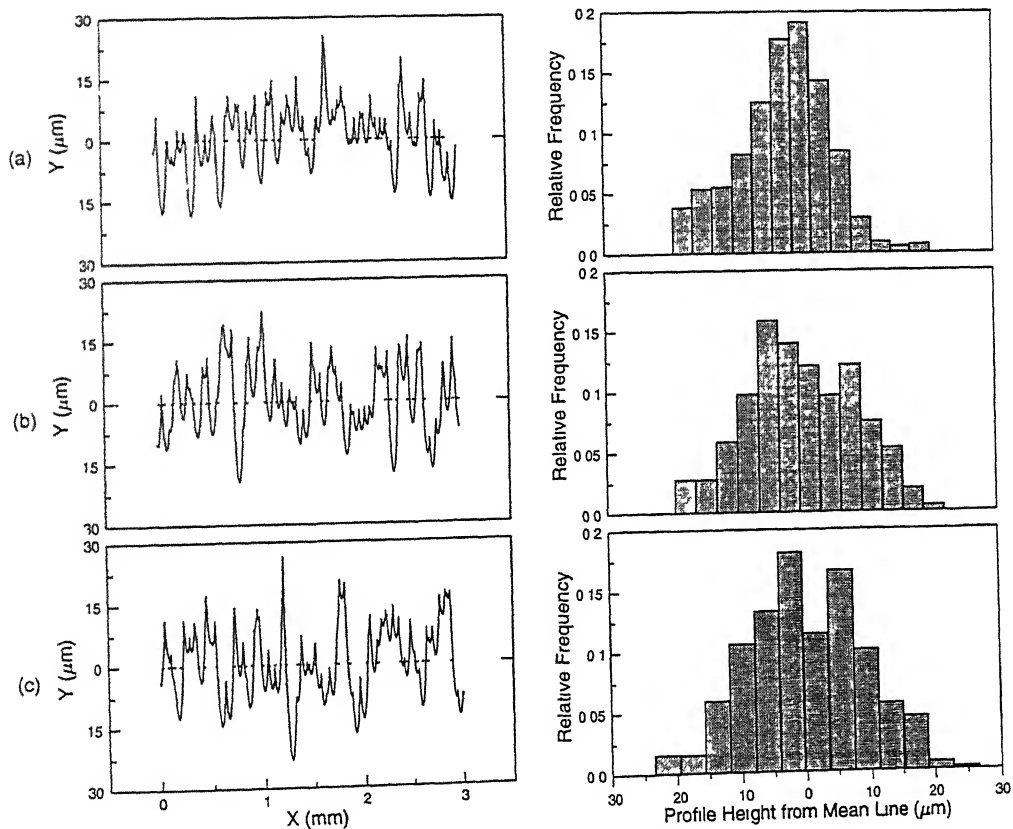


Figure 4.10 Representative simulated ground work profiles and their profile height distribution at an active grain number of (a) 250 (b) 500 and (c) 1000 (100/120 grit,  $40\text{ }\mu\text{m}$  gap-width, cut-off)

The height distribution of ground surfaces is generally cited to be gaussian, in line with what is postulated by the Central Limit Theorem. The distribution of profile height in Figure 4.10 however indicates the presence of a skewness. Sayles and Thomas [91], based on their experimental investigations report that the height distribution of surfaces ground by conventional wheels exhibit significant negative skewness, their theoretical analysis of the grinding process explained this to be the direct consequence of the positive skewness of the height distribution of the grinding wheel.

The nature of variation of the skewness of the generated profile as each active grain removes material in cut-off configuration is shown in Figure 4.11. The plot indicates that the skewness is predominantly positive, and varies cyclically similar to the trend exhibited by the roughness characteristics (Figure 4.5). A discrete infeed given to the wheel renders the profile positively skewed, and subsequent removal of material in the same cycle with the ram remaining stationary, predominantly removes the peaks leaving the valleys in the profile relatively unscathed which is denoted by the trend of the curve.

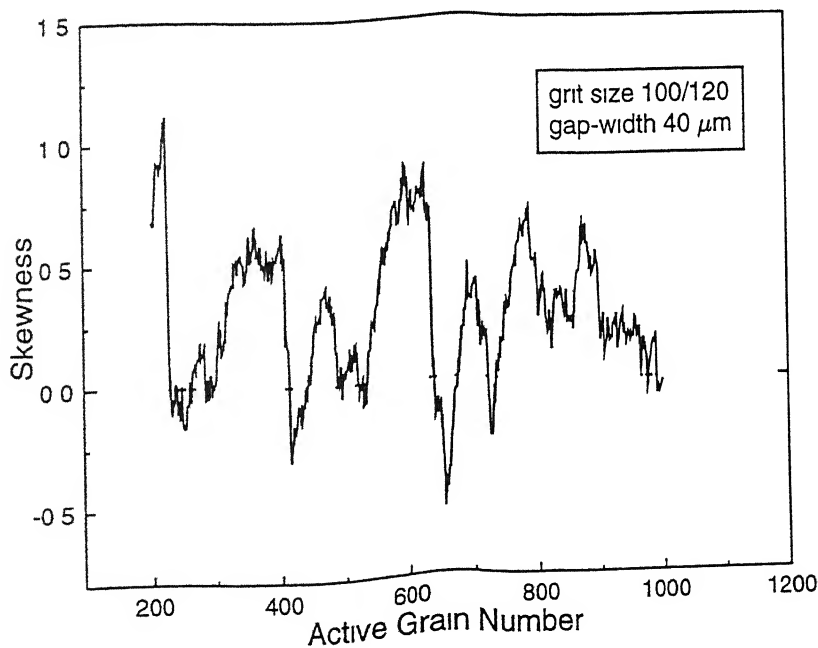


Figure 4.11 The skewness of the simulated profile as a function of active grain number (cut-off)

which approaches zero skewness. This is in agreement with the statistical theory of skewed distributions due to Kapteyn, discussed in reference [91]. This theory predicts that a gaussian height distribution would result where light cuts are involved and several passes are taken without increasing the feed, whereas heavy cuts with single pass would lead to a truncated distribution. The simulation supports the view of Sayles and Thomas [91] that a strictly gaussian distribution of profile height generally accepted as the norm is only an artifact of the care taken to obtain a specimen, and that surfaces ground routinely would exhibit significant skewness, the simulation, however, indicates positive rather than negative skewness as reported by them.

The mean uncut chip cross-sectional area  $a_m$  which is the two-dimensional counterpart of the undeformed chip-thickness is an important parameter in grinding which depends on the topography of the wheel and the kinematics of the grinding process. Responses like the grinding forces, work surface roughness and integrity, and the mode of material removal have been characterized in terms of  $a_m$  for advanced ceramic materials [94]. The distribution of the cross-sectional area  $a_c$  of chips obtained by simulation for various grit sizes, in cut-off configuration, at a gap-width of 40  $\mu\text{m}$  is given in Figure 4.12. It is evident that the distribution becomes increasingly skewed to the right as the grit size becomes coarser.

Experimental investigations [95] have revealed that the average cross-sectional area of chips is related to the roughness of the generated surface in grinding for a particular work material — a concept which comes in handy for predicting roughness corresponding to different grinding conditions and operations, for that material. The relationship between  $R_a$  and  $a_m$  as brought out by the simulation, based on geometrical considerations alone is presented in Figure 4.13.

It is interesting to note that the extrapolation of the best-fit second-order polynomial which relates  $R_a$  and  $a_m$  in Figure 4.13 to the range of  $a_m$  pertinent to experiments reported in reference [95] indicates that the simulated characteristic is in fair agreement with experimental data reported therein (Figure 4.14).

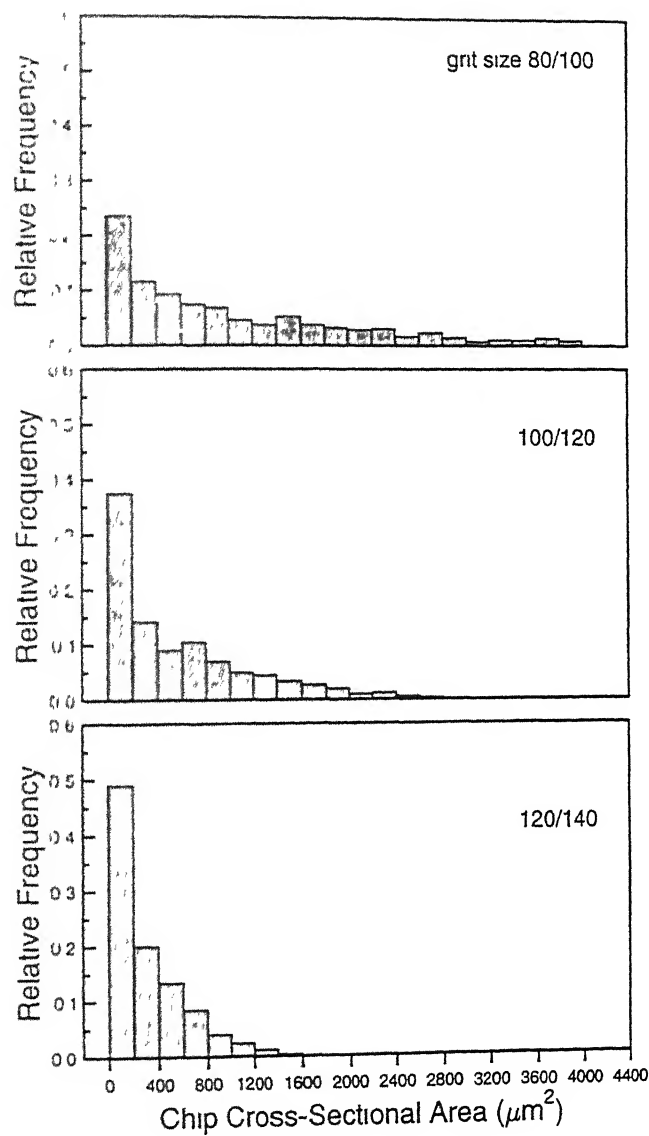


Figure 4.12 The distribution of chip cross-sectional area for various grit sizes obtained by simulation (40  $\mu\text{m}$  gap-width, cut-off)



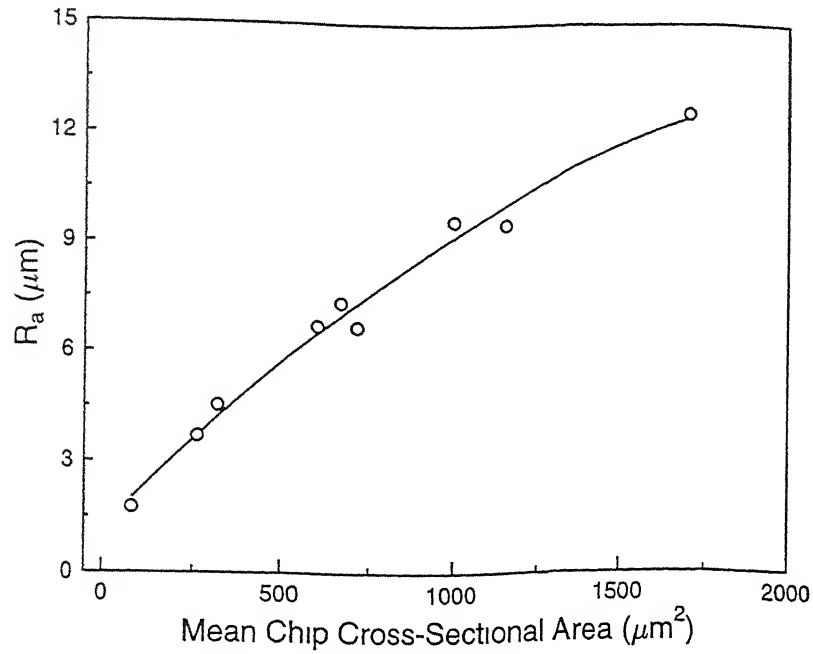


Figure 4.13 The roughness parameter  $R_a$  as a function of the average chip cross-sectional area (obtained by simulation)

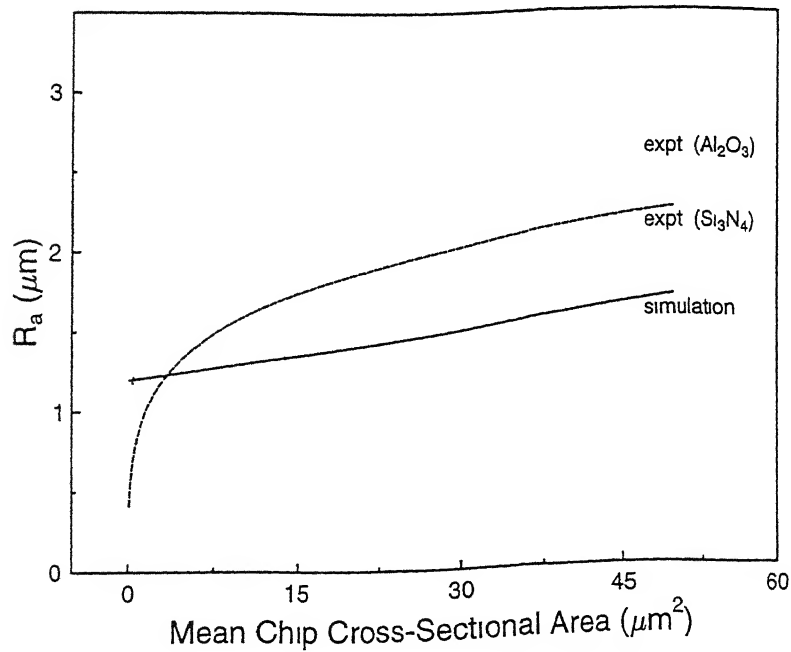


Figure 4.14 A comparison of the  $R_a$  vs  $a_m$  characteristic obtained by simulation with that of experiment cited in reference [95]

# Chapter 5

## Conclusions and Future Work

---

### 5.1 Conclusions

On the basis of the experimental and theoretical investigations reported in this thesis, the following general conclusions have been drawn

#### Mechanism of Material Removal in EDDG

- EDDG experiments on high speed steel indicate that the introduction of electrical spark discharges in the grinding zone is technologically appealing for grinding electrically conducting hard materials, carbide-steel combinations and materials that tend to rapidly blunt the abrasives and/or load the wheel
- The improved grinding performance in EDDG is on account of continuous in-process dressing and declogging of the wheel, the wheel wear, however, has to be optimized for EDDG to be economically viable
- The spark discharges thermally soften the work material in the grinding zone and thus diminish the normal force. The significance of the thermal softening effect is that it can be taken advantage of to substitute diamond abrasives by relatively inexpensive aluminum oxide abrasives for grinding hard materials

- While grinding cemented carbides, loading of the wheel is more of a problem rather than the formation of wear-flats on the abrasives. The enhancement of grinding performance by the spark discharges incorporated in the wheel-work interface is hence due to declogging of the wheel surface.
- With an increase in the discharge power, cemented carbide workpieces are subject to thermal softening, resulting in a decrease of the normal grinding force, but at the expense of premature pull-out of abrasives from the wheel, which is unacceptable. In such an instance, it is expedient to decouple the grinding and dressing zones, and accomplish electrodischarge dressing of the wheel with a separate electrode outside the grinding zone, as depicted in Figure 1.1b.
- WC-TiC-(TaNb)C-Co cemented carbide studied in the present work exhibits an increase in wear resistance while electrodischarge grinding at low discharge power due to an increase in the fracture toughness of the material with temperature. Thermal relief of the inherent tensile residual stress in the cementing phase of the composite, through which the rupturing cracks propagate appears to be responsible for the rise in fracture toughness, and the concomitant increase in wear resistance.

### Topography Models for Diamond Grinding Wheels

- Two approaches to modeling diamond wheel topography — a mathematical model and a simulation methodology have been evolved to estimate the indices that characterize the wheel topography viz, the protrusion height distribution, the static grain density, the distribution of inter-grain spacing and the projected area due to exposed abrasives, with reference to abrasive grit size and concentration. The results of the models are in agreement with experimental data available in the literature.
- The models indicate that (1) the protrusion height distribution of a freshly dressed diamond wheel is approximately uniform, and is inde-

percent of abrasive concentration, (ii) the inter-grain spacing of diamond wheels conforms to a gamma distribution, and (iii) the percentage of the total projected area due to exposed abrasives is a function of abrasive concentration alone and is independent of the grit size

### Simulation of Surface Generation in EDDG

- Experiments on high speed steel and cemented carbide workpieces indicate that the inclusion of electrical spark discharges in the grinding zone in EDDG, though beneficial in so far as they dress and declog the wheel and reduce the normal grinding force, is however detrimental to the finish of the ground surface. Finish-grinding of components may hence be carried out with the current switched off.
- The roughness of electrical discharge diamond ground surfaces is higher than what is obtained in conventional diamond grinding, for identical grit size. This is evidently due to the higher maximum abrasive protrusion height associated with the former.
- A simulation of surface generation in EDDG utilizing simulated wheel topography data is presented to predict the surface roughness parameter  $R_a$  with reference to abrasive grit size, under conditions of no current flow. The simulation results are validated by experiments conducted on the EDDG set-up.
- The simulation indicates that the profile height of surfaces ground in cut-off configuration is predominantly positively skewed. The simulation also yields the relationship between the surface roughness parameter  $R_a$  and the average uncut chip cross-sectional area, based on geometrical considerations.

## 5.2 Scope for Future Work

EDDG process is in its early stages of development. In this thesis, certain fundamental aspects relating to the mechanism of material removal and mod-

clung of the process have been presented. Some of the issues which could be examined in future are summarized as follows

- The mechanism of material removal in EDDG can be comprehensively studied by conducting single-grit experiments with diamond indentors of known geometry
- Metal-bonded aluminum oxide wheels can be tried in EDDG in light of the thermal softening of the work, to test their efficacy in grinding hard materials like cemented carbides, which hitherto could be ground effectively only with diamond abrasives. Design of grinding wheels which would include development of suitable bonding materials especially suited to EDDG is also worthy of consideration
- The roughness of ground surfaces obtained in the present study are in the coarse machining range. Further work in EDDG may be carried out with finer grit wheels
- A parametric study of the EDDG process to study the effect of the wheel parameters viz., abrasive grit size and concentration, and the electrical pulse parameters on various process responses like the MRR and grinding forces is essential to generate the technological data for EDDG. This would also pave the way for optimization of the process. Another process response which is to be studied is the integrity of surfaces obtained in EDDG
- The discharge energy is an important parameter which considerably influences the wheel topography while electrodischarge dressing. Sufficient grit protrusion is obtained with increasing discharge energy but at the expense of dislodging some abrasive grains, arriving at the appropriate level of discharge energy is a compromise between these conflicting factors. With this in view, the effect of discharge energy on the wheel topography could be studied, and then correlated with wheel performance by conducting grinding tests

- The simulation of surface generation in EDDG in the present work is based on geometrical considerations. The wear of abrasives and the pile-up of the work material could be incorporated in the simulation for more realistic results. The simulation can further be extended to predict the forces and the material removal rate.

# References

- [1] S JAHANMIR, L K IVES, A W RUFF and M B PETERSON, *Ceramic Machining Assessment of Current Practice and Research Needs in the United States*, NIST Special Publication 834, U S Department of Commerce, 1992
- [2] W KONIG, R KOMANDURI, H K TONSHOFF and G ACKERSHOTT, Machining of hard materials, *Ann CIRP* **33** (2), 417-427 (1984)
- [3] W KONIG, L CRONJAGER, G SPUR, H K TONSHOFF, M. VIGNEAU and W J ZDEBLICK, Machining of new materials, *Ann CIRP* **39** (2), 673-681 (1990)
- [4] I INASAKI, Grinding of hard and brittle materials, *Ann CIRP* **36** (2), 463-471 (1987)
- [5] T G BIFANO, S C FAWCETT and R O SCATTERGOOD, Ductile-regime grinding A new technology for machining brittle materials, *J Eng Ind* **113**, 184-189 (1991)
- [6] W KONIG, D F DAUW, G LEVY and U PANTEN, EDM — Future steps towards the machining of ceramics, *Ann CIRP* **37** (2) 623-631 (1988)
- [7] G F BENEDICT, *Nontraditional Manufacturing Processes* Marcel Dekker Inc , New York (1987)
- [8] J A MCGEOUGH, *Advanced Methods of Machining*, Chapman and Hall, London (1988)

- [9] S KOSHIMIZU and I INASAKI, Hybrid machining of hard and brittle materials, *J Mech Work Tech* 17, 333-341 (1988)
- [10] T UEMATSU, K SUZUKI, T YANASE and T NAKAGAWA, A new complex grinding method for ceramic materials combined with ultrasonic vibration and electrodischarge machining, *Intersociety Symposium on Machining of Ceramic Materials*, Eds S CHANDRASEKHAR et al, American Society of Mechanical Engineers, New York, 135-140 (1988)
- [11] T KITAGAWA and K MAEKAWA, Plasma hot machining for new engineering materials, *Wear* 139, 251-267 (1990)
- [12] W KONIG and A K ZABOKLICKI, Laser assisted hot machining of ceramics and composite materials, *Proc Int Conference on Machining of Advanced Materials*, Ed S JAHANMIR, NIST Special Publication 847, U S Department of Commerce, 455-464 (1993)
- [13] E WESTKAMPER, Grinding assisted by Nd YAG lasers, *Ann CIRP* 44 (1), 317-320 (1995)
- [14] H LIANG and S JAHANMIR Boric acid as an additive for core-drilling of alumina, *J Tribology* 117, 65-73 (1995)
- [15] E YA GRODZINSKII, Grinding with electrical activation of the wheel surface, *Mach Tooling* 50 (12), 10-13 (1979)
- [16] V B VITLIN, Model of the electrocontact-abrasive cutting process, *Sov Eng Res* 1 (5), 88-91 (1981)
- [17] E YA GRODZINSKII and L S ZUBOTAVA, Electrochemical and electrical-discharge abrasive machining, *Sov Eng Res* 2 (3), 90-92 (1982)
- [18] H W ZHENG, G Q CAI, S L WANG and S X YUAN, An experimental study on mechanism of cermet grinding, *Ann CIRP* 38 (1), 335-338 (1989).



- [19] R WYSS and E POLLAK, A machining concept for PCD tools, *Ind Ma Rev* **51**, 280-283 (1991)
- [20] C E DAVIS, The dependence of grinding wheel performance on dressing procedure, *Int J Mach Tool Des Res* **14**, 33-52 (1974)
- [21] K SUZUKI, T UEMATSU and T. NAKAGAWA, On-machine trueing/dressing of metal bond grinding wheels by electrodischarge machining, *Ann CIRP* **36** (1), 115-118 (1987)
- [22] SH A BAKHTIAROV, Efficiency of diamond wheels after contact-erosion dressing, *Stanki Instrument* **60** (1), 18-19 (1989)
- [23] A ERDEN and B KAFTANOGLU, Heat transfer modeling of electric discharge machining, *Proc 21st Int Machine Tool Design and Research Conference*, Ed J M ALEXANDER, Macmillan, London, 351-358 (1981)
- [24] T AOYAMA and I INASAKI, Hybrid machining — Combination of electrical discharge machining and grinding, *14th North American Manufacturing Research Conference*, Society of Manufacturing Engineers, 654-661 (1986)
- [25] K P RAJURKAR, B WEI, J KOZAK and S R NOOKA Abrasive electrodischarge grinding of advanced materials, *11th Int Symposium for Electromachining*, Eds J P VAN GRIETHUYSEN and D KIRITSIS, Presses Polytechniques et Universitaires Romandes, Laussane, 863-869 (1995)
- [26] C RUBENSTEIN, The mechanics of grinding, *Int J Mach Tool Des Res* **12**, 127-139 (1972)
- [27] T TANAKA, N IKAWA and H TSUWA, Affinity of diamond for metals, *Ann CIRP* **30**(1), 241-245 (1981)
- [28] W GRAHAM and A NEE, The grinding of tool steels with a diamond abrasive wheel, *Int J Mach Tool Des Res* **14**, 175-185 (1974)

- [29] J F PRINS Single diamond particle interaction on steels, *Ind Dia Rev* . 364-370 (1971)
- [30] G A ROBERTS and R A CARY, *Tool steels*, American Society for Metals, Ohio (1980)
- [31] M R PATEL, M A BARRUFET, P T EUBANKS and D D DiBITONTO, Theoretical models of the electrical discharge machining process - The anode erosion model, *J App Phy* 66(9), 4104 - 4111 (1989)
- [32] N IKAWA and T TANAKA, Thermal aspects of wear of diamond grain in grinding, *Ann CIRP* 19(1), 153-157 (1971)
- [33] R KOMANDURI and M C SHAW, Wear of synthetic diamond when grinding ferrous metals, *Nature* 255, 211-213 (1975)
- [34] A G THORNTON and J WILKS, Tool wear and solid state reactions during machining, *Wear* 53, 165-187 (1979)
- [35] G M MAGISTRI, C V COOPER and J E WILLIAMS, The deposition of electrically conductive films as a measure to improve the electrical discharge truing behavior of metal-bonded c-BN grinding wheels, *Surf Coat Tech* 62, 649-654 (1993)
- [36] T T SOONG, *Probabilistic modeling and analysis in science and engineering*, John Wiley, New York (1981)
- [37] R.L MEHAN and L E HIBBS, Thermal degradation of sintered diamond compacts, *J Mater Sci* 24, 942-950 (1989)
- [38] M A MOORE, Abrasive Wear, *Fundamentals of friction and wear of materials*, Ed D A Rigney, American Society of Metals, USA (1981)
- [39] E D DOYLE and L E SAMUELS, Further developments of a model of grinding, *Proc Int Conf Prod Eng* , p 45, Tokyo (1974)

- [40] D M TURLEY and E D DOYLE, Factors affecting workpiece deformation during grinding, *Mater Sci Eng* 21, 261-271 (1975)
- [41] B M SCHUMACHER, About the role of debris in the gap during electrical discharge machining, *Ann CIRP* 39(1), 197-199 (1990)
- [42] F P BOWDEN and D TABOR, *The friction and lubrication of solids*, (Oxford University Press, New York (1986)
- [43] K IWATA and J AIHARA, Shear strength of the adhesion junction between contact surfaces formed at high pressures and temperatures, *Wear* 97, 275-290 (1984)
- [44] S MALKIN, *Grinding Technology — Theory and applications of machining with abrasives*, Ellis Horwood Ltd, Chichester, U K (1989)
- [45] K H ZUM GHAR, *Microstructure and wear of materials*, Elsevier Science, Amsterdam (1987)
- [46] J LARSEN-BASSE and N DEVNANI, Binder extrusion as a controlling mechanism in abrasion of WC-Co cemented carbides, *Proc Int Conf Science of Hard Materials*, Eds E A Almond, C A Brookes and R Warren, Adam Hilger Ltd, Bristol, 883-895 (1986)
- [47] O ZELWER and S MALKIN, Grinding of WC-Co cemented carbides, *J Eng Ind* 102, 209-220 (1980)
- [48] A M GADALLA and W TSAI, Electrical discharge machining of tungsten carbide-cobalt composites, *J Am Ceram Soc* 72 (8), 1396-1401 (1989)
- [49] C J HEUVELMAN, Summary report on the CIRP co-operative research on spark-erosion machining of cemented carbides (die-sinking), *Ann CIRP* 29 (2), 541-544 (1980)
- [50] M A MOORE and F S KING, Abrasive wear of brittle solids, *Wear* 60, 123-140 (1980)

- 
- [51] I M OGHAY, On the indentation fracture of cemented carbide – Survey of operative fracture modes, *Wear* **43**, 239–252 (1977)
- [52] J L METZGER and A TORRANCE, Dry versus wet grinding of carbide, *Industrial Diamond Review*, No 6, 296–303 (1990)
- [53] M BAILEY and H JUCHEM, Grinding cermets with diamond, *Industrial Diamond Review*, No 6, 298–302 (1992)
- [54] A K SRIVASTAVA, K SRIRAM and G K LAL, A new technique for evaluating wheel loading, *Int J Mach. Tool Des Res* **25** (1), 33–38 (1985)
- [55] K H ZUM GHAR, Modeling of two-body abrasive wear, *Wear* **124**, 87–103 (1988)
- [56] G S KREIMER, *Strength of Hard Alloys*, Consultants Bureau, New York (1968)
- [57] R WARREN and B JOHANNESSON, The fracture toughness of hardmetals, *Sintered metal-ceramic composites*, Ed G S UPADHYAYA, Elsevier Science, Amsterdam, 365–375 (1984)
- [58] W BETTERIDGE, *Cobalt and it's alloys*, Ellis Horwood Ltd, Chichester, U K (1982)
- [59] S B LUYCKX, W B JONES, A KONRASIS and N MASTRANTONIS, Healing of cracks in WC-Co in the temperature range 600 to 800°C, *Int J Refractory Metals and Hard Materials* **12**, 89–93 (1993-94)
- [60] B JOHANNESSON and R WARREN, Fracture of hardmetals upto 1000°C, *Proc Int Conf Science of Hard Materials*, Eds E.A ALMOND, C A BROOKES and R. WARREN, Adam Hilger Ltd., Bristol, 713–723 (1986)
- [61] J VERKERK, Final report concerning CIRP co-operative work in the characterization of grinding wheel topography, *Ann CIRP* **26** (2), 385–395 (1977)

- [62] J TAMAKI and T KITAGAWA, Evaluation of surface topography of metal-bonded diamond wheel utilizing three-dimensional profilometry, *Int J Mach Tools Manufact* **35** (10), 1339–1351 (1995)
- [63] H T MCADAMS, Markov chain models of grinding profiles, *J Eng Ind* **86** 383–388 (1964)
- [64] J PEKLENIK, Contribution to the correlation theory for the grinding process, *J Eng Ind* **86**, 85–94 (1964)
- [65] S M PANDIT and S M WU, *Time series and system analysis with applications*, Wiley, New York (1983)
- [66] T WARREN LIAO, Fractal and DDS characterization of diamond wheel profiles, *J Matl Process Tech* **53**, 567–581 (1995)
- [67] H K TONSHOFF, J PETERS, I INASAKI and T PAUL, Modeling and simulation of grinding processes, *Ann CIRP* **41** (2), 677–688 (1992)
- [68] S MALKIN and R B ANDERSON, Active grains and dressing particles in grinding, *Proc Int Conference on New Developments in Grinding*, Ed M C SHAW, Carnegie Press, Pittsburg (1972)
- [69] A BUTTNER, Das schleifen sprodharter werkstoffe mit diamanttopfscheiben unter besonderer berucksichtigung des tiefschleifens, Dr Ing Dissertation, Technical University of Hannover, 1968
- [70] H RUMPF, *Particle Technology*, Hanser, Munich (1990)
- [71] J L METZGER, *Superabrasive grinding*, Butterworth, London (1986)
- [72] H OHMORI and T NAKAGAWA, Mirror surface grinding of silicon wafers with electrolytic in-process dressing, *Ann CIRP* **39** (1), 329–332 (1990)
- [73] C.E DAVIS, The dependence of grinding wheel performance on dressing procedure, *Int J Mach Tool Des Res* **14**, 33–52 (1974)

- [74] G. ELSNER, Bonding strength of ceramic-metal joints, *Proc European Colloquium on Designing Interfaces for Technological Applications*, Ed S D PETEVES, Elsevier, Barking (1988)
- [75] T. YUHTA, S. IGARASHI, R. OKUMA and T. SATOH, On the surface nature of diamond wheel in the process of grinding carbon steel, *Ann CIRP* 27 (1), 255-259 (1976)
- [76] K. SYOJI, L. ZHOU and S. MATSUI, Studies on truing and dressing of diamond wheels, *Bull Jpn Soc Prec Eng* 24 (2), 124-129 (1990)
- [77] N. DEO, *System simulation with digital computer*, Prentice Hall, New Delhi (1987)
- [78] W. J. CONOVER, *Practical nonparametric statistics*, John Wiley & Sons, New York (1971)
- [79] Y. NAMBA, Y. YAMADA, A. TSUBOI, K. UNNO and H. NAKAO, Surface structure of Mn-Zn ferrite single crystals ground by an ultraprecision surface grinder with various diamond wheels, *Ann CIRP* 41 (1), 347-351 (1992)
- [80] K. V. BURY, *Statistical models in applied science*, John Wiley & Sons, New York (1975)
- [81] S. MALKIN and T. MURRAY, Mechanics of rotary dressing of grinding wheels, *J Eng Ind* 100, 95-102 (1978)
- [82] W. H. PRESS, B. P. FLANNERY, S. A. TEUKOLSKY and W. T. VETTERLING, *Numerical recipes — The art of scientific computing*, Cambridge University Press, Cambridge (1989)
- [83] R. M. BAUL and R. SHILTON, Mechanics of metal grinding with particular reference to Monte Carlo simulation, *Proc 8th Int. Machine Tool Design and Research Conference*, Eds S. A. TOBIAS and F. KOENIGSBERGER, Pergamon, Oxford (1967), 923-946

- [84] H YOSHIKAWA and T SATA, Simulated grinding process by Monte Carlo method, *Ann CIRP* **16**, 297-302 (1968)
- [85] C P BHATEJA, An enveloping profile approach for the generation of ground surface texture, *Ann CIRP* **25** (1), 333-337 (1971)
- [86] T SUTO and T SATA, Simulation of grinding process based on wheel surface characteristics, *Bull. Japan Soc Prec Engg* **15** (1), 27-33 (1981)
- [87] M S HAMED D J WHITEHOUSE and T C BUTTERY, Random surface generation — an integrated approach, *Ann CIRP* **27** (1), 499-504 (1978)
- [88] S S LAW and S M WU, Simulation study of the grinding process, *J Eng Ind* **95**, 972-978 (1973).
- [89] K STEFFENS Closed loop simulation of grinding, *Ann CIRP* **32** (1), 255-259 (1983)
- [90] P K BASURAY, B SAHAY and G K LAL, A simple model for evaluating surface roughness in fine grinding, *Int J Mach Tool Des Res* **20**, 265-273 (1980)
- [91] R S SAYLES and T R THOMAS, A stochastic explanation of some structural properties of a ground surface, *Int J Prod Res* **14** (6), 641-655 (1976)
- [92] S JACOBSON, P WALLEN and S HOGMARK, Fundamental aspects of abrasive wear studied by a new numerical simulation model, *Wear* **123**, 207-223 (1988)
- [93] J E MEYER and G P FANG, Effect of grinding parameters on surface finish of ground ceramics, *Ann. CIRP* **44** (1), 279-282 (1995)
- [94] I INASAKI, Speed-stroke grinding of advanced ceramics, *Ann. CIRP* **37** (1), 299-302 (1988)

- 
- [9] E. BRINKSMEIER, H. K. TONSHOFF, I. INASAKI and J. PEDDINGHAUS Basic parameters in grinding, *Ann. CIRP* **42** (2), 795–799 (1993)



